IRON TRAFFICKING IN THE CYTOSOL AND VACUOLES OF SACCHAROMYCES CEREVISIAE

A Dissertation

by

TRANG QUYNH NGUYEN

Submitted to the Office of Graduate and Professional Studies of
Texas A&M University
in partial fulfillment of the requirements for the degree of

DOCTOR OF PHILOSOPHY

Chair of Committee,	Paul A. Lindahl
Committee Members,	Marcetta Y. Darensbourg
	Vishal M. Gohil
	Frank M. Raushel
Head of Department,	Simon W. North

December 2019

Major Subject: Chemistry

ABSTRACT

Iron (Fe) is an essential trace metal for all eukaryotes. *Saccharomyces cerevisiae* is an excellent model organism to study eukaryotic iron metabolism. Much Fe enters the cytosol and shuttles to the mitochondria for heme and iron-sulfur clusters biosynthesis. Little is known about cytosolic iron. Circumstantial evidence suggests that cytosolic Fe is high-spin Fe^{II} but further evidence is required to validate this. Cytosolic Fe flows not only into mitochondria but also into vacuoles. They are acidic organelles that can store Fe under Fe-overload conditions. The endogenous ligand of vacuolar Fe is proposed to be polyphosphate, but no direct evidence has been shown. The main goal of this dissertation was to investigate the vacuolar and cytosolic Low-Molecular-Mass (LMM) iron complexes in *S. cerevisiae.*

To characterize these complexes, vacuolar and cytosolic fractions were first isolated from whole cells of yeast under low and high iron. LMM complexes were contained in flow through solutions (FTSs) by passing vacuolar and cytosolic fractions through a 10 kDa membrane cut-off. These FTSs were then loaded onto a LC size exclusion column interfaced to an ICP-MS.

The results of LMM metal complexes from vacuoles were described in Chapter II. 29 batches of vacuoles were isolated from *S.cerevisiae*. Since ICP-MS can detect multiple elements simultaneously, I found that nearly all iron, zinc, and manganese ions in the vacuolar FTSs were present as LMM complexes. Phosphorus-detected peaks generally comigrated with metal-detected speaks at 500 – 1700 Da, thus suggesting polyphosphate is the common ligand for metals stored in the vacuoles. The binding of transition metals and vacuolar polyphosphate was further demonstrated by the treatment with phosphatase, which resulted in the loss of LMM metal-bound species.

The second aim was to study the speciation of cytosolic iron (Chapter III). Iron with peaks range from 700 – 1300 Da dominated. Cytosol from cells of different genetic knockout strains were isolated and collected the FTSs to study the behavior of these Fe complexes. Interestingly, a pool of copper LMM complexes were detected in the cytosol at 300 – 1300 Da under high copper growth condition and disruption of copper homeostasis.

DEDICATION

For my parents, Khanh Duc Nguyen and Ninh Thi Kim Nguyen, who have worked very hard for their entire life and made a lot of sacrifice to give me and my sister, Phuong Thuy Nguyen, the best education that they did not have the opportunities to pursue.

ACKNOWLEDGEMENTS

I would like to thank my research advisor, Dr. Paul A. Lindahl for giving me the opportunity to learn and do science in your laboratory. Thank you for your understanding, your patience and your unlimited support to train me to be a scientific researcher. Thank you for your extremely hard work ethics and infinite enthusiasm which have inspired me to love chemistry even more and nurture my curiosity. Thank you for pushing me and believing in me so that I could do my best during my time at Texas A&M University.

I also would like to thank all of my committee members. First of all, I would like to thank Dr. Marcetta Darensbourg for your encouragement, spiritual support and wonderful lessons of organometallic chemistry. Thank you for being such a great role model whom I deeply respect, admire and want to grow up and become a person like you. I would like to thank Dr. Frank Raushel for being such an excellent teacher who transformed enzymatic mechanisms to be interesting for me learn and understand them better. I would like to specially thank Dr. Vishal Gohil for your constructive criticism, suggestions and willingness to let me learn and work in your lab. Thank you to Dr. Yohannes Rezenom at the Chemistry Mass Spectrometry Facility for your dedicated assistance to help me obtain ESI-MS results. Thank you to Dr. Lisa Perez for being very patient, friendly and supportive to teach me Marvin Sketch and Avogadro. Thank you to Dr. Roula Mouneimne at the College of Veterinary Medicine & Biomedical Sciences for being very kind and nice to help me obtain good confocal images of vacuoles. Thank you to Dr. Dennis Thiele at Duke University for your helpful discussion to my research and your generous gifts of *cup1*Δ and *CUP1R* strains.

I would also like to thank the Lindahl lab members. Special thanks to Nathaniel Dziuba for always being helpful and patient to teach me LC-ICP-MS. Thank you for not only being a supportive labmate, a wonderful colleague but also being an invaluable friend of mine. Thank you for always being by my side whenever I have difficulties. Thank you to Waseem Vali for teaching me Mössbauer and your willingness to help me with heavy lab tasks. Thank you to Joshua Kim, Raynelle Nash and Carmen Wiggin for giving me the opportunities to become your mentor so that I can improve my teaching and communication skills. It was my great honor to mentor such talented and hardworking students like three of you. Thank you to Rachel Shepherd for always being friendly and sharing the same passion for cats just like me. Thank you to Hayley Brawley for your dedication to keep the lab clean and organized.

In addition, I would like to thank my friend Ms. Sasha Chihak for being a great "essential vitamin" helping me get through the tough time in grad school. I thank Dr. Charli Baker for being such a wonderful person who was willing to teach me Western blots and giving me insightful suggestions for my research projects.

Moreover, I would like to thank my parents and my sister, Phuong Thuy Nguyen, for always being there to listen to me and encourage me to never give up. Thank you to my American families, the Deffendall and the Turner for always loving and caring about me even though I am so far away from you. I could not complete this degree without your endless support and love.

Last but not least, I would like to thank my undergraduate advisor, Dr. Kayla Green. Thank you for being my academic mother who taught me bio-inorganic chemistry and made me fall in love with the subject, who was the reason why I got accepted and went to TAMU, and who always believed in me and motivated me to do my best. Thank you for everything you have done for me.

CONTRIBUTORS AND FUNDING SOURCES

Contributors:

This work was supervised by a dissertation committee consisting of Professors Paul Lindahl, Marcetta Darensbourg and Frank Raushel of the Department of Chemistry and Professor Vishal Gohil of the Department of Biochemistry and Biophysics.

The results for the LC calibration curve in Chapter II (Figure 2.S1) was provided by Mr. Nathaniel Dziuba.

All other work conducted for the dissertation was completed by the student independently.

Funding Sources:

Graduate study was supported by a teaching and research assistant fellowship from Texas A&M University.

This work was also made possible in part by National Institutes of Health under Grant Number R35 GM127021 and the Robert A. Welch under Grant Number A1170 to Professor Paul Lindahl. The content is solely the responsibility of the authors and does not necessarily represent the official views of the National Institutes of Health or the Welch Foundation.

TABLE OF CONTENTS

LIST OF FIGURES

LIST OF TABLES

LIST OF SCHEMES

CHAPTER I

INTRODUCTION

Trace metals are indispensable for virtually all living organisms. Iron, copper, zinc, and manganese in particular serve as cofactors for hundreds of enzymes required for cell growth and survival (1) (2) (3). These metal cofactors are small, simple but versatile to enable difficult chemistry due to their unique properties such as electron-donor/acceptor ability, multivalence state, ligand selectivity with flexible coordination geometry and great mobility (4) (5) (6). However, the toxicity of excess metals can be detrimental if cells fail to properly control a balance between supply and demand (3) (7). Additionally, the number of available donor ligands in biological systems is limited to oxygen, nitrogen, and sulfur (8) (9). So how do cells avoid mismetallation and choose the correct metal to perform the desired role? How can the native metal cofactor overcome displacement by other metal ions? What principles are followed to control the selectivity and competition among different metals? What strategies are adopted to protect the cells against potential lethality of metals?

Living organisms have developed a sophisticated system of metal regulation and trafficking to maintain intracellular metal homeostasis. This includes three primary sub-processes: [1] acquiring metal from the environment, [2] sensing the intracellular metal status, [3] distributing metal ions for storage, utilization, and recycling (7) (10) (11). As a genetically tractable and unicellular eukaryotic organism, the budding yeast *Saccharomyces cerevisiae* has been used extensively to study trafficking and regulation of metal ions (12) (13).

The aim of this dissertation is to investigate the trafficking of iron, copper, zinc, and manganese in the cytosol and vacuoles of *Saccharomyces cerevisiae*. We hope to gain a better

understanding of trafficking as well as the exquisite regulatory mechanisms used to control these processes.

Iron Trafficking

Iron (Fe) is involved in a variety of metabolic processes including electron transport, respiration, enzyme catalysis and DNA biosynthesis (14). The unique redox activity of Fe allows it to function as an electron donor or acceptor by recycling between the ferrous (Fe^{II}) and ferric (Fe^{III}) states. Due to this property, intracellular iron can catalyze the Haber-Weiss reaction (Eq.3), which makes use of Fenton chemistry (Eq.2), to generate reactive hydroxyl radicals in the cells (15).

$$Fe^{3+} + O_2^{-\bullet} \rightarrow Fe^{2+} + O_2 \qquad \text{(Eq.1)}$$

$$Fe^{2+} + H_2O_2 \rightarrow Fe^{3+} + OH^{\bullet} + OH^{-} \qquad \text{(Eq.2)}$$

$$\text{Net reaction: } H_2O_2 + O_2^{-\bullet} \rightarrow O_2 + OH^{\bullet} + OH^{-} \qquad \text{(Eq.3)}$$

Hydroxyl radicals ($OH^{\bullet}$), superoxide ($O_2^{-\bullet}$) and hydrogen peroxide (H_2O_2) are reactive oxygen species (ROS) which can be extremely toxic. High level of ROS can induce DNA damage, enzymes inactivation and eventually cell death (16). The accumulation of iron, ROS and both is linked to degenerative diseases, the immune response and cancer (17) (18).

Budding yeast has established complex regulatory mechanisms to survive despite substantial fluctuations of nutrient iron availability. Primary subcellular compartments involved in yeast iron metabolism include mitochondria, vacuoles, the cytosol, the nucleus and the plasma membrane as shown in Figure 1.1 (19).

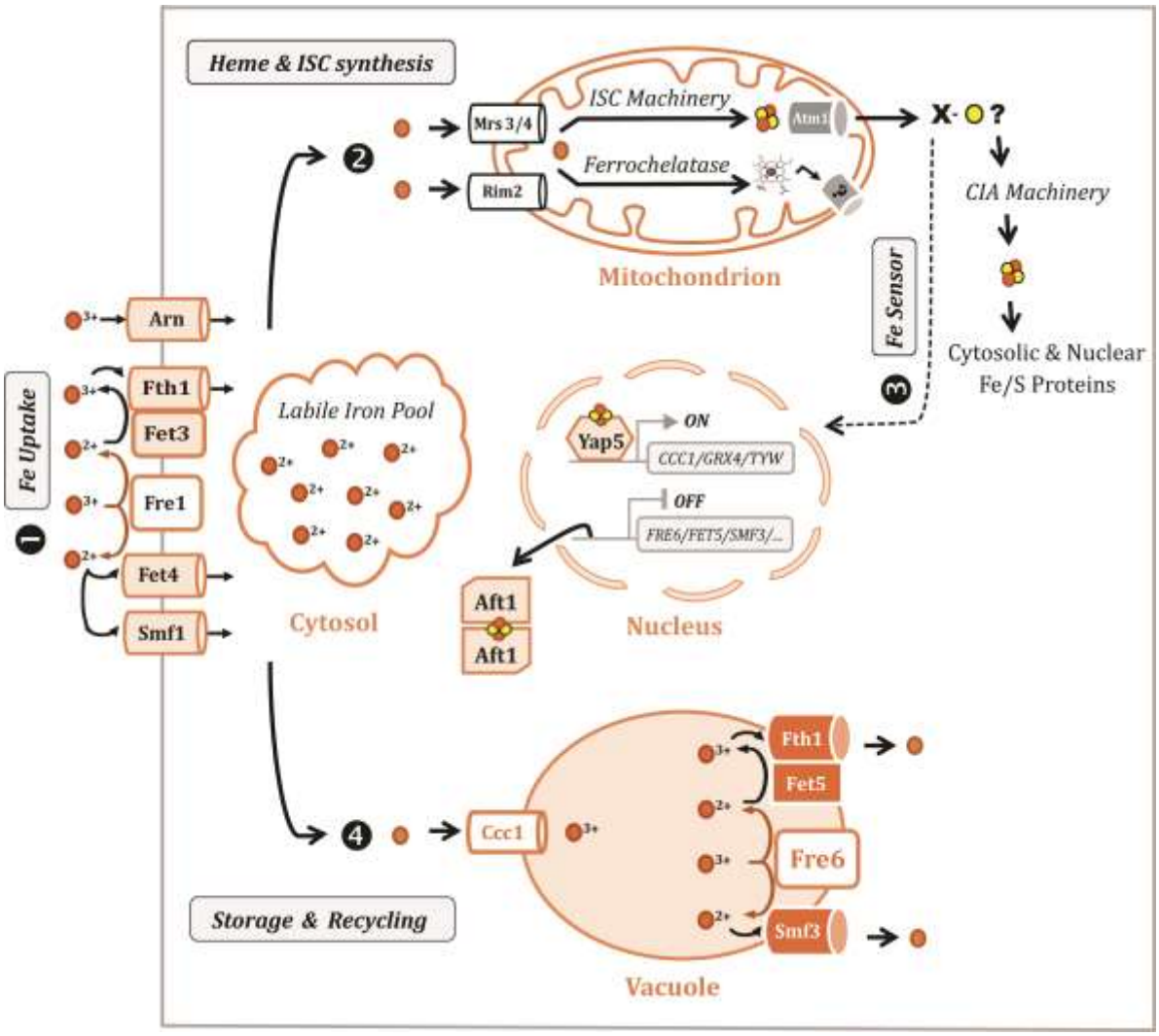

Figure 1.1: Iron trafficking in *Saccharomyces cerevisiae* (adapted from references 10 and 19).

$^{3+}$: ferric ion

$^{2+}$: ferrous ion

: iron-sulfur cluster (ISC)

X-S: unknown X-S species

Iron acquisition

Due to the high reactivity with oxygen, environmental Fe is usually found in biological unavailable forms such as ferric hydroxide $Fe(OH)_3$. Iron hydroxide with an oxidation state of 3+ has extremely low solubility with $K_{sp} = 3 \times 10^{-39}$ (20). Budding yeast has evolved with intricate strategies to cope with this challenge and maximize iron acquisition under iron scarcity by 2 primary uptake mechanisms.

The first pathway, which is widely used in bacteria, fungi, and plants, utilizes siderophores (21). These are small molecules that bind to ferric ions with high affinity to form six-coordinate, octahedral complexes (22). For example, desferrioxamine, a hydroxamate-type siderophore produced by several species of actinomycetes, has a complex formation constant of $\log \beta = 30.5$ with iron (23). These iron-bound siderophore complexes are then captured by specific transport systems on the plasma membrane, thus permitting ferric ions to be solubilized, imported and utilized (24). Although *S. cerevisiae* do not synthesize their own siderophores, they can express 4 of the siderophore transporters Arn1, Arn2, Arn3, and Arn4 to capture the siderophores secreted by other organisms (25). Once bound to siderophores, Fe can be either utilized as a substrate for the ferrireductases Fre1-3 on the plasma membrane or endocytosed (26). The endocytic vesicle of Fe-bound siderophores is acidified to release Fe to the cytosol. Siderophores can be degraded or accumulated in intracellular vesicles (27). This siderophore-mediated iron uptake mechanism is promoted by a family of 3 cell wall mannoproteins called Fit1, Fit2, and Fit3 (facilitator of iron transport) (28). The cell wall from yeast cells, which have transitioned to post-exponential growth phase, can accumulate iron in a magnetically ordered form (29). Expression of Arn and Fit proteins is induced under iron starvation by the Aft1/2-dependent iron regulon (30).

The second uptake mechanism requires metalloreductase activity supplied by a family of Fre proteins. There are 7 Fre proteins in *S.cerevisiae* (31). All are heme-containing transmembrane proteins utilizing NADPH as a reducing agent to convert Fe^{III} to Fe^{II} (32). Fre1-3 localize to the plasma membrane and labilize Fe^{III} from either exogenous Fe source or ferric-siderophore importer complexes (26). The resulting ferrous ions can then be transported to the cells via a high-affinity or low-affinity importers.

The high-affinity transport systems involves a complex of Fet3 and Ftr1 with a K_m = 0.2 μM for iron (33). Both of these proteins are controlled by Aft1 transcription factor (34). They must be synthesized simultaneously to be correctly targeted to the cell surface together as a complex (35). The Fet3-Ftr1 transport system is post-transcriptionally regulated by iron levels in the media. Transcription of *FET3* is down-regulated when cells are exposed to as little as 10 μM $FeSO_4$. Decreased protein levels are observed at higher Fe concentrations. Incubation of cells with 1 mM $FeSO_4$ causes 50% loss of Fet3 protein expression within 1 hour, and 80% loss within 2 hours (36). As a multicopper oxidase, Fet3 depends on Cu (see below) and molecular oxygen to convert Fe^{II} to Fe^{III}. This enzyme is analogous to mammalian ceruloplasmin (37). Three ferrous ions are oxidized in sequential fashion and the extracted electrons are stored in the protein. After the oxidation of a fourth Fe^{II}, the multicopper oxidase reduces molecular oxygen to water, thus inhibiting the formation of free radicals (37). The reduction-oxidation reaction of Fet3 is shown as follows: $4Fe^{2+} + O_2 + 4H^+ \rightarrow 4Fe^{3+} + 2H_2O$. The transmembrane permease Ftr1 then binds to the ferric ions generated in this reaction, and transports them into the cells. Such binding of Ftr1 to Fe^{III} is thought to give rise to the selectivity of Fet3/Ftr1 system for transporting iron over other transition metals (38).

In contrast, the low-affinity importers have a broad specificity towards a variety of transition metals in addition to iron. One transporter, Fet4 has a K_m of 35 μM with ferrous iron (39). It can also transport copper, zinc, manganese and cadmium (40). Due to this property, upregulation of Fet4 in the absence of the high affinity iron transporters results in overload metal acquisition, thus diminishing metal resistance in yeast cells (41). Expression of Fet4 is also strongly induced under hypoxic conditions by Rox1 (42). The other low-affinity iron transporter, Smf1, is not oxygen-sensitive and primarily transports manganese (43). Smf1p is an H^+/transition metal symporter which utilizes a pH gradient to drive iron and manganese uptake (44).

Mitochondria are the major "hubs" for iron trafficking

Nutrient Fe enters the cytosol and is trafficked primarily into the vacuoles and mitochondria. Mitochondria are the ATP-generating sites where heme and iron-sulfur clusters (ISC) are synthesized for the respiratory complexes and other important Fe-containing enzymes (45) (46). Much cytosolic Fe flows into this organelle for use in those critical metabolic processes via 2 transport systems: high-affinity transporters Mrs3/Mrs4 and low-affinity transporter Rim2. All three reside in the mitochondrial inner membrane.

Mrs3 and Mrs4, which belong to the mitochondrial carrier family (MCF), are homologs of vertebrate mitoferrin1 and mitoferrin 2 (47). In low-iron media, deletion of *MRS3* and *MRS4* genes causes loss of mitochondrial iron in frataxin-deficient cells (48), which results in decreased biogenesis of ISC and heme proteins (49). This phenomenon has been further studied by Moore and coworkers using Mössbauer spectroscopy to characterize the cellular iron-ome (50). Mitochondrial iron from *mrs3*Δ*mrs4*Δ cells grown under iron-deficient respiring medium are

primarily present as an inaccessible form of Fe^{III} nanoparticles, thus limiting the cell ability for ISC and heme synthesis. *mrs3*Δ*mrs4*Δ mutants also grow slowly in iron-deficient respiring media but recover to wild-type (WT) growth rate under iron-sufficient condition. The restoration of growth implies the defects of heme and ISC biogenesis are rescued by the adequate supply of nutrient iron, which is proved by Mössbauer spectroscopy. Mitochondria from iron-sufficient *mrs3*Δ*mrs4*Δ cells compose of ISC, heme, and non-heme high spin (NHHS) Fe^{II} Mössbauer signals as usually observed in mitochondria of healthy cells. Surprisingly, total intracellular iron concentrations in these double mutants were found to be higher compared with WT cells regardless of the nutrient Fe status. This indicates a failure of sensing iron status in the *mrs3*Δ*mrs4*Δ mutants, implying a dysregulation of iron homeostasis (50).

Rim2 is also a member of MCF. Similar to *MRS3/4* genes, the *RIM2* gene was discovered as a multicopy suppressor to rescue the respiratory defects of *mrs2* null mutant (51) (52). This nuclear gene is required for proper cell growth and mitochondrial DNA replication. The substrate of Rim2 was unknown until 2006 when pyrimidine triphosphates were identified to be transported into mitochondrial matrix via Rim2 in exchange for the export of pyrimidine monophosphates to the cytosol (53). Yoon and coworkers subsequently showed that Rim2 is also involved in mitochondrial iron metabolism by serving as a back-up for Mrs3/4 (54). Overexpression of Rim2 in WT and *mrs3*Δ*mrs4*Δ cells increases heme and ISC synthesis. Depletion of Rim2 in the absence of Mrs3 and Mrs4 is associated with reduced heme synthesis *in vitro* (54), but not *in vivo* (55). While Froschauer *et al.* concluded that iron transport activity of Rim2 required pyrimidine nucleotides (55), recent work of Knight and coworkers demonstrated that 2 point mutations at the substrate binding sites of Rim2 had nonoverlapping effects on iron and pyrimidine transport, thus

implying Rim2 transport activities of these 2 substrates occur independently with separate mechanisms (56).

The driving force of iron transport by Mrs3/4 and Rim2 depends on media Fe^{II} concentration and pH gradient (56) (57). Little is known about the chemical nature of the Fe complexes recognized by these carrier proteins. Based on the basket-shaped structures of mitochondrial carrier proteins (58), the Fe substrates of Mrs3/4 are speculated to be small enough to fit and pass through the narrow channels of these transporters (59). Low-Molecular-Mass (LMM) complexes are the ideal candidates satisfying this requirement (60). A LMM iron complex with an appoximate mass of 580 Da (Fe_{580}) repeatedly found in mitochondiral extracts may serve such role (61). Fe_{580} was not observed in mitochondria isolated from respiring *mrs3*Δ*mrs4*Δ cells grown in iron-deficient media but recovered under iron-sufficient condition (50). This pool of Fe_{580} was also characterized by Mössbauer to yield a NHHS Fe^{II} signal (62). Treatment of intact mitochondria with a membrane-permeable chelator was found to inhibit ISC assembly (63). This result is consistent with the Mössbauer signal of Fe_{580}, suggesting its role as a feedstock for ISC synthesis and that it is likely transported via Mrs3/4.

Intracellular iron sensing and regulation

As the focal point of iron trafficking, mitochondria exert a strong influence on whole-cell iron metabolism. In addition to producing hemes and ISC, mitochondria export a poorly characterized "X-S" species that is essential for the molecular mechanism of iron regulation. This species is hypothesized to be translocated to the cytosol by an ATP-binding cassette (ABC) transporter Atm1 in the mitochondrial inner membrane (64). The chemical structure of X-S is still controversial. The crystal structure of Atm1 proposes X-S to be glutathione or glutathione

persulfide (65). Using transportomics approach with mass spectrometry, Schaedler and coworkers concluded that glutathione trisulfide (GS-S-SG) was the substrate of Atm1 (66). On the contrary, Cowan suggests that X-S composes an Fe_2S_2 cluster coordinated with four glutathiones as exoligands (67). Recent work by Pain and coworkers reveals that Atm1 exports 2 different sulfur-containing species. One of them is called S_{int} with a mass in the range of 500 – 1000 Da. S_{int} is produced by the mitochondrial ISC assembly machinery and then exported to the cytosol for tRNA modification (68). The other species is an Fe-S intermediate, which might be related to Cowan's glutathione-coordinated iron-sulfur cluster (69).

The mysterious X-S species exported by Atm1 has attracted interest for the past two decades due to its suggested role as a means of communication between mitochondria and the cytosol (70). X-S is produced in proportion to the mitochondrial Fe/S cluster assembly activity, and this is central for the cell's ability to respond to different iron conditions. Aft1 and Aft2 are activated in response to Fe deficiency, while another transcription factor Yap5 is activated in response to iron Fe sufficiency (71) (72). Under low iron conditions, Aft1/2 stay in the nucleus and bind to the promoter site to activate the iron regulon of approximately 20 Fe-related proteins (73) (74). Iron uptake is stimulated since Aft1 induces the expression of the plasma membrane Fe importer genes *FET3/FTR1* and *FET4*, a family of metalloreductase genes *FRE1-3*, and the cell wall mannoprotein genes *FIT1-3* (75). Fe is also mobilized from a different subcellular compartment called vacuoles where excess Fe is stored (see below). The shuttling of Fe from the vacuoles to the cytosol is induced by the upregulation of the vacuolar metalloreductase Fre6 and two vacuolar Fe exporters Fet5/Fth1 and Smf3 (76).

In response to iron overload condition, Aft1 is first exported out of the nucleus via Msn5, then it is inhibited by Fe_2S_2 cluster-binding complexes formed by Grx3 and Grx4 along with two

Protein	Subcellular localization	Function	Regulation
Arn1	Plasma membrane, endosome	Ferrichrome siderophore transporter	Aft1p
Arn2/ Taf1	Unknown	TAFC siderophore transporter	Aft1p
Arn3/ Sit1	Plasma membrane, endosome	Hydroxamate siderophore transporter	Aft1p
Arn4/ Enb1	Plasma membrane	Enterobactin siderophore transporter	Aft1p
Fit1	Cell wall	Mannoprotein, facilitator of Fe-siderophore transport	Aft1p
Fit2	Cell wall	Mannoprotein, facilitator of Fe-siderophore transport	Aft1p
Fit3	Cell wall	Mannoprotein, facilitator of Fe-siderophore transport	Aft1p
Fre1	Plasma membrane	Ferric/ cupric reductase	Aft1p
Fre2	Plasma membrane	Ferric/ cupric reductase	Aft1p
Fre3	Plasma membrane	Ferric/ cupric reductase	Aft1p
Fet3p	Plasma membrane	Multicopper oxidase	Aft1p
Ftr1	Plasma membrane	Ferric permease	Aft1p
Fet4	Plasma membrane	Low-affinity Fe^{II} transporter	Aft1p, Aft2p, Rox1p
Smf1	Plasma membrane	Divalent metal transporter, Nramp family	---
Mrs3	Inner mitochondrial membrane	High-affinity Fe transporter	Aft1p
Mrs4	Inner mitochondrial membrane	High-affinity Fe transporter	Aft1p, Aft2p
Rim2	Inner mitochondrial membrane	Low-affinity Fe transporter, pyrimidine nucleotide transporter	---
Ccc1	Vacuolar membrane	Fe transporter	Yap5p
Fre6	Vacuolar membrane	Ferric/ cupric reductase	Aft1p
Fet5	Vacuolar membrane	Multicopper oxidase	Aft1p
Fth1	Vacuolar membrane	Ferric permease	Aft1p
Smf3	Vacuolar membrane	Divalent metal transporter, Nramp family	Aft1p. Aft2p
Grx4	Cytosol	Monothiol glutaredoxin	Yap5p
Tyw1	Endoplasmic reticulum	Fe/S protein required for wybutosine modified tRNA synthesis	Yap5p

Table 1: Proteins involved in Fe trafficking and that are discussed in this dissertation. Information is extracted from references 30, 71, and 74.

cytosolic proteins Fra1 and Fra2 (77) (78) (79). At the same time, the high iron regulator Yap5 is activated via binding with an Fe_2S_2 cluster to turn on the transcription of a vacuolar Fe importer gene *CCC1* and Fe-S cluster binding protein genes *GRX4* and *TYW1* (72) (80) (81). Thus, cells can be protected from Fe toxicity since excess cytosolic Fe is shuttled via Ccc1 and stored in the vacuoles (82). Table 1.1 summarizes all of the proteins required for iron trafficking and that are discussed in this dissertation (30) (71) (74).

Vacuoles as the storage and recycling site for iron

Despite the important role of vacuoles as mediators of Fe homeostasis, little is known about the speciation and ligands of vacuolar iron. Yeast vacuoles are comparable to the mammalian lysosomes; thus, the vacuolar lumen has an acidic pH and a variety of hydrolases (83). The acidity of vacuolar compartments is crucial for cell growth, which maintained by a number of vacuolar proton translocating V-ATPases (84). They are multisubunit enzymes composed of two functional domains: the cytoplasmic V_1 sector participating in ATP hydrolysis and the membrane-bound V_0 sector functioning in proton translocation (85) (86). Acidification of vacuoles is indispensable for a number of cellular processes including protein sorting and degradation, membrane trafficking, zymogen activation, and also transport of small molecules such as metal ions (87) (88) (89) (90). The organelle serves to detoxify Fe, other toxic metals, and metabolites. Figure 1.2 represents the role of vacuoles in storing, detoxifying and mobilizing cellular transition metals. Defects in any subunit of the yeast V-ATPases (*vma* mutant) result in enzyme dysfunction, which is linked to vacuolar alkalinization and disruption of overall cellular pH homeostasis (91) (92). Loss of V-ATPase activity inhibits the delivery of copper to apo-Fet3p, part of the high-affinity iron transport system (93) (94) (95). Interestingly, *vma2*Δ cells induce an iron deprivation signal, which results

in overaccumulation of intracellular iron despite the activation of Aft1 (96). This is the first evidence bridging pH homeostasis and iron-regulatory pathways, emphasizing the critical role of vacuoles in cellular Fe metabolism.

Vacuoles store Fe in cells grown under Fe-rich conditions. 85% of Fe is transported into the vacuoles via Ccc1, which is mainly controlled by the Yap5-dependent iron regulon (82) (97). *CCC1* transcription is also activated by the low-glucose sensor Snf1 and two stress factors Msn2 and Msn4 (98). The remaining ~15% of vacuolar Fe transport is mediated by End4-dependent endocytosis (82).

Once Fe is imported into the vacuolar lumen, it has been proposed ferric ions coordinated (poly)phosphate due to the oxidizing environment of the vacuole and high abundance of phosphate/polyphosphate (99). At the same time, vacuoles can serve as a reservoir for Fe to help cells survive under Fe-poor conditions (19). When Aft1/2-dependent regulon is active under low iron condition, mRNA-binding proteins Cth1/2 are expressed to degrade *CCC1* mRNA (80). In addition, the metalloreductase Fre6 is also upregulated by Aft1 to reduce Fe^{III} back to Fe^{II}, which is then mobilized to the cytosol via two pathways: the low-affinity transporter Smf3 and the high-affinity transporter Fet5-Fth1 (100) (101) (102). The export mechanism of vacuolar Fe by these 2 systems is similar to the metalloreductase Fre1-mediated Fe uptake pathway on the plasma membrane.

Extensive genetic and biochemical studies on iron-related genes and proteins have mapped out the general scheme of iron acquisition and storage of yeast vacuoles (103) (104). However, the chemical and molecular details of iron trafficking and regulation of vacuolar Fe are not fully understood. For that reason, significant biophysical methods have been utilized to characterize and detect different types of Fe centers within entire yeast cells and isolated organelles. Mössbauer

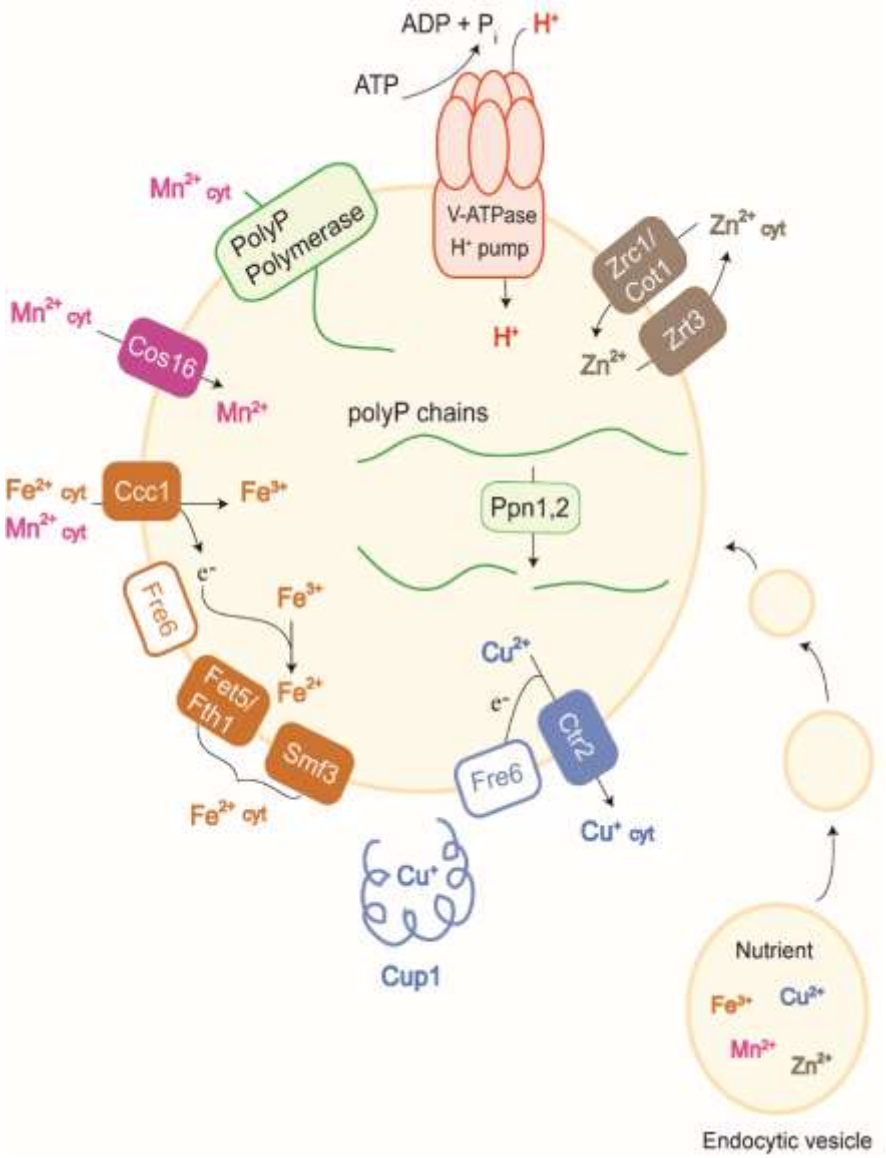

Figure 1.2: **Model of vacuole showing the dynamics of metal ions storage and mobilization** (adapted from references 85, 104, 113, and 144)**.** Nutrient metals also enter the vacuoles via endocytosis. Polyphosphate (polyP) chains are synthesized on the membrane, a Mn-dependent process, and are imported simultaneously. Under static conditions, this is balanced PolyP degradation as catalyzed by phosphatases Ppn1 and Ppn2. Cytosolic Fe^{II} and Mn^{II} ions enter vacuoles via Ccc1 (and Cos16 for Mn), while Zn^{II} ions enter via Zrc1 and Cot1. Nutrient metals also enter vacuoles via End4-dependent endocytosis. Fe^{II} ions become oxidized once they enter the vacuole. Fe^{III} ions are mobilized by Fre6-dependent reduction; the resulting Fe^{II} ions are exported via Fet5/Fth1 and Smf3. Zn^{II} ions are exported via Zrt3 on the vacuolar membrane. Metallothionein Cup1 is a cytosolic protein that stores copper.

spectroscopy is a powerful tool in such analysis. Cockrell *et al.* discovered that vacuolar Fe exists in an equilibrium between a non-heme high spin (NHHS) Fe^{III}-polyphosphate species, which is dominant at pH ~ 5, and supramagnetic Fe^{III}-oxyhydroxo nanoparticles, which are dominant at pH ~ 7 (105). The vacuolar iron Mössbauer spectrum was simulated assuming a magnetically isolated $S = 5/2$ iron with rhombic symmetry. The hyperfine counpling constant A value of -230 kG suggests Fe^{III} is coordinated with hard oxygen donors in octahedral symmetry. The conversion between (NHHS) Fe^{III}-polyphosphate and Fe^{III}-oxyhydroxo nanoparticles is reversible and pH-dependent. However, the number of species and the chemical composition of vacuolar Fe^{III}-polyphosphate complex remains unresolved.

Inorganic polyphosphates (polyP) are linear polymers of orthophosphate residues linked by phosphoanhydride bonds. They are ubiquitous in most subcellular compartments, but primarily accumulate in the vacuoles of yeast cells (106). Phosphate transport and uptake into the vacuoles decrease with increasing pH (107). The yeast polyP polymerase or vacuolar transport chaperone (VTC complexes) on the vacuolar membrane synthesizes polyP from ATP (108). In concert with the synthesis, VTC translocates the growing chain of polyP into the vacuolar lumen to prevent the toxicity of polyP accumulation in the cytosol. This transport is also driven by the vacuolar pH gradient (108). Thus, it is not surprising that *vma2*Δ mutants are defective in polyP synthesis (109). It will be exciting to further investigate whether this is a coincidence or an actual cause-and-effect relationship between the reduced vacuolar polyP concentration and the enhanced level of cellular iron in *vma2*Δ cells.

Once inside the vacuoles, polyP can be hydrolyzed in the middle of the chain by an endopolyphosphatase called Ppn1 (110). Unexpectedly, the final products of Ppn1 are triphosphates and orthophosphates, thus implying that exopolyphosphatase activity can also occur

(111). In 2017, another endopolyphosphatase in the vacuolar lumen was discovered. Ppn2 belongs to the PPP-superfamily of metalloproteases, requiring zinc ions for activity (112). Together, polyP polymerase and phosphatases regulate vacuolar phosphate concentrations and chain length. Stored polyP can be mobilized to the cytosol under phosphate scarcity via the Pho91 transporter (113) (114).

Phosphate and polyphosphate have been suggested to be ligands for Fe^{III} due to their high concentrations in the vacuoles and strong binding constant of polyphosphate with Fe^{III} (106) (115). The bond angles of O-P-O and P-O-P from literature as 132^o, 117^o respectively suggest is that polyP can bind to Fe as a bidentate ligand on the equatorial plane (116) . Rosenfeld and colleagues also showed the effect of phosphate accumulation on cellular metal ion homeostasis (117). All these pieces of evidence provide more insights to further investigate the chemical composition of vacuolar Fe^{III}-polyphosphate species and its regulation.

Cytosolic iron as the Labile Iron Pool (LIP)

Vacuolar Fe almost certainly originates from the cytosol. Many details of cytosolic Fe regulation and trafficking also remains unclear. Park *et al.* discovered that cells grown under adenine-deficient minimal media contain a high concentration of NHHS Fe^{II} (118). Neither mitochondria nor vacuoles isolated from such cells contained this species, suggesting that this NHHS Fe^{II} species are located in the cytosol. The exact ligand environment of cytosolic Fe has not been resolved.

Greenberg, G. R. and Wintrobe, M. M. in 1946 coined the term “labile iron pool” or LIP to describe a pool of non-transferrin bound iron in the blood complexed by LMM organic chelators

with low Fe affinities (119) (120). Labile iron pools in the cytosol have been studied by incubating live intact cells with custom-designed fluorescence-based chelator probes (121). These probes penetrate the cell membrane to bind the iron centers that constitute the LIP. This coordination of metal ions will change the fluorescence properties of the probes so that the concentration of the LIP can be measured from the fluorescence intensity. However, enhancing or quenching of the fluorescence intensity of these probes requires the dissociation of endogenous ligands from the iron center (122). This is a major disadvantage since the native ligand environment dictates important chemical properties of the LIP. Also, nonspecific binding with other metals such as Cu and Zn can occur once the fluorescence probes enter the cells. The required K_D of a fluorescence chelator probe to bind iron in the LIP is unknown. A stronger binding probe might chelate more Fe overestimating the LIP size, while a weaker binding probe will underestimate it (122). Figueroa and colleagues demonstrated the poor specificity and selectivity of small molecule fluorescence dyes that have been extensively used to quantify intracellular Ca^{2+} and Zn^{2+} concentrations (123). Their work indicates that Ca^{2+} and Zn^{2+} binding dyes yield fluorescence responses that are not unique to the recognition of particular labile metals. These dyes also show broad interaction with other metals such as Cu and Fe. This further shows that using fluorescent chelator probes is not the best method to quantify labile metal pools in living cells.

Another common approach to measure cytosolic Fe is using a genetic LacZ reporter of certain cytosolic Fe metalloenzymes such as IRP-1 or the Fe regulon Aft1/2 (100). Kaplan used the cytosolic gentisate 1,2-dioxygenase (GDO) assay to quantify cytosolic Fe concentration based on the following rationale (81). The Fe binding site of GDO is solvent-accessible. Also, GDO has a relatively low affinity for iron since it binds Fe with only 3 His residues (124). GDO activity can

be measured using gentisate as a substrate. Again, this is an indirect method to quantify cytosolic Fe concentration. Thus, the ligand environment of cytosolic Fe species remains unknown.

Hider and Kong have proposed glutathione that is the primary ligand for the cytosolic labile iron species. Based on the affinity constant and high concentration of glutathione (GSH) in the cytosol, they proposed that cytosolic Fe is primarily coordinated to the sulfur ligand of glutathione (125). However, this model is only based on the relative concentration of glutathione and the redox potential in the cytosol. There is no direct experimental evidence for such species in the cytosol. Together, the exact chemical composition of the cytosolic Fe complexes is not well-characterized. To address these deficiencies, we aimed to detect such species in the vacuole and cytosol and characterize their properties.

Copper Trafficking

Iron homeostasis also depends on copper (Cu). Diseases relating to iron deficiency such as ataxia, reduced hematocrit, and mitochondrial malfunction link with decreased intracellular copper (126) (127) (128). Cu is an essential trace element that forms the most stable complexes according to the Irving-William series: $Mn^{II} < Fe^{II} < Co^{II} < Ni^{II} < Cu^{II} > Zn^{II}$ [127]. Due to this property, Cu is tightly regulated to be distributed to appropriate subcellular compartments or proteins for utilization and storage. By this way, free Cu ions are limited to spontaneously bind with solvent-exposed sulfur ligands, thus minimizing protein mismetallation (1). Figure 1.3 represents major trafficking pathways of intracellular copper in *S.cerevisiae* (128) (130) (131).

Nutrient copper in the oxidized form Cu^{II} is transported into the cell via the low-affinity system Fet4p (132). The high affinity transport system of copper requires metalloreductase activity supplied by Fre1, since Ctr proteins are only selective for the reduced form Cu^{I} rather than Cu^{II}

(133) (134). *S.cerevisiae* cells encode two plasma membrane Ctr proteins, Ctr1 and Ctr3. Along with Fre1, Ctr1/3 transporters are induced by the Mac1 transcription factor in response to low copper (135). Ctr1 and Ctr3 possess methionine and cysteine-rich N-terminal domains, respectively, to concentrate Cu^{I} at the transmembrane pore (133) (136) (137) (138). Recent crystal structure reveals Ctr1 adopts a trimeric-ion like architecture, in which the methionine triads serve as selectivity filters for cuprous ions over other divalent metals (139). Cu^{I} is permeated through an enlarged central cavity formed by tilted transmembrane helices TM 1 and 2. The C-terminal tail then acts an intracellular gate for ion passage and transfers Cu to cytosolic Cu chaperones and proteins (139). Ctr2 is another Ctr member in budding yeast, which mediates the shuttling of copper ions from the vacuolar lumen back into the cytosol (140). Copper is thought to be stored as Cu^{II} ions in vacuoles, and then reduced to Cu^{I} by Fre6 prior to export via Ctr2 (141). It is unknown how Cu enters the vacuoles for detoxification (141).

Yeast cells express Cu-buffering proteins and chaperones as another defense mechanism against potential Fenton-like chemistry of free Cu^{I}. All of these proteins are upregulated under high Cu condition by the Ace1 transcription factor (142). Two metallothioneins, Cup1 and Crs5 are abundant in the cytosol to buffer free Cu^{I}. Each metallothionein can bind up to 8 cuprous ions in a trigonal coordination geometry with thiol ligands of cysteine residues (143) (144) (145). The other copper-buffering agent is the copper-zinc superoxide dismutase Sod1, which plays a role in sequestering cytosolic Cu as well as protecting the cells from oxidative stress (146). Cu is delivered to Sod1 via direct protein-protein interaction with the cytosolic chaperone Ccs (147) (148) (149).

A similar strategy of metallochaperone-mediated transport is applied to deliver Cu to the secretory compartment, where Cu is installed into the multicopper oxidase apo-Fet3 of the high affinity iron importer. Thus, Fet3 activity is a useful reporter of copper trafficking to the secretory

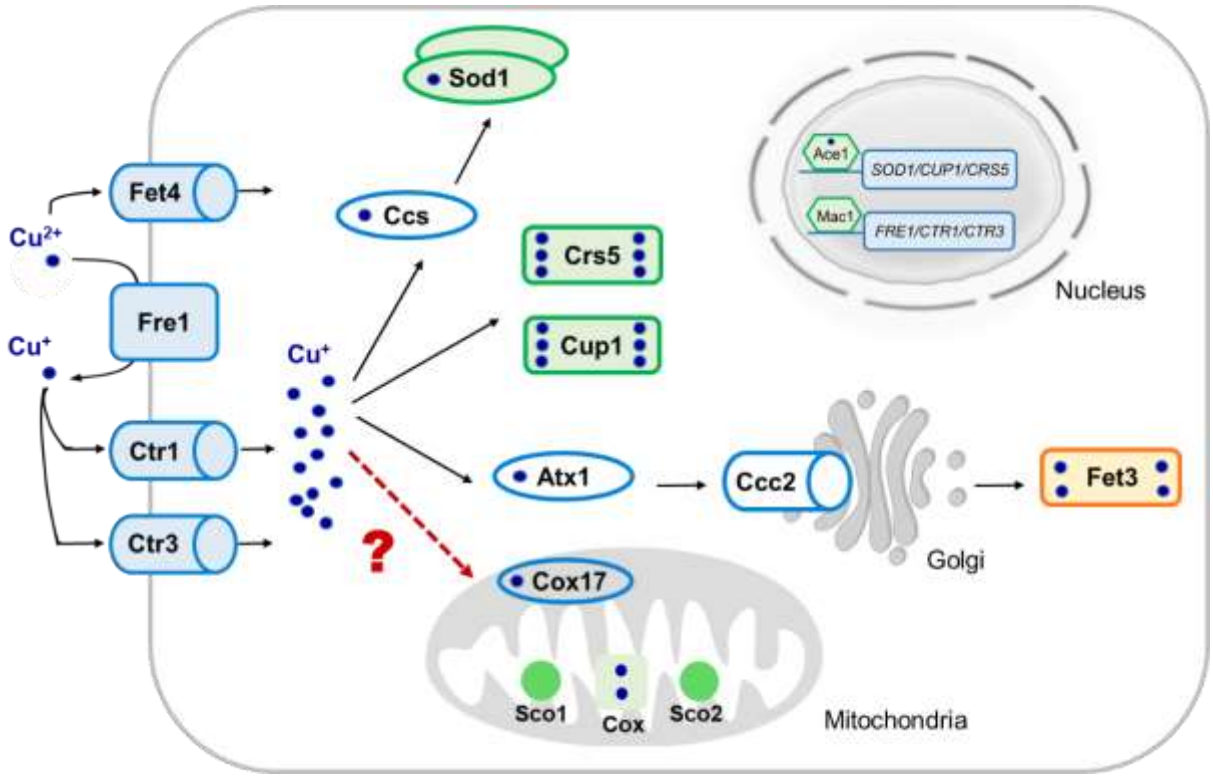

Figure 1.3: Copper trafficking in *Saccharomyces cerevisiae*
(adapted from references 131, 135, and 142**).**

pathway (93) (94) (95). First, an 8kDa chaperone Atx1 binds to cytosolic Cu^{I} and directs it to an integral membrane Cu^{I} -transporting ATPase, Ccc2 (150) (151) (152). This protein is localized in the Golgi apparatus and conserved from bacteria to human (153). Deletion of *CCC2* gene negatively impacts Fet3 activity, leading to iron deficiency (93) (154). In addition to Ccc2, loading of Cu onto apo-Fet3 requires 2 other factors. One of them is the acidification of post-Golgi vesicles. This process depends on a functional V-ATPase/H^{+} pump as well as a CLC chloride (Cl^{-}) channel Gef1 localized in the post-Golgi compartment (94) (155). Gef1 generates an influx of Cl^{-} anions to counterbalance the accumulation of protons as a result of acidification (155). Cl^{-} ions may function as an allosteric effector for copper insertion into apo-Fet3 (156). The binding of Cu^{I} to Fet3 is also shown to be promoted by potassium ions. Thus, Kha1 as a K^{+}/H^{+} transporter is necessary for the compartmentalization of K^{+} in the *trans*-Golgi network to enable proper copper metalation of Fet3 (157).

In contrast with the secretory compartment, the Cu trafficking mechanism to the mitochondria is not well characterized. Mitochondria are the "power house" of the cells where cytochrome *c* oxidase (COX) or complex IV of the respiratory chain localizes. COX catalyzes the reduction of oxygen to water coupling with proton translocating activity (158). It requires 3 copper atoms and 2 heme groups for function (159). Defects in COX protein assembly or copper metalation result in mitochondrial diseases in humans such as hypertrophic cardiomyopathy (160) (161). Mrs3/4 and Rim2 can transport copper into the mitochondria in addition to iron (55) (57). Whether this is the primary trafficking pathway of Cu to this organelle is elusive. Cobine proposes the majority of mitochondrial copper is non-proteinaceous, low molecular weight and kinetically labile. This pool is called Cu-L which displays anionic properties and resists to protein digestion (162). They suggest that Cu-L enters via Pic2 into the mitochondrial matrix as a feedstock for

metalation of COX (163). Fluorescent-chelator probes have also been utilized to detect this labile pool of copper, but failed to give any information about its concentration or its identity (164). The chemical nature of Cu-L still remains mysterious after 15 years of discovery.

Zinc Trafficking

Approximately 9% of metalloenzymes in *S.cerevisiae* contain zinc (Zn) as cofactors (165). Zap1 is the main transcription factor regulating the expression of many genes that involve in homeostatic and adaptive responses to zinc deficiency (166). Two Zn^{II}-specific transporters, Zrt1 and Zrt2, are controlled by Zap1 (167) (168). Fet4 and Pho84 are the low-affinity Zn transporters. Expression of *PHO84* does not depend on zinc status, but Fet4 is induced under zinc limiting conditions (166). Once zinc is transported into the cells, over half of the metal is located in vacuoles (169). Zinc is imported into these organelles by Zrc1 and Cot1 transporters on the vacuolar membrane, and exported through Zrt3 (170) (171) (172) (173). In Zn-deficient cells, Zrt3 expression increases while Cot1 is degraded. In zinc-replete cells, Zrt3 is degraded (171) (174). Besides storing and sequestering zinc, vacuoles help regulate a zinc-dependent alkaline phosphatase (Pho8) located in the organelle (175). Pho8 is metallated and activated by Zn ions in the vacuole (176). The metallated Pho8 catalyzes the hydrolysis of phosphate from various phosphorylated substrates to facilitate the recycling of monophosphates (177).

Manganese Trafficking

Manganese is well-known to play a crucial role in oxidative stress protection. Much interest focuses on the manganese-containing superoxide dismutase Sod2 in the mitochondria. Under high Mn^{II} conditions, two Nramp proteins, Smf1p and Smf2p transporters are degraded in the vacuoles.

When Mn^{II} levels are low, these proteins localize to the plasma membrane (43) (101) (178). It is unclear how cells sense intracellular Mn^{II} concentrations to control and mobilize this protein localization. One of the main pathways of intracellular manganese trafficking is the Golgi apparatus. This compartment acquires manganese via Pmr1, a P-type Ca^{II} and Mn^{II} –transporting ATPase (179). Manganese and calcium are transported by Pmr1 are essential for proper trafficking of polypeptides entering the secretory pathway (180) (181) (182). Manganese ions also traffic to vacuoles via both Ccc1 and Cos16/ Per1 transporters (183) (184). Mutations in either protein render cells sensitive to nutrient manganese, probably because high cytosolic manganese levels are intoxicating (185) . Yeast cells respond to manganese toxicity by increasing the rate of polyP synthesis and by decreasing polyphosphatase activities ; both responses serve to increase the average length of polyP chains (186) (187). This diminishes toxicity, perhaps by increasing the capacity for manganese to coordinate to polyP chains in the vacuole (187). Whole-cell ENDOR spectra indicate that manganese is coordinated to both orthophosphate and polyP in WT yeast cells (188). However, the cellular location of such complexes within the cell was not established.

Objectives

This dissertation aims to detect, isolate, and characterize the Low-Molecular-Mass (LMM) metal complexes (primarily Fe) from vacuoles and the cytosol of *S. cerevisiae*. Fe species in these two subcellular compartments are proposed to be weakly-coordinated LMM complexes with a molecular mass less than 10 kDa, The lability of these complexes allows the cells to easily access and direct Fe to the appropriate subcellular compartments for utilization. Moreover, LMM complexes are responsive to different intracellular Fe “quota”, and can potentially be used as an internal Fe sensor. The liquid chromatography (LC) size exclusion column interfaced with an

online inductively coupled plasma mass spectrometer (ICP-MS) was the primary biophysical tool used in this study. This setup allowed the LMM complexes of interest to be separated intact based on size and their chemical nature to be characterized further with other methods. Moreover, ICP-MS is an analytical technique with a detection limit of 1 part per billion (10^6), permitting precise quantification of low metal concentrations in biological samples.

The general scheme of experimental approach for this dissertation is illustrated in Scheme 1.1. The first step was to isolate the vacuolar and cytosol fractions from whole cells of yeasts. After that, the LMM complexes of each of these subcellular fractions were collected as a flow through solution of a 10 kDa nitrocellulose membrane cutoff in an amicon stirred cell. This flow through solution was run through the LC-ICP-MS. A portion of the LC eluent was split to the ICP-MS for detection of different Fe species. The area, eluent volume, and linewidth of all ICP-MS peaks were quantified. The column was calibrated such that apparent molecular masses could be determined from eluent volumes of standards. The detector response was calibrated to estimate the concentrations of each observed species.

Iron chromatograms are our main focus. However, we are also interested in analyzing data of other biologically-relevant metals including Cu, Zn, Mn and nonmetals such as S, P since collecting these extra datasets requires little additional effort. This helps us understand better the interplay between the trafficking pathways of different trace metals in living cells. This experimental approach using the LC-ICP-MS system set up the basis to investigate the trafficking mechanism of metal ions on the molecular level from the cytosol to two major organelles: the mitochondria and the vacuoles.

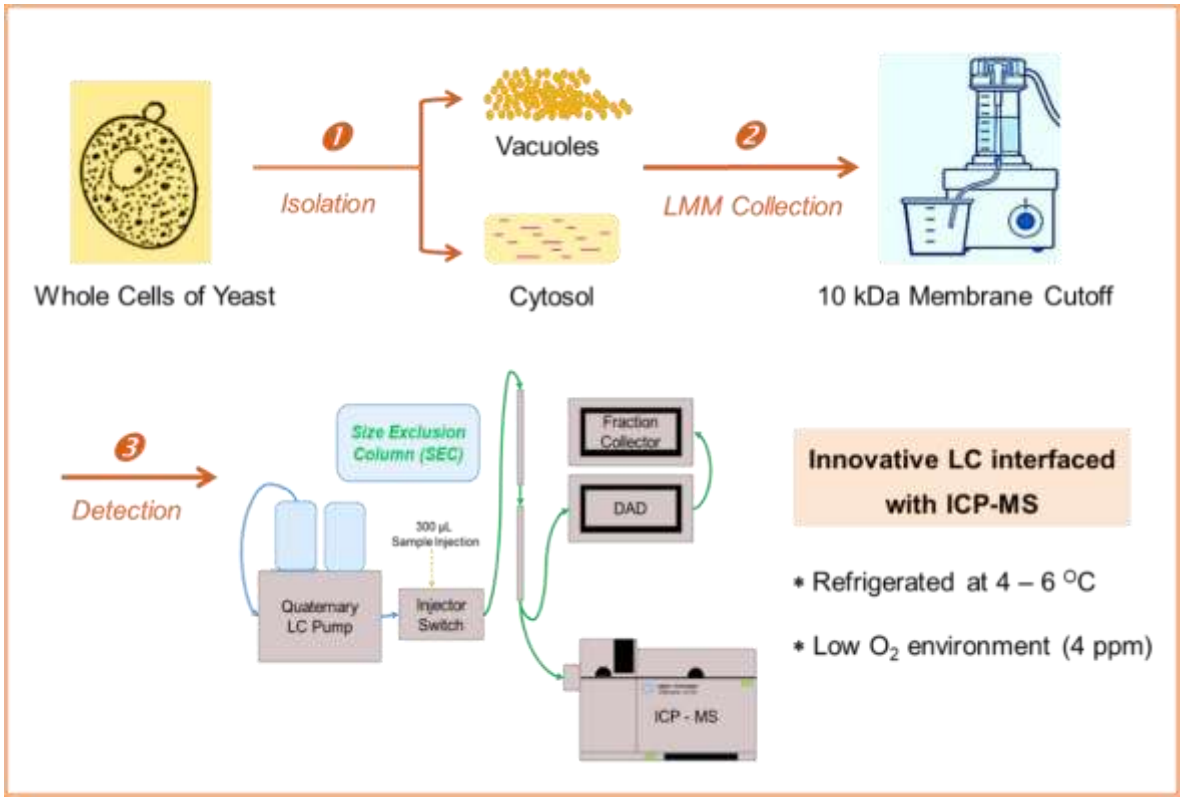

Scheme 1.1: General scheme of experimental approach

References

1. Palmer, A. E., and Franz, K. J. (2009) Introduction to cellular metal homeostasis and trafficking. *Chem. Rev.* **109**, 4533–4535
2. Cyert, M. S., and Philpott, C. C. (2013) Regulation of cation balance in *Saccharomyces cerevisiae*. *Genetics*. **193**, 677–713
3. Maret, W. (2016) The metals in the biological periodic system of the elements: Concepts and conjectures. *Int. J. Mol. Sci.* **17**, 1–8
4. Campos-Bermudez, V. A., Leite, N. R., Krog, R., Costa-Filho, A. J., Soncini, F. C., Oliva, G., and Vila, A. J. (2007) Biochemical and structural characterization of *Salmonella typhimurium* glyoxalase II: New insights into metal ion selectivity. *Biochemistry*. **46**, 11069–11079
5. Dudev, T., and Lim, C. (2008) Metal binding affinity and selectivity in metalloproteins: insights from computational studies. *Annu. Rev. Biophys.* **37**, 97–116
6. Dudev, T., and Lim, C. (2014) Competition among metal ions for protein binding sites: Determinants of metal ion selectivity in proteins. *Chem. Rev.* **114**, 538–556
7. Gilston, B. A., and O'Halloran, T. V. (2004) Metals in cells: Control of cellular metal concentration. *Encycl. Inorg. Bioinorg. Chem.* 10.1002/9781119951438.eibc2107
8. Finney, L. A. (2003) Transition metal speciation in the cell: insights from the chemistry of metal ion receptors. *Science.* **300**, 931–936
9. Foster, A. W., Osman, D., and Robinson, N. J. (2014) Metal preferences and metallation. *J. Biol. Chem.* **289**, 28095–28103
10. Philpott, C. C., Leidgens, S., and Frey, A. G. (2012) Metabolic remodeling in iron-deficient fungi. *Biochim. Biophys. Acta - Mol. Cell Res.* **1823**, 1509–1520

11. Kosman, D. J. (2013) Iron metabolism in aerobes: Managing ferric iron hydrolysis and ferrous iron autoxidation. *Coord. Chem. Rev.* **257**, 210–217

12. Anderson, G. J., Dancis, A., Roman, D. G., Klausner, R. D., Lesuisse, E., and Labbe, P. (1992) Ferric iron reduction and iron assimilation in *Saccharomyces cerevisiae*. *J. Inorg. Biochem.* **47**, 249–255

13. Klausner, R. D., and Dancis, A. (1994) A genetic approach to elucidating eukaryotic iron metabolism. *FEBS Lett.* **355**, 109–113

14. Cairo, G., Bernuzzi, F., and Recalcati, S. (2006) A precious metal: Iron, an essential nutrient for all cells. *Genes Nutr.* **1**, 25–39

15. Halliwell, B., and Gutteridge, J. M. C. (1986) Oxygen free radicals and iron in relation to biology and medicine: Some problems and concepts. *Arch. Biochem. Biophys.* **246**, 501–514

16. Dixon, S. J., and Stockwell, B. R. (2014) The role of iron and reactive oxygen species in cell death. *Nat. Chem. Biol.* **10**, 9–17

17. Kell, D. B. (2009) Iron behaving badly: inappropriate iron chelation as a major contributor to the aetiology of vascular and other progressive inflammatory and degenerative diseases. *BMC Med. Genomics*. **2**, 2

18. Torti, S. V., and Torti, F. M. (2013) Iron and cancer: More ore to be mined. *Nat. Rev. Cancer*. **13**, 342–355

19. Kosman, D. J. (2003) Molecular mechanisms of iron uptake in fungi. *Mol. Microbiol.* **47**, 1185–1197

20. Pesterfield, L. L. (2001) Ions in solution - Basic principles of chemical interaction, 2nd edition. *J. Chem. Educ.* **78**, 456

21. Lesuisse, E., Raguzzi, F., and Crichton, R. R. (1987) Iron uptake by the yeast *Saccharomyces cerevisiae*: involvement of a reduction step. *Microbiology*. **133**, 3229–3236

22. Griffin, D. H., Winkelmann, G., and Winge, D. R. (1995) Metal ions in fungi. *Mycologia*. **87**, 425

23. Muller, G., Matzanke, B. F., and Raymond, K. N. (1984) Iron transport in *Streptomyces pilosus* mediated by ferrichrome siderophores, rhodotorulic acid, and enantio-rhodotorulic acid. *J. Bacteriol.* **160**, 313–318

24. Byers, B. R., and Arceneaux, J. E. (1998) Microbial iron transport: iron acquisition by pathogenic microorganisms. *Met. Ions Biol. Syst.* **35**, 37–66

25. Neilands, J. B. (1995) Siderophores: Structure and function of microbial iron transport compounds. *J. Biol. Chem.* **270**, 26723–26726

26. Yun, C. W., Bauler, M., Moore, R. E., Klebba, P. E., and Philpott, C. C. (2001) The role of the Fre family of plasma membrane reductases in the uptake of siderophore-iron in *Saccharomyces cerevisiae*. *J. Biol. Chem.* **276**, 10218–10223

27. Moore, R. E., Kim, Y., and Philpott, C. C. (2003) The mechanism of ferrichrome transport through Arn1p and its metabolism in *Saccharomyces cerevisiae*. *Proc. Natl. Acad. Sci.* **100**, 5664–5669

28. Protchenko, O., Ferea, T., Rashford, J., Tiedeman, J., Brown, P. O., Botstein, D., and Philpott, C. C. (2001) Three cell wall mannoproteins facilitate the uptake of iron in *Saccharomyces cerevisiae*. *J. Biol. Chem.* **276**, 49244–49250

29. Wofford, J. D., Park, J., McCormick, S. P., Chakrabarti, M., and Lindahl, P. A. (2016) Ferric ions accumulate in the walls of metabolically inactivating *Saccharomyces cerevisiae* cells and are reductively mobilized during reactivation. *Metallomics*. **8**, 692–708

30. Outten, C. E., and Albetel, A.-N. (2013) Iron sensing and regulation in *Saccharomyces cerevisiae*: Ironing out the mechanistic details. *Curr. Opin. Microbiol.* **16**, 662–668

31. Martins, L. J., Jensen, L. T., Simons, J. R., Keller, G. L., and Winge, D. R. (1998) Metalloregulation of *FRE1* and *FRE2* homologs in *Saccharomyces cerevisiae*. *J. Biol. Chem.* **273**, 23716–23721

32. Lesuisse, E., Casteras-Simon, M., and Labbe, P. (1996) Evidence for the *Saccharomyces cerevisiae* ferrireductase system being a multicomponent electron transport chain. *J. Biol. Chem.* **271**, 13578–13583

33. De Silva, D. M., Askwith, C. C., Eide, D., and Kaplan, J. (1995) The *FET3* gene product required for high affinity iron transport in yeast is a cell surface ferroxidase. *J. Biol. Chem.* **270**, 1098–1101

34. Hassett, R. F., Romeo, A. M., and Kosman, D. J. (1998) Regulation of high affinity iron uptake in the yeast *Saccharomyces cerevisiae*: Role of dioxygen and Fe(II). *J. Biol. Chem.* **273**, 7628–7636

35. Stearman, R., Yuan, D. S., Yamaguchi-Iwai, Y., Klausner, R. D., and Dancis, A. (1996) A permease-oxidase complex involved in high-affinity iron uptake in yeast. *Science.* **271**, 1552–1557

36. Felice, M. R., De Domenico, I., Li, L., Ward, D. M. V., Bartok, B., Musci, G., and Kaplan, J. (2005) Post-transcriptional regulation of the yeast high affinity iron transport system. *J. Biol. Chem.* **280**, 22181–22190

37. Williams, D., Lee, G., and Cartwright, G. (1974) Ferroxidase activity of rat ceruloplasmin. *Am. J. Physiol. Content*. **227**, 1094–1097

38. Askwith, C., Eide, D., Van Ho, A., Bernard, P. S., Li, L., Davis-Kaplan, S., Sipe, D. M.,

and Kaplan, J. (1994) The *FET3* gene of *S. cerevisiae* encodes a multicopper oxidase required for ferrous iron uptake. *Cell*. **76**, 403–410

39. Dix, D. R., Bridgham, J. T., Broderius, M. A., Byersdorfer, C. A., and Eide, D. J. (1994) The *FET4* gene encodes the low affinity Fe(II) transport protein of *Saccharomyces cerevisiae*. *J. Biol. Chem.* **269**, 26092–26099

40. Waters, B. M., and Eide, D. J. (2002) Combinatorial control of yeast *FET4* gene expression by iron, zinc, and oxygen. *J. Biol. Chem.* **277**, 33749–33757

41. Li, L., and Kaplan, J. (1998) Defects in the yeast high affinity iron transport system result in increased metal sensitivity because of the increased expression of transporters with a broad transition metal specificity. *J. Biol. Chem.* **273**, 22181–22187

42. Jensen, L. T., and Culotta, V. C. (2002) Regulation of *Saccharomyces cerevisiae FET4* by oxygen and iron. *J. Mol. Biol.* **318**, 251–260

43. Portnoy, M. E., Jensen, L. T., and Culotta, V. C. (2002) The distinct methods by which manganese and iron regulate the Nramp transporters in yeast. *Biochem. J.* **362**, 119–124

44. Chen, X. Z., Peng, J. Bin, Cohen, A., Nelson, H., Nelson, N., and Hediger, M. A. (1999) Yeast Smf1 mediates H^+-coupled iron uptake with concomitant uncoupled cation currents. *J. Biol. Chem.* **274**, 35089–35094

45. Lill, R., and Kispal, G. (2000) Maturation of cellular Fe–S proteins: an essential function of mitochondria. *Trends Biochem. Sci.* **25**, 352–356

46. Ajioka, R. S., Phillips, J. D., and Kushner, J. P. (2006) Biosynthesis of heme in mammals. *Biochim. Biophys. Acta - Mol. Cell Res.* **1763**, 723–736

47. Wiesenberger, G., Link, T. A., von Ahsen, U., Waldherr, M., and Schweyen, R. J. (1991) *MRS3* and *MRS4*, two suppressors of mtRNA splicing defects in yeast, are new members

of the mitochondrial carrier family. *J. Mol. Biol.* **217**, 23–37

48. Foury, F., and Roganti, T. (2002) Deletion of the mitochondrial carrier genes *MRS3* and *MRS4* suppresses mitochondrial iron accumulation in a yeast frataxin-deficient strain. *J. Biol. Chem.* **277**, 24475–24483

49. Mühlenhoff, U., Stadler, J. A., Richhardt, N., Seubert, A., Eickhorst, T., Schweyen, R. J., Lill, R., and Wiesenberger, G. (2003) A specific role of the yeast mitochondrial carriers Mrs3/4p in mitochondrial iron acquisition under iron-limiting conditions. *J. Biol. Chem.* **278**, 40612–40620

50. Moore, M. J., Wofford, J. D., Dancis, A., and Lindahl, P. A. (2018) Recovery of *mrs3Δmrs4Δ Saccharomyces cerevisiae* cells under iron-sufficient conditions and the role of Fe_{580}. *Biochemistry*. **57**, 672–683

51. Démolis, N., Mallet, L., Bussereau, F., and Jacquet, M. (1993) *RIM2*, *MSI1* and *PGI1* and located within an 8 kb segment of *Saccharomyces cerevisiae* chromosome II, which also contains the putative ribosomal gene L21 and a new putative essential gene with a leucine zipper motif. *Yeast*. **9**, 645–659

52. Van Dyck, E., Jank, B., Ragnini, A., Schweyen, R. J., Duyckaerts, C., Sluse, F., and Foury, F. (1995) Overexpression of a novel member of the mitochondrial carrier family rescues defects in both DNA and RNA metabolism in yeast mitochondria. *Mol. Gen. Genet. MGG*. **246**, 426–436

53. Marobbio, C. M. T., Di Noia, M. A., and Palmieri, F. (2006) Identification of a mitochondrial transporter for pyrimidine nucleotides in *Saccharomyces cerevisiae*: Bacterial expression, reconstitution and functional characterization. *Biochem. J.* **393**, 441–446

54. Yoon, H., Zhang, Y., Pain, J., Lyver, E. R., Lesuisse, E., Pain, D., and Dancis, A. (2011) Rim2, a pyrimidine nucleotide exchanger, is needed for iron utilization in mitochondria. *Biochem. J.* **440**, 137–146

55. Froschauer, E. M., Rietzschel, N., Hassler, M. R., Binder, M., Schweyen, R. J., Lill, R., Uhlenhoff, U. M., and Wiesenberger, G. (2013) The mitochondrial carrier Rim2 co-imports pyrimidine nucleotides and iron. *Biochem. J.* **455**, 57–65

56. Knight, S. A. B., Yoon, H., Pandey, A. K., Pain, J., Pain, D., and Dancis, A. (2019) Splitting the functions of Rim2, a mitochondrial iron/pyrimidine carrier. *Mitochondrion*. **47**, 256–265

57. Froschauer, E. M., Schweyen, R. J., and Wiesenberger, G. (2009) The yeast mitochondrial carrier proteins Mrs3p/Mrs4p mediate iron transport across the inner mitochondrial membrane. *Biochim. Biophys. Acta - Biomembr.* **1788**, 1044–1050

58. Robinson, A. J., and Kunji, E. R. S. (2006) Mitochondrial carriers in the cytoplasmic state have a common substrate binding site. *Proc. Natl. Acad. Sci. U. S. A.* **103**, 2617–22

59. Brazzolotto, X., Pierrel, F., and Pelosi, L. (2014) Three conserved histidine residues contribute to mitochondrial iron transport through mitoferrins. *Biochem. J.* **460**, 79–89

60. Lindahl, P. A., and Moore, M. J. (2016) Labile low-molecular-mass metal complexes in mitochondria: trials and tribulations of a burgeoning field. *Biochemistry*. **55**, 4140–4153

61. McCormick, S. P., Moore, M. J., and Lindahl, P. A. (2015) Detection of labile low-molecular-mass transition metal complexes in mitochondria. *Biochemistry*. **54**, 3442–3453

62. Holmes-Hampton, G. P., Miao, R., Garber Morales, J., Guo, Y., Münck, E., and Lindahl, P. A. (2010) A nonheme high-spin ferrous pool in mitochondria isolated from fermenting *Saccharomyces cerevisiae*. *Biochemistry*. **49**, 4227–4234

63. Pandey, A., Pain, J., Ghosh, A. K., Dancis, A., and Pain, D. (2015) Fe-S cluster biogenesis in isolated mammalian mitochondria: Coordinated use of persulfide sulfur and iron and requirements for GTP, NADH, and ATP. *J. Biol. Chem.* **290**, 640–657

64. Kispal, G., Csere, P., Guiard, B., and Lill, R. (1997) The ABC transporter Atm1p is required for mitochondrial iron homeostasis. *FEBS Lett.* **418**, 346–50

65. Srinivasan, V., Pierik, A. J., and Lill, R. (2014) Crystal structures of nucleotide-free and glutathione-bound mitochondrial ABC transporter Atm1. *Science.* **343**, 1137–1140

66. Schaedler, T. A., Thornton, J. D., Kruse, I., Schwarzländer, M., Meyer, A. J., van Veen, H. W., and Balk, J. (2014) A conserved mitochondrial ATP-binding cassette transporter exports glutathione polysulfide for cytosolic metal cofactor assembly. *J. Biol. Chem.* **289**, 23264–74

67. Li, J., and Cowan, J. A. (2015) Glutathione-coordinated [2Fe-2S] cluster: a viable physiological substrate for mitochondrial ABCB7 transport. *Chem. Commun. (Camb).* **51**, 2253–5

68. Pandey, A., Pain, J., Dziuba, N., Pandey, A. K., Dancis, A., and Lindahl, P. A. (2018) Mitochondria export sulfur species required for cytosolic tRNA thiolation. *Cell Chem. Biol.* **25**, 738–748

69. Pandey, A. K., Pain, J., Dancis, A., and Pain, D. (2019) Mitochondria export iron-sulfur and sulfur intermediates to the cytoplasm for iron-sulfur cluster assembly and tRNA thiolation in yeast. *J. Biol. Chem.* **294**, 9489–9502

70. Lill, R., Dutkiewicz, R., Freibert, S. A., Heidenreich, T., Mascarenhas, J., Netz, D. J., Paul, V. D., Pierik, A. J., Richter, N., Stümpfig, M., Srinivasan, V., Stehling, O., and Mühlenhoff, U. (2015) The role of mitochondria and the CIA machinery in the maturation of cytosolic

and nuclear iron–sulfur proteins. *Eur. J. Cell Biol.* **94**, 280–291

71. Rutherford, J. C., Ojeda, L., Balk, J., Mühlenhoff, U., Lill, R., and Winge, D. R. (2005) Activation of the iron regulon by the yeast Aft1/Aft2 transcription factors depends on mitochondrial but not cytosolic iron-sulfur protein biogenesis. *J. Biol. Chem.* **280**, 10135–10140

72. Li, L., Miao, R., Bertram, S., Jia, X., Ward, D. M., and Kaplan, J. (2012) A role for iron-sulfur clusters in the regulation of transcription factor Yap5-dependent high iron transcriptional responses in yeast. *J. Biol. Chem.* **287**, 35709–35721

73. Yamaguchi-Iwai, Y., Ueta, R., Fukunaka, A., and Sasaki, R. (2002) Subcellular localization of Aft1 transcription factor responds to iron status in *Saccharomyces cerevisiae*. *J. Biol. Chem.* **277**, 18914–18918

74. Martínez-Pastor, M. T., Perea-García, A., and Puig, S. (2017) Mechanisms of iron sensing and regulation in the yeast *Saccharomyces cerevisiae*. *World J. Microbiol. Biotechnol.* **33**, 75

75. Dlouhy, A. C., and Outten, C. E. (2013) The iron metallome in eukaryotic organisms. in *Met. Ions in Life Sci.* **12**, 241–278

76. Philpott, C. C., and Protchenko, O. (2008) Response to iron deprivation in *Saccharomyces cerevisiae*. *Eukaryot. Cell*. **7**, 20–27

77. Ueta, R., Fujiwara, N., Iwai, K., and Yamaguchi-Iwai, Y. (2007) Mechanism underlying the iron-dependent nuclear export of the iron-responsive transcription factor Aft1p in *Saccharomyces cerevisiae*. *Mol. Biol. Cell*. **18**, 2980–2990

78. Kumánovics, A., Chen, O. S., Li, L., Bagley, D., Adkins, E. M., Lin, H., Dingra, N. N., Outten, C. E., Keller, G., Winge, D., Ward, D. M., and Kaplan, J. (2008) Identification of

FRA1 and *FRA2* as genes involved in regulating the yeast iron regulon in response to decreased mitochondrial iron-sulfur cluster synthesis. *J. Biol. Chem.* **283**, 10276–10286

79. Poor, C. B., Wegner, S. V., Li, H., Dlouhy, A. C., Schuermann, J. P., Sanishvili, R., Hinshaw, J. R., Riggs-Gelasco, P. J., Outten, C. E., and He, C. (2014) Molecular mechanism and structure of the S*accharomyces cerevisiae* iron regulator Aft2. *Proc. Natl. Acad. Sci.* **111**, 4043–4048

80. Li, L., Bagley, D., Ward, D. M., and Kaplan, J. (2008) Yap5 Is an iron-responsive transcriptional activator that regulates vacuolar iron storage in yeast. *Mol. Cell. Biol.* **28**, 1326–1337

81. Li, L., Jia, X., Ward, D. M., and Kaplan, J. (2011) Yap5 protein-regulated transcription of the *TYW1* gene protects yeast from high iron toxicity. *J. Biol. Chem.* **286**, 38488–38497

82. Li, L., Chen, O. S., Ward, D. M. V., and Kaplan, J. (2001) Ccc1 is a transporter that mediates vacuolar iron storage in yeast. *J. Biol. Chem.* **276**, 29515–29519

83. Li, S. C., and Kane, P. M. (2009) The yeast lysosome-like vacuole: Endpoint and crossroads. *Biochim. Biophys. Acta - Mol. Cell Res.* **1793**, 650–663

84. Yamashiro, C. T., Kane, P. M., Wolczyk, D. F., Preston, R. A., and Stevens, T. H. (1990) Role of vacuolar acidification in protein sorting and zymogen activation: a genetic analysis of the yeast vacuolar proton-translocating ATPase. *Mol. Cell. Biol.* **10**, 3737–3749

85. Kane, P. M., and Stevens, T. H. (1992) Subunit composition, biosynthesis, and assembly of the yeast vacuolar proton-translocating ATPase. *J. Bioenerg. Biomembr.* **24**, 383–393

86. Anraku, Y., Umemoto, N., Hirata, R., and Ohya, Y. (1992) Genetic and cell biological aspects of the yeast vacuolar H^+-ATPase. *J. Bioenerg. Biomembr.* **24**, 395–405

87. Forgac, M. (1989) Structure and function of vacuolar class of ATP-driven proton pumps.

Physiol. Rev. **69**, 765–796

88. Recchi, C., and Chavrier, P. (2006) V-ATPase: a potential pH sensor. *Nat. Cell Biol.* **8**, 107–109

89. Beyenbach, K. W. (2006) The V-type H^+ ATPase: molecular structure and function, physiological roles and regulation. *J. Exp. Biol.* **209**, 577–589

90. Forgac, M. (2007) Vacuolar ATPases: rotary proton pumps in physiology and pathophysiology. *Nat. Rev. Mol. Cell Biol.* **8**, 917–929

91. Martínez-Muñoz, G. A., and Kane, P. (2008) Vacuolar and plasma membrane proton pumps collaborate to achieve cytosolic pH homeostasis in yeast. *J. Biol. Chem.* **283**, 20309–20319

92. Au-Yeung, H. Y., Chan, J., Chantarojsiri, T., and Chang, C. J. (2013) Molecular imaging of labile iron(II) pools in living cells with a turn-on fluorescent probe. *J. Am. Chem. Soc.* **135**, 15165–15173

93. Yuan, D. S., Stearman, R., Dancis, A., Dunn, T., Beeler, T., and Klausner, R. D. (1995) The Menkes/Wilson disease gene homologue in yeast provides copper to a ceruloplasmin-like oxidase required for iron uptake. *Proc. Natl. Acad. Sci.* **92**, 2632–2636

94. Radisky, D. C., Snyder, W. B., Emr, S. D., and Kaplan, J. (1997) Characterization of *VPS41*, a gene required for vacuolar trafficking and high-affinity iron transport in yeast. *Proc. Natl. Acad. Sci.* **94**, 5662–5666

95. Yuan, D. S., Dancis, A., and Klausner, R. D. (1997) Restriction of copper export in *Saccharomyces cerevisiae* to a late Golgi or post-Golgi compartment in the secretory pathway. *J. Biol. Chem.* **272**, 25787–25793

96. Diab, H. I., and Kane, P. M. (2013) Loss of vacuolar H^+-ATPase (V-ATPase) activity in yeast generates an iron deprivation signal that is moderated by induction of the

peroxiredoxin *TSA2*. *J. Biol. Chem.* **288**, 11366–11377

97. Pimentel, C., Vicente, C., Menezes, R. A., Caetano, S., Carreto, L., and Rodrigues-Pousada, C. (2012) The Role of the Yap5 transcription factor in remodeling gene expression in response to Fe bioavailability. *PLoS One*. **7**, 1–11

98. Li, L., Kaplan, J., and Ward, D. M. (2017) The glucose sensor Snf1 and the transcription factors Msn2 and Msn4 regulate transcription of the vacuolar iron importer gene *CCC1* and iron resistance in yeast. *J. Biol. Chem.* **292**, 15577–15586

99. Raguzzi, F., Lesuisse, E., and Crichton, R. R. (1988) Iron storage in *Saccharomyces cerevisiae*. *FEBS Lett.* **231**, 253–258

100. Singh, A., Kaur, N., and Kosman, D. J. (2007) The metalloreductase Fre6p in Fe-efflux from the yeast vacuole. *J. Biol. Chem.* **282**, 28619–28626

101. Portnoy, M. E., Liu, X. F., and Culotta, V. C. (2000) *Saccharomyces cerevisiae* expresses three functionally distinct homologues of the Nramp family of metal transporters. *Mol. Cell. Biol.* **20**, 7893–7902

102. Urbanowski, J. L., and Piper, R. C. (1999) The iron transporter Fth1p forms a complex with the Fet5 iron oxidase and resides on the vacuolar membrane. *J. Biol. Chem.* **274**, 38061–38070

103. Bode, H. P., Dumschat, M., Garotti, S., and Fuhrmann, G. F. (1995) Iron sequestration by the yeast vacuole: a study with vacuolar mutants of *Saccharomyces cerevisiae*. *Eur. J. Biochem.* **228**, 337–342

104. Blaby-Haas, C. E., and Merchant, S. S. (2014) Lysosome-related organelles as mediators of metal homeostasis. *J. Biol. Chem.* **289**, 28129–28136

105. Cockrell, A. L., Holmes-Hampton, G. P., McCormick, S. P., Chakrabarti, M., and Lindahl,

P. A. (2011) Mössbauer and EPR study of iron in vacuoles from fermenting *Saccharomyces cerevisiae*. *Biochemistry*. **50**, 10275–10283

106. Urech, K., Dürr, M., Boller, T., Wiemken, A., and Schwencke, J. (1978) Localization of polyphosphate in vacuoles of *Saccharomyces cerevisiae*. *Arch. Microbiol.* **116**, 275–278
107. Booth, J. W., and Guidotti, G. (1997) Phosphate transport in yeast vacuoles. *J. Biol. Chem.* **272**, 20408–20413
108. Gerasimaite, R., Sharma, S., Desfougeres, Y., Schmidt, A., and Mayer, A. (2014) Coupled synthesis and translocation restrains polyphosphate to acidocalcisome-like vacuoles and prevents its toxicity. *J. Cell Sci.* **127**, 5093–5104
109. Tomaschevsky, A. A., Ryasanova, L. P., Kulakovskaya, T. V., and Kulaev, I. S. (2010) Inorganic polyphosphate in the yeast *Saccharomyces cerevisiae* with a mutation disturbing the function of vacuolar ATPase. *Biochem.* **75**, 1052–1054
110. Sethuraman, A., Rao, N. N., and Kornberg, A. (2001) The endopolyphosphatase gene: essential in *Saccharomyces cerevisiae*. *Proc. Natl. Acad. Sci. U. S. A.* **98**, 8542–8547
111. Lichko, L., Kulakovskaya, T., and Kulaev, I. (2004) Inactivation of endopolyphosphatase gene *PPN1* results in inhibition of expression of exopolyphosphatase *PPX1* and high-molecular-mass exopolyphosphatase not encoded by *PPX1* in *Saccharomyces cerevisiae*. *Biochim. Biophys. Acta - Gen. Subj.* **1674**, 98–102
112. Gerasimaitė, R., and Mayer, A. (2017) Ppn2, a novel Zn^{2+}-dependent polyphosphatase in the acidocalcisome-like yeast vacuole. *J. Cell Sci.* **130**, 1625–1636
113. Gerasimaite, R., and Mayer, A. (2016) Enzymes of yeast polyphosphate metabolism: Structure, enzymology and biological roles. *Biochem. Soc. Trans.* **44**, 234–239
114. Hürlimann, H. C., Stadler-Waibel, M., Werner, T. P., and Freimoser, F. M. (2007) Pho91

is a vacuolar phosphate transporter that regulates phosphate and polyphosphate metabolism in *Saccharomyces cerevisiae*. *Mol. Biol. Cell*. **18**, 4438–4445

115. Irani, R. R., and Morgenthaler, W. W. (1963) Iron sequestration by polyphosphates. *J. Am. Oil Chem. Soc.* **40**, 283–285

116. Nixon, J. F. (1985) Phosphorus. An outline of its chemistry, biochemistry and technology. *J. Organomet. Chem.* **296**, 56–57

117. Rosenfeld, L., Reddi, A. R., Leung, E., Aranda, K., Jensen, L. T., and Culotta, V. C. (2010) The effect of phosphate accumulation on metal ion homeostasis in *Saccharomyces cerevisiae*. *J. Biol. Inorg. Chem.* **15**, 1051–1062

118. Park, J., McCormick, S. P., Cockrell, A. L., Chakrabarti, M., and Lindahl, P. A. (2014) High-spin ferric ions in *Saccharomyces cerevisiae* vacuoles are reduced to the ferrous state during adenine-precursor detoxification. *Biochemistry*. **53**, 3940–3951

119. Greenberg, G. R., and Wintrobe, M. M. (1946) A labile iron pool. *J. Biol. Chem.* **165**, 397–398

120. Linder, M. C., Mulligan, M., and Henley, D. (1983) Low molecular weight iron pools in tissues of the rat and pig. in *Struct. Funct. Iron Storage Transp. Proteins, Proc. Int. Conf., 6th*

121. Ma, Y., Abbate, V., and Hider, R. C. (2015) Iron-sensitive fluorescent probes: monitoring intracellular iron pools. *Metallomics*. **7**, 212–222

122. Petrat, F., de Groot, H., Sustmann, R., and Rauen, U. (2002) The chelatable iron pool in living cells: A methodically defined quantity. *Biol. Chem.* **383**, 489–502

123. Landero Figueroa, J. A., Subramanian Vignesh, K., S. Deepe, G., and Caruso, J. (2014) Selectivity and specificity of small molecule fluorescent dyes/probes used for the detection

of Zn^{2+} and Ca^{2+} in cells. *Metallomics*. **6**, 301–315

124. Hintner, J.-P., Lechner, C., Riegert, U., Kuhm, A. E., Storm, T., Reemtsma, T., and Stolz, A. (2001) Direct ring fission of salicylate by a salicylate 1,2-dioxygenase activity from *Pseudaminobacter salicylatoxidans*. *J. Bacteriol.* **183**, 6936–6942

125. Hider, R. C., and Kong, X. L. (2011) Glutathione: A key component of the cytoplasmic labile iron pool. *BioMetals*. **24**, 1179–1187

126. Salmon, H. A. (1962) The cytochrome c content of the heart, kidney, liver and skeletal muscle of iron-deficient rats. *J. Physiol.* **164**, 17–30

127. Gambling, L., Kennedy, C., and McArdle, H. J. (2011) Iron and copper in fetal development. *Semin. Cell Dev. Biol.* **22**, 637–644

128. Festa, R. A., and Thiele, D. J. (2011) Copper: An essential metal in biology. *Curr. Biol.* **21**, 877–883

129. Irving, H., and Williams, R. J. P. (1948) Order of stability of metal complexes. *Nature*. **162**, 746–747

130. Kim, B.-E., Nevitt, T., and Thiele, D. J. (2008) Mechanisms for copper acquisition, distribution and regulation. *Nat. Chem. Biol.* **4**, 176–185

131. Smith, A. D., Logeman, B. L., and Thiele, D. J. (2017) Copper acquisition and utilization in fungi. *Annu. Rev. Microbiol.* **71**, 597–623

132. Hassett, R. F., Dix, D. R., Eide, D. J., and Kosman, D. J. (2000) The Fe(II) permease Fet4p functions as a low affinity copper transporter and supports normal copper trafficking in *Saccharomyces cerevisiae*. *Biochem. J.* **351**, 477

133. Dancis, A., Yuan, D. S., Haile, D., Askwith, C., Eide, D., Moehle, C., Kaplan, J., and Klausner, R. D. (1994) Molecular characterization of a copper transport protein in *S.*

*cerevisia*e: An unexpected role for copper in iron transport. *Cell*. **76**, 393–402

134. Dancis, A., Haile, D., Yuan, D. S., and Klausner, R. D. (1994) The *Saccharomyces cerevisiae* copper transport protein (Ctr1p). Biochemical characterization, regulation by copper, and physiologic role in copper uptake. *J. Biol. Chem.* **269**, 25660–25667

135. Jungmann, J., Reins, H. A., Lee, J., Romeo, A., Hassett, R., Kosman, D., and Jentsch, S. (1993) Mac1, a nuclear regulatory protein related to Cu-dependent transcription factors is involved in Cu/Fe utilization and stress resistance in yeast. *EMBO J.* **12**, 5051–5056

136. Knight, S. A. B., Labbé, S., Kwon, L. F., Kosman, D. J., and Thiele, D. J. (1996) A widespread transposable element masks expression of a yeast copper transport gene. *Genes Dev.* **10**, 1917–1929

137. Peña, M. M. O., Puig, S., and Thiele, D. J. (2000) Characterization of the *Saccharomyces cerevisiae* high affinity copper transporter Ctr3. *J. Biol. Chem.* **275**, 33244–33251

138. Puig, S., Lee, J., Lau, M., and Thiele, D. J. (2002) Biochemical and genetic analyses of yeast and human high affinity copper transporters suggest a conserved mechanism for copper uptake. *J. Biol. Chem.* **277**, 26021–26030

139. Ren, F., Logeman, B. L., Zhang, X., Liu, Y., Thiele, D. J., and Yuan, P. (2019) X-ray structures of the high-affinity copper transporter Ctr1. *Nat. Commun.* **10**, 1386

140. Rees, E. M., Lee, J., and Thiele, D. J. (2004) Mobilization of intracellular copper stores by the Ctr2 vacuolar copper transporter. *J. Biol. Chem.* **279**, 54221–54229

141. Rees, E. M., and Thiele, D. J. (2007) Identification of a vacuole-associated metalloreductase and its role in Ctr2-mediated intracellular copper mobilization. *J. Biol. Chem.* **282**, 21629–21638

142. Dameron, C. T., Winge, D. R., George, G. N., Sansone, M., Hu, S., and Hamer, D. (1991)

A copper-thiolate polynuclear cluster in the Ace1 transcription factor. *Proc. Natl. Acad. Sci. U. S. A.* **88**, 6127–6131

143. Lerch, K. (1980) Copper metallothionein, a copper-binding protein from *Neurospora crassa*. *Nature*. **284**, 368–370

144. Winge, D. R., Nielson, K. B., Gray, W. R., and Hamer, D. H. (1985) Yeast metallothionein. Sequence and metal-binding properties. *J. Biol. Chem.* **260**, 14464–14470

145. George, G. N., Byrd, J., and Winge, D. R. (1988) X-ray absorption studies of yeast copper metallothionein. *J. Biol. Chem.* **263**, 8199–8203

146. Joh, H.-D. (1995) A physiological role for *Saccharomyces cerevisiae* copper/zinc superoxide dismutase in copper buffering. *J. Biol. Chem.* **270**, 29991–29997

147. Culotta, V. C., Klomp, L. W. J., Strain, J., Casareno, R. L. B., Krems, B., and Gitlin, J. D. (1997) The copper chaperone for superoxide dismutase. *J. Biol. Chem.* **272**, 23469–23472

148. Rae, T. D. (1999) Undetectable intracellular free copper: the requirement of a copper chaperone for superoxide dismutase. *Science.* **284**, 805–808

149. Schmidt, P. J., Kunst, C., and Culotta, V. C. (2000) Copper activation of superoxide dismutase 1 (SOD1) in Vivo. *J. Biol. Chem.* **275**, 33771–33776

150. Lin, S. J., Pufahl, R. A., Dancis, A., O'Halloran, T. V., and Culotta, V. C. (1997) A role for the *Saccharomyces cerevisiae ATX*1 gene in copper trafficking and iron transport. *J. Biol. Chem.* **272**, 9215–9220

151. Pufahl, R. A. (1997) Metal ion chaperone function of the soluble Cu(I) receptor Atx1. *Science.* **278**, 853–856

152. Huffman, D. L., and O'Halloran, T. V. (2000) Energetics of copper trafficking between the Atx1 metallochaperone and the intracellular copper transporter, Ccc2. *J. Biol. Chem.* **275**,

18611–18614

153. La Fontaine, S., and Mercer, J. F. B. (2007) Trafficking of the copper-ATPases, Atp7A and Atp7B: Role in copper homeostasis. *Arch. Biochem. Biophys.* **463**, 149–167

154. Lowe, J., Vieyra, A., Catty, P., Guillain, F., Mintz, E., and Cuillel, M. (2004) A mutational study in the transmembrane domain of Ccc2p, the yeast Cu(I)-ATPase, shows different roles for each Cys-Pro-Cys Cysteine. *J. Biol. Chem.* **279**, 25986–25994

155. Gaxiola, R. A., Yuan, D. S., Klausner, R. D., and Fink, G. R. (1998) The yeast CLC chloride channel functions in cation homeostasis. *Proc. Natl. Acad. Sci. U. S. A.* **95**, 4046–4050

156. Davis-Kaplan, S. R., Askwith, C. C., Bengtzen, A. C., Radisky, D., and Kaplan, J. (1998) Chloride is an allosteric effector of copper assembly for the yeast multicopper oxidase Fet3p: An unexpected role for intracellular chloride channels. *Proc. Natl. Acad. Sci. U. S. A.* **95**, 13641–13645

157. Wu, X., Kim, H., Seravalli, J., Barycki, J. J., Hart, P. J., Gohara, D. W., Di Cera, E., Jung, W. H., Kosman, D. J., and Lee, J. (2016) Potassium and the K^+/H^+ exchanger Kha1p promote binding of copper to apo Fet3p multi-copper ferroxidase. *J. Biol. Chem.* **291**, 9796–9806

158. Ostermeier, C. (1996) Cytochrome c oxidase. *Curr. Opin. Struct. Biol.* **6**, 460–466

159. Michel, H., Behr, J., Harrenga, A., and Kannt, A. (1998) Cytochrome c oxidase: Structure and spectroscopy. *Annu. Rev. Biophys. Biomol. Struct.* **27**, 329–356

160. Shoubridge, E. A. (2001) Cytochrome c oxidase deficiency. *Am. J. Med. Genet.* **106**, 46–52

161. Baertling, F., A.M. van den Brand, M., Hertecant, J. L., Al-Shamsi, A., P. van den Heuvel, L., Distelmaier, F., Mayatepek, E., Smeitink, J. A., Nijtmans, L. G. J., and Rodenburg, R. J. T. (2015) Mutations in *COA6* cause cytochrome c oxidase deficiency and neonatal

hypertrophic cardiomyopathy. *Hum. Mutat.* **36**, 34–38

162. Cobine, P. A., Ojeda, L. D., Rigby, K. M., and Winge, D. R. (2004) Yeast contain a non-proteinaceous pool of copper in the mitochondrial matrix. *J. Biol. Chem.* **279**, 14447–14455

163. Vest, K. E., Leary, S. C., Winge, D. R., and Cobine, P. A. (2013) Copper import into the mitochondrial matrix in *Saccharomyces cerevisiae* is mediated by Pic2, a mitochondrial carrier family protein. *J. Biol. Chem.* **288**, 23884–23892

164. Dodani, S. C., Leary, S. C., Cobine, P. A., Winge, D. R., and Chang, C. J. (2011) A targetable fluorescent sensor reveals that copper-deficient *SCO1* and *SCO2* patient cells prioritize mitochondrial copper homeostasis. *J. Am. Chem. Soc.* **133**, 8606–8616

165. Andreini, C., Bertini, I., Cavallaro, G., Holliday, G. L., and Thornton, J. M. (2008) Metal ions in biological catalysis: From enzyme databases to general principles. *JBIC J. Biol. Inorg. Chem.* **13**, 1205–1218

166. Eide, D. J. (2009) Homeostatic and adaptive responses to zinc deficiency in *Saccharomyces cerevisiae*. *J. Biol. Chem.* **284**, 18565–18569

167. Zhao, H., and Eide, D. (1996) The yeast *ZRT1* gene encodes the zinc transporter protein of a high-affinity uptake system induced by zinc limitation. *Proc. Natl. Acad. Sci.* **93**, 2454–2458

168. Zhao, H., and Eide, D. (1996) The *ZRT2* gene encodes the low affinity zinc transporter in *Saccharomyces cerevisiae*. *J. Biol. Chem.* **271**, 23203–23210

169. White, C., and Gadd, G. M. (1987) The uptake and cellular distribution of zinc in *Saccharomyces cerevisiae*. *J. Gen. Microbiol.* **133**, 727–737

170. Kamizono, A., Nishizawa, M., Teranishi, Y., Murata, K., and Kimura, A. (1989) Identification of a gene conferring resistance to zinc and cadmium ions in the yeast

Saccharomyces cerevisiae. *MGG Mol. Gen. Genet.* **219**, 161–167

171. MacDiarmid, C. W. (2000) Zinc transporters that regulate vacuolar zinc storage in *Saccharomyces cerevisiae*. *EMBO J.* **19**, 2845–2855

172. Miyabe, S., Izawa, S., and Inoue, Y. (2001) The Zrc1 is involved in zinc transport system between vacuole and cytosol in *Saccharomyces cerevisiae*. *Biochem. Biophys. Res. Commun.* **282**, 79–83

173. Conklin, D. S., McMaster, J. A., Culbertson, M. R., and Kung, C. (1992) *COT1*, a gene involved in cobalt accumulation in *Saccharomyces cerevisiae*. *Mol. Cell. Biol.* **12**, 3678–3688

174. Li, M., Rong, Y., Chuang, Y.-S., Peng, D., and Emr, S. D. (2015) Ubiquitin-dependent lysosomal membrane protein sorting and degradation. *Mol. Cell*. **57**, 467–478

175. Kizawa, K., Aono, T., and Ohtomo, R. (2016) *PHO8* gene coding alkaline phosphatase of *Saccharomyces cerevisiae* is involved in polyphosphate metabolism. *J. Gen. Appl. Microbiol.* **62**, 297–302

176. Qiao, W., Ellis, C., Steffen, J., Wu, C.-Y., and Eide, D. J. (2009) Zinc status and vacuolar zinc transporters control alkaline phosphatase accumulation and activity in *Saccharomyces cerevisiae*. *Mol. Microbiol.* **72**, 320–334

177. Coleman, J. E. (1992) Structure and mechanism of alkaline phosphatase. *Annu. Rev. Biophys. Biomol. Struct.* **21**, 441–483

178. Liu, X. F., and Culotta, V. C. (1999) Post-translation control of Nramp metal transport in yeast. *J. Biol. Chem.* **274**, 4863–4868

179. Rudolph, H. K., Antebi, A., Fink, G. R., Buckley, C. M., Dorman, T. E., LeVitre, J., Davidow, L. S., Mao, J., and Moir, D. T. (1989) The yeast secretory pathway is perturbed

by mutations in Pmr1, a member of a Ca^{2+} ATPase family. *Cell*. **58**, 133–145

180. Antebi, A., and Fink, G. R. (1992) The yeast Ca^{2+}-ATPase homologue, *PMR1*, is required for normal Golgi function and localizes in a novel Golgi-like distribution. *Mol. Biol. Cell*. **3**, 633–654

181. Dürr, G., Strayle, J., Plemper, R., Elbs, S., Klee, S. K., Catty, P., Wolf, D. H., and Rudolph, H. K. (1998) The medial -Golgi ion pump Pmr1 supplies the yeast secretory pathway with Ca^{2+} and Mn^{2+} required for glycosylation, sorting, and endoplasmic reticulum-associated protein degradation. *Mol. Biol. Cell*. **9**, 1149–1162

182. Sorin, A., Rosas, G., and Rao, R. (1997) Pmr1, a Ca^{2+}-ATPase in yeast Golgi, has properties distinct from sarco/endoplasmic reticulum and plasma membrane calcium pumps. *J. Biol. Chem.* **272**, 9895–9901

183. Lapinskas, P. J., Lin, S. J., and Culotta, V. C. (1996) The role of the *Saccharomyces cerevisiae CCC1* gene in the homeostasis of manganese ions. *Mol. Microbiol.* **21**, 519–528

184. Paidhungat, M., and Garrett, S. (1998) Cdc1 and the vacuole coordinately regulate Mn^{2+} homeostasis in the yeast *Saccharomyces cerevisiae*. *Genetics*. **148**, 1787–1798

185. Culotta, V. C., Yang, M., and Hall, M. D. (2005) Manganese transport and trafficking: lessons learned from *Saccharomyces cerevisiae*. *Eukaryot. Cell*. **4**, 1159–1165

186. Jensen, L. T., Ajua-Alemanji, M., and Culotta, V. C. (2003) The *Saccharomyces cerevisiae* high affinity phosphate transporter encoded by *PHO84* also functions in manganese homeostasis. *J. Biol. Chem.* **278**, 42036–42040

187. Rosenfeld, L., and Culotta, V. C. (2012) Phosphate disruption and metal toxicity in *Saccharomyces cerevisiae*: effects of Rad23 and the histone chaperone Hpc2. *Biochem. Biophys. Res. Commun.* **418**, 414–419

188. McNaughton, R. L., Reddi, A. R., Clement, M. H. S., Sharma, A., Barnese, K., Rosenfeld, L., Gralla, E. B., Valentine, J. S., Culotta, V. C., and Hoffman, B. M. (2010) Probing in vivo Mn^{2+} speciation and oxidative stress resistance in yeast cells with electron-nuclear double resonance spectroscopy. *Proc. Natl. Acad. Sci. U. S. A.* **107**, 15335–15339

CHAPTER II

ISOLATED SACCHAROMYCES CEREVISIAE VACUOLES CONTAIN LOW-MOLECULAR-MASS TRANSITION-METAL POLYPHOSPHATE COMPLEXES [*]

Chapter II is a reprint of a published paper on *Metallomics* which I was the first author. I prepared all of the figures and obtained all of the experimental results except the LC calibration curve (Figure 2.S1). Mr. Nathaniel Dziuba maintained the LC-ICP-MS instrument, trained me on the instrument and obtained the LC calibration curve. We thank Dr. Dennis Thiele (Duke University School of Medicine) for the *cup1*Δ strain and helpful discussion. We thank Dr. Vishal Gohil (TAMU Department of Biochemistry and Biophysics) for the *cox17*Δ strain. I appreciate Dr. Charlie Baker and Ms. Natalie Garza from the Gohil lab for their help with Western blots, and Dr. Roula Barhoumi Mouneimne (TAMU Department of Veterinary Integrative Biosciences) for her assistance with the confocal microscopy.

Summary

Vacuoles play major roles in the trafficking, storage, and homeostasis of metal ions in fungi and plants. In this study, 29 batches of vacuoles were isolated from *Saccharomyces cerevisiae*. Flow-through solutions (FTS) obtained by passing vacuolar extracts through a 10 kDa cut-off membrane were characterized for metal content using an anaerobic liquid chromatography system interfaced to an online ICP-MS. Nearly all iron, zinc, and manganese ions in these solutions were present as low-molecular-mass (LMM) complexes. Metal-detected peaks with masses between 500–1700 Da dominated; phosphorus-detected peaks generally comigrated. The distribution of metal:polyphosphate complexes was dominated by particular chain-lengths rather than a broad binomial distribution. Similarly treated synthetic Fe^{III}-polyphosphate complexes showed similar peaks. Treatment with a phosphatase disrupted the LMM metal-bound species in vacuolar FTSs. These results indicated metal:polyphosphate complexes 6–20 phosphate units in length and coordinated by 1–3 metals on average per chain. The speciation of iron in FTSs from iron-deficient cells was qualitatively similar, but intensities were lower. Under healthy conditions, nearly all copper ions in vacuolar FTSs were present as 1–2 species with masses between 4800–7800 Da. The absence of these high-mass peaks in vacuolar FTS from *cup1*Δ cells suggests that they were due to metallothionein, Cup1. Disrupting copper homeostasis increased the amount of LMM copper:polyphosphate complexes in vacuoles (masses between 1500–1700 Da). Potentially dangerous LMM copper species in the cytosol of metallothionein-deficient cells may traffic into vacuoles for sequestration and detoxification.

Introduction

Vacuoles are acidocalcisome-like organelles found in fungi and plants (1) (2) (3) (4). These acidic structures are related to endosomes and lysosomes in humans, and are used in endocytosis, secretory trafficking, autophagy, and metabolite recycling. Vacuoles in S. cerevisiae cells grown to stationary phase in media buffered at pH = 6 have a pH of 6.2 (5). The pH gradient with cytosol drives the import of metal ions into the organelle (3), allowing vacuoles to store essential metals (1) (6) (7) (8) (9) (10) (11) and sequester toxic metal ions that would otherwise engage in deleterious cellular reactions (12) (13).

Iron fits in both of these categories; it is essential for cell growth and can generate reactive oxygen species via Fenton-based reactions (14). Some cellular iron enters vacuoles through the Ccc1 protein located on the vacuolar membrane (15) (16). Some extracellular iron enters vacuoles through endocytosis (15). Vesicular fluid-phase endocytic transport to and from vacuoles plays a major role in metal homeostasis (17). Vacuoles concentrate nutrient metal ions in the environment for eventual delivery to the cytosol.

Iron in vacuoles can be mobilized and exported to the cytosol through specific iron-export proteins on the vacuolar membrane. These include the Fet5:Fth1 ferroxidase:permease complex and the Nramp protein Smf3 (18) (19) (20). The ultimate concentration of vacuolar iron is controlled by opposing rates of iron import and export.

These organelles are oxidizing relative to the cytosol, and so iron is typically stored as Fe^{III} rather than Fe^{II} (9) (20) (21) (22) (23). EPR spectra of isolated vacuoles exhibit a g = 4.3 signal indicating high-spin S = 5/2 Fe^{III} ions with rhombic symmetry. Fe^{III} ions in vacuoles must be reduced to Fe^{II} prior to export to the cytosol. This process is controlled by ferrireductase Fre6 (20).

An important aspect of vacuolar metabolism involves polyphosphate (polyP) ions, linear polyanionic polymers of phosphate units linked by phosphoanhydride bonds (24). WT yeast cells contain 25–42 mM orthophosphate (P_i) and 23–250 mM polyP (concentration given in terms of phosphate units) (6) (25). Most polyP ions are located in vacuoles (26).

Preassembled polyP chains cannot be imported into vacuoles (3). Rather they must be synthesized on the vacuolar membrane and inserted ratchet-like into the lumen (3) (26) (27). Once in the lumen, polyP chains can be hydrolyzed by vacuolar phosphatases Ppn1 and Ppn2 (28). Ppn1 has both exopolyphosphatase and endopolyphosphatase activities. Activity requires manganese or magnesium ions (26). Ppn2 is exclusively an endophosphatase that is activated by zinc (29). Both enzymes are delivered to the vacuole via the multivesicular body pathway in which proteins are packaged into luminal vesicles that fuse with vacuoles and release their contents (30) (31).

The length of polyP chains (defined in terms of residues n) depends on the carbon and nitrogen source in the growth medium, as well as on metal ion availability (5) (32) (33) (34). Reported values of n include 7, 15, 20, and 60–100 (5) (17) (33) (34). In the presence of high concentrations of metals, n reportedly increases to 45–75, ∼200, and >300 (3) (17) (34). Each internal P_i residue has a mass of 79 Da; thus, polyP chains with n = 7–100 units have masses between 600–8000 Da.

The high concentration of polyP in vacuoles and the strong binding of Fe^{III} to polyP chains (35) (36) led Raguzzi *et al*. to hypothesize that Fe^{III} ions must be coordinated to polyP in vacuoles (9). Supporting this, Mössbauer spectra of intact vacuoles reveal high-spin S = 5/2 Fe^{III} ions whose spectra can be simulated using parameters expected for coordination to hard-oxygen ligands like polyP (21) (22). Moreover, spectra of authentic Fe^{III} –polyP in acidic pH are nearly indistinguishable from those of intact vacuoles. Fe^{III} –oxyhydroxide nanoparticles form when Fe^{III}

–polyP solutions are adjusted to high pH similar to those observed spectroscopically in some batches of isolated vacuoles (21) (22).

Vacuoles are also involved in the trafficking, storage, and regulation of other metal ions such as zinc, manganese, and copper (1) (6) (8) (10) (11) (36). Importers and exporters for zinc and manganese are known. Copper enters vacuoles through an unknown mechanism but exits via membrane-bound Ctr2 (37) (38). Copper is thought to be stored as Cu^{II} ions in vacuoles, and then reduced to Cu^{I} by Fre6 prior to export (20) (38) (39).

Here, we have detected and partially characterized low-molecular-mass (LMM) iron, zinc, manganese and copper complexes from isolated vacuoles using a liquid chromatography system located in a refrigerated anaerobic glove box and interfaced with an online inductively coupled plasma mass spectrometer. Using this LC-ICP-MS system, we provide new additional evidence that most of these metal species in vacuoles are indeed present as metal–polyP complexes, with particular chain lengths dominating. Under healthy conditions, most copper ions in vacuolar extracts were present as high-molecular-mass (HMM) species (primarily or exclusively bound to metallothionein, Cup1) whereas in cells lacking Cup1, significant amounts of copper ions were coordinated to polyP chains. Implications of these results for cellular metal metabolism are discussed.

Materials and Methods

Cell growth

Saccharomyces cerevisiae strains W303 wild type (*MATα, ura3-1, ade2-1, trp1-1, his3-11,15, leu2-3,112; ATCC*), *cup1*Δ (*MAT α, trpl-1, gal-l, met13, can1, cup1S, ura3-50, Ade−His−cup1Δ::ura3*), and *cox17*Δ (*Mat a, his3Δ1, leu2Δ0, met15Δ0, ura3Δ0, cox17::HphMX4*)

were used in this study. The background for *cup1*Δ cells was *MAT α, trp1l-1, gal-l, met13, can1, cup1S, ura3-50, Ade−His−* whereas that for *cox17*Δ cells was BY4741. WT cells were typically grown in 500 mL of either complete synthetic medium (CSM) or minimal medium (MM). *cup1*Δ and *cox17*Δ cells were grown in 1 L of CSM. The composition for MM included 2% (w/v) glucose, 0.5% (w/v) ammonium sulfate, 0.17% (w/v) modified YNB lacking copper and iron (MP Bio), 20 mg L^{-1} uracil, 20 mg L^{-1} histidine, 50 mg L^{-1} tryptophan, 100 mg L^{-1} adenine, and 100 mg L^{-1} leucine. CSM composition is similar to MM with the exceptions of using 6% (w/v) glucose and replacing most of the specific amino acids with the Yeast Synthetic Drop-out Medium Supplements (Y1376, Sigma-Aldrich). The growth medium was typically supplemented with 10 μM $CuSO_4$ and either 1 or 40 μM $^{56}Fe^{III}$–citrate. Starting with a single colony on YPAD plates, 50 mL (for WT strain) or 100 mL (for *cup1*Δ and *cox17*Δ strains) of precultures were grown in either CSM or MM at 30 °C for 24–48 hours. Cells were then inoculated into either 500 mL or 1 L of CSM or MM in a 2.8 L baffle flask and grown at 30 °C and 130 rpm. WT cells were harvested either at mid-exponential phase (OD_{600} = 0.8 ± 0.1 for MM) or early stationary phase (OD_{600} = 3.0 ± 0.1 for MM and OD_{600} = 8.5 ± 0.1 for CSM). *cup1*Δ and *cox17*Δ cells were harvested at OD_{600} = 5 and 8, respectively. Typical yields were 13 ± 2 g of wet cell pellet. Additional conditions for individual batches of isolated vacuoles are listed in Table 2.S1.

Isolation of vacuoles

Vacuoles were isolated using the protocol of Li *et al.* (15) with some modifications for large-scale batches. Harvested cells were washed (centrifuged at 4000 × g for 5 min, supernatant-disposed, and pellet resuspended) 3 times with 5 mL of Buffer A (1 mM EDTA, 1.2 M sorbitol, and 200 mM KP_i, pH = 7.4) per g wet-pellet, followed by 3 additional washes with DI water. Cells

were suspended in 5 mL of Buffer B (5 mM TCEPS, 100 mM Tris, pH = 7.4) per g wet cell mass. After 30 min incubation at 30 °C, cells were centrifuged and resuspended in 10 mL of Buffer C (0.6 M sorbitol, 10 mM KP_i, pH = 7.4,) per g of wet cells. PMSF was added to a final concentration of 8 mM. In addition, 3 mg of 200 KU-lyticase (Sigma Aldrich) per g wet cells were dissolved in 1 mL of Buffer C, and quantitatively transferred to the cell suspension. The initial OD600 (immediately after adding lyticase) was measured by mixing 10 μL of cell suspension with 990 μL of water. Once OD_{600} was 10–20% of the initial value, the suspension was centrifuged at 2200 × g for 5 min. Spheroplasts were gently resuspended in 3.5 mL of pre-chilled 15% Ficoll in Buffer D (200 mM sorbitol, 20 mM PIPES, pH = 6.8), and transferred to a prechilled 16 × 102 mm polypropylene ultracentrifuge tube (Beckman Coulter). A suspension of diethylaminoethyl dextran (DEAE-Dextran, Sigma-Aldrich) was prepared fresh in Buffer D (1–4 mg solid per mL of Buffer D), and was added to the spheroplast suspension to a final concentration of 200 μg mL^{-1}. The suspension was incubated for 3 min on ice followed by 5 min at 30 °C. The resulting subcellular fractionate was chilled on ice and overlaid first with 3 mL of 8% Ficoll, then 4 mL of 4% Ficoll, and finally 0% Ficoll to fill the tube to within 5 mm of the top. All Ficoll solutions were prepared in Buffer D and kept on ice. After centrifugation at 110 000 × g for 90 min with Beckman Coulter SW 32 Ti rotor in an Optima L-90K Ultracentrifuge, the vacuoles were collected at the 0–4% Ficoll interphase with a plastic disposable pipet (trimmed at the orifice to ~3 mm OD).

Western blotting

Protein concentrations were quantified by Pierce™ BCA Protein Assay Kit (Thermo Scientific™). Whole cells protein extract and vacuolar fractions were run on a NuPAGE™ 10% Bis–Tris protein gel (Invitrogen™). Separated proteins were transferred to PVDF membranes

using a Trans-Blot transfer cell (Bio-Rad). Membranes were blocked with 5% milk dissolved in Tris-buffered saline with 0.1% Tween (TBST-milk) for 1 h at RT before incubating with primary antibodies overnight at 4 °C. All primary antibodies were prepared in TBST-milk at the following dilutions: 1 : 2000 of anti-CPY antibody for vacuole/late endosome marker (Life Technologies, A-6428), 1 : 1000 of anti-ALP antibody for vacuole marker (Abcam, 1D3A10), 1 : 2000 of anti-Kar2 antibody for endoplasmic reticulum marker (Santa Cruz Biotechnology, sc-33630), 1 : 2000 of anti-PGK antibody for cytosol marker (Life Technologies, H0460) and 1 : 1000 of anti-porin antibody for mitochondria marker (Thermo Fisher, 16G9E6BC4). Goat anti-rabbit IgG HRP-conjugated secondary antibody was from Santa Cruz Biotechnology (clone sc-2004) and goat anti-mouse IgG HRP-conjugated secondary antibody was from Invitrogen (clone G-21040). Both secondary antibodies were used at 1 : 5000 dilution for 1 hour at RT. Clarity™ Western ECL Substrate (Bio-Rad) was added, and images were obtained (FujiFilm LAS-4000 mini) with a 15 s exposure using the precision mode of chemiluminescence setting.

Confocal microscopy

A 2-well Lab-Tek™ Chambered Borosilicate Coverglass (Fisher Scientific) was coated with 20 mL of 0.1% (w/v) poly-L-lysine solution (Sigma Aldrich) for 30 min and dried in air overnight. A stock solution of 10 mM green fluorescent Yeast Vacuole Membrane Marker MDY-64 dye (Fisher Scientific) was prepared by dissolving 1 mg of solid in 260 μL of DMSO. Aliquots of 4 μL were frozen in liquid nitrogen, stored at −20 °C in the dark. Freshly isolated vacuoles (20–50 μL) were gently mixed, affording a final dye concentration of 10 μM. The mixture was incubated at RT for 5 min. Fluorescent stained vacuoles were then applied to the coated coverglass and imaged with a Zeiss LSM 780 confocal microscope at TAMU Department of Veterinary

Integrative Biosciences using an excitation wavelength of 451 nm and emission wavelength of 497 nm.

Preparation of Fe^{III}- polyphosphate

0.5 mg/mL of sodium polyphosphate (Acros Organics) was prepared in Buffer D and passed through an Ultracel regenerated cellulose 10 kDa NMWL membrane (EMD Millipore) using an Amicon® EMD Millipore Stirred Cell (Model 8003, 3 mL). To 10 mL of the resulting flow-through solution (FTS) was added 270 mg of $FeCl_3.6H_2O$ (Sigma Aldrich). The resulting 100 mM $FeCl_3$ stock solution was serially diluted using polyphosphate FTS to yield 5, 10, 25, and 50 μM of $FeCl_3$ in 0.5 mg/mL polyphosphate.

Preparation of vacuolar FTS and LC-ICP-MS chromatography

2–2.5 mL of isolated vacuolar extract (in Buffer D, obtained from the 0–4% Ficoll interface) were treated with 2% (v/v, final) Triton X-100 and passed through a 10 kDa cut-off membrane (EMD Millipore) using the stirred cell described above. Almost 90% of the vacuolar extract passed through the 10 kDa membrane in ca. 1 h. The FTS (150 or 500 μL) was loaded onto a dipeptide size-exclusion (SEC) Superdex™ Peptide 10/300 GL column (GE Life Sciences) connected to an Agilent 1260 Bioinert quaternary pump (G5611A). A flow rate of 0.35 mL/min was used with the mobile phase of either 20 mM $(NH_4)HCO_3$, pH = 8.5 or 20 mM (NH_4)OAc, pH = 6.5. The SEC column was calibrated such that apparent molecular masses could be estimated from eluent volumes of standards (Figure 2.S1). LC-ICP-MS parameters, column cleaning procedure, and molecular mass calibration have been described (40).

Vacuolar FTS treatment with acid phosphatase

1.5 mg of lyophilized acid phosphatase powder (P1146-50UN, Sigma-Aldrich) was dissolved in 525 μL of DI water. Vacuolar FTSs from batches 13 and 14 were mixed with the resulting acid phosphatase solution in a 1: 1 v/v ratio and incubated at 37 °C for 3 h. The resulting solution was injected onto the LC using a mobile phase with pH 8.5.

Elemental analysis

Elemental concentrations were measured as described (40). Briefly, vacuolar extract and vacuolar FTSs of 4 independent batches were separated into 50 μL quadruplicates using 15 mL polypropylene screw-top vials. 400 μL of trace-metal-grade 70% w/v nitric acid (Fisher Scientific) was added to each vial. Vials were sealed with caps and electrical tape, then incubated at 85 °C for ca. 15 h. Each replicate was diluted with 7.55 mL of high-purity trace-metal-free double-distilled-deionized water. Samples were analyzed using ICP-MS (Agilent 7700x) in He collision mode. ICP standards were prepared from customized stock solutions (Inorganic Ventures), 5% w/v final concentration of trace-metal-grade nitric acid, and double-distilled-deionized water to generate calibration curves for each element.

Results

Twenty nine batches of vacuoles were isolated

After density-gradient ultracentrifugation, the organelle congregated at the 0–4% Ficoll interphase (Figure 2.1, panel A, arrow). Western blots of soluble extracts of whole cells and isolated vacuolar lysates from this interface revealed that the organelle was significantly purified

(Figure 2.1, panel A) but also contaminated with endoplasmic reticulum (ER) and cytosol. No contamination from mitochondria was evident.

We evaluated the integrity of isolated vacuole batches using confocal fluorescence microscopy. Samples were treated with a fluorescent dye that localized to vacuolar membranes. Images revealed intact membranes (Figure 2.1, panel B). Vacuoles were distributed in size, ranging from 1–3 μm in diameter. Unidentified contaminating small punctate structures were also evident.

Due to the limited quantities, we did not determine absolute metal ion concentrations in isolated organelle batches. Rather, we determined the ratio of metal concentrations (nM) of vacuolar extracts and FTSs to the overall protein concentration (mg/mL) of the vacuolar extract ($[proteins]_{avg}$ = 0.5 ± 0.1 mg/mL, n = 6). FTSs are the portion of soluble vacuolar extracts that passed through a 10 kDa cut-off membrane and contained LMM species. The average concentration-ratios of iron, zinc, copper and manganese in our FTSs and in soluble vacuolar extracts (Figure 2.2) indicate that nearly all of the considered metal ions in vacuolar extracts are present as LMM complexes.

Ratios of [metal]/[protein] for Fe and Mn in vacuolar suspensions were similar to previous results (21), especially for iron. The current [copper]/[protein] ratio was similar to the previous low-concentration group. The current [zinc]/[protein] ratio was 5-times lower than previous while the [phosphorus]/[protein] ratio was 3-times higher. Absolute concentrations in isolated vacuoles were previously determined to be: $[P_{vac}]$ = 14 ± 9 mM; $[Fe_{vac}]$ = 220 ± 100 μM; $[Zn_{vac}]$ = 160 ± 120 μM; $[Cu_{vac}]$ = 30 ± 30 μM (low group); $[Mn_{vac}]$ = 1.7 ± 0.6 μM; [protein] = 6.3 mg/mL (21). Some iron probably leached from vacuoles during isolation. Current P : Fe : Zn : Cu : Mn ratios were 10 : 1: 0.12 : 0.11 : 0.02; previous ratios were 64 : 1 : 0.73 : 0.14 : 0.01.

Iron-detected chromatograms of vacuolar FTS exhibit several LMM species

FTSs were passed down a size-exclusion chromatography column designed for optimal resolution of small peptides. We initially used a mobile phase of ammonium bicarbonate at pH 8.5 but later used ammonium acetate at pH 6.5. All of the elemental chromatograms of vacuolar FTS from WT cells are the average of individual traces that were categorized by the growth medium (complete synthetic media CSM vs. minimal media MM), growth phase at harvest (exponential vs. stationary phase), and the pH of the mobile phase. See Table 2.S1 for all conditions. Individual chromatograms associated with Figure 2.S3, 2.S4, 2.S7–2.S10 are shown in Supplemental Information.

Chromatography traces of FTSs from cells grown on MM and harvested in exponential and stationary phases exhibited three major iron-containing peaks with estimated masses of 1400, 1100, and 700 Da (Figure 2.3, top 2 traces). We will refer to the species affording these peaks as Fe_{1400}, Fe_{1100}, and Fe_{700}. Masses were estimated from calibrated migration rates of known metal complexes and small metalloproteins under the same column conditions; we assume an uncertainty in mass of ±25%. Traces of FTSs from MM-grown cells harvested at stationary phase were more reproducible than those harvested during exponential phase, but major peaks were routinely in the same chromatographic region (700–1400 Da). More diverse peaks were observed using FTS from vacuoles isolated from cells grown on CSM and harvested during stationary phase (Figure 2.3, middle 2 traces). The particular peaks observed depended on the pH of the mobile phase. At pH 8.5, major peaks were at 1700, 1400, 800, and 500 Da; at pH 6.5, they shifted to higher masses (2200, 1700, and 1200). Peaks of greater masses were evident in some traces. In summary, virtually all of the iron present in vacuolar extracts was present in LMM forms. These included ca. 8 LMM iron species, with apparent masses ranging from 2200–500 Da. There was some batch-to-batch

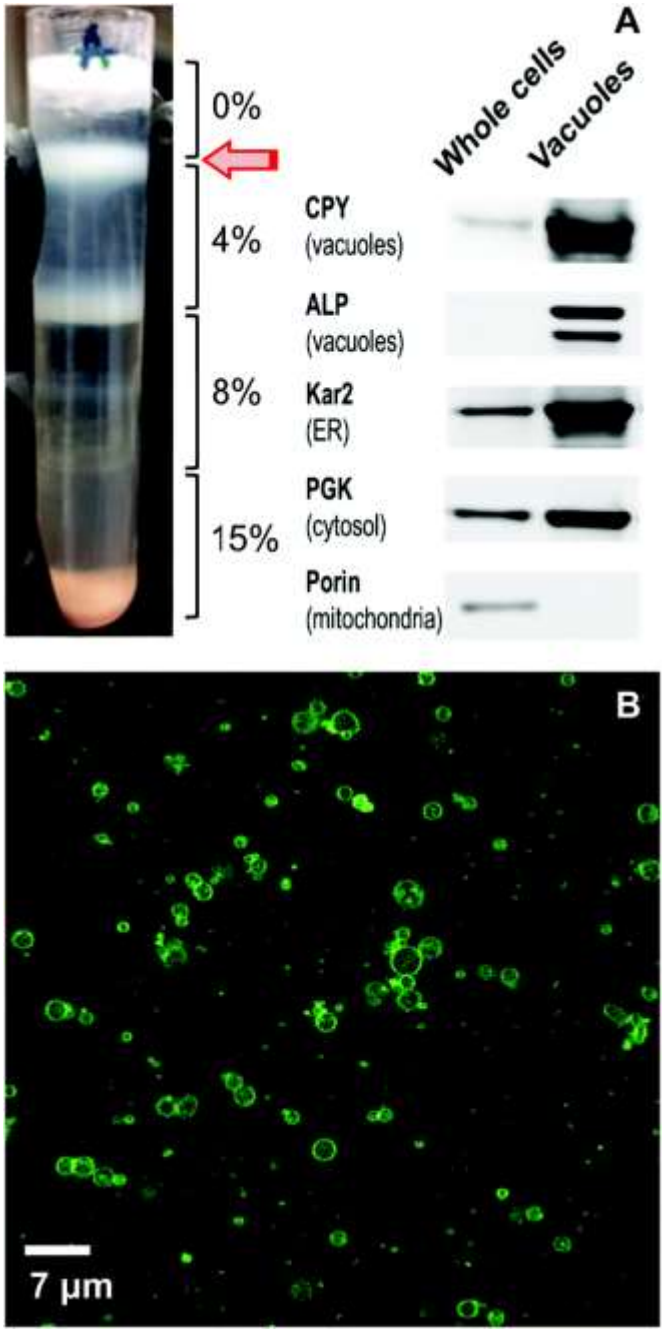

Figure 2.1: Purity and integrity of isolated vacuoles (reprinted from reference 41)**.**
A, centrifugation tube after density gradient step of the isolation procedure. The white band at the 0%:4% Ficoll interface (arrow) was collected and called the isolated vacuole fraction. A Western blot of whole cells and the corresponding isolated vacuolar fraction is shown; 8 µg proteins were loaded into each lane (n = 2) (41).
B, Confocal microscopic image of isolated vacuolar fraction (n = 2) (41).

variability, and species with higher masses were stabilized when the mobile phase of the chromatography column was slightly acidic.

Two batches were supplemented with 1 rather than 40 μM Fe in CSM. The speciation of iron in these batches was similar to that in batches grown with 40 μM iron; however, the intensities

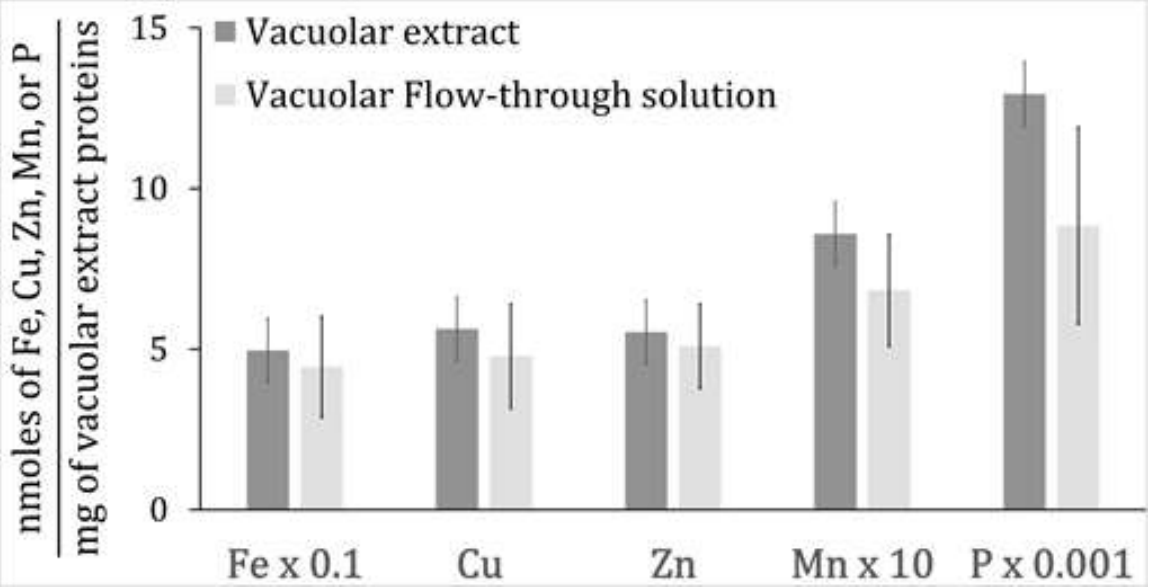

Figure 2.2: Histogram of elemental concentrations in vacuolar extracts and FTSs (n = 4) (reprinted from reference 41).

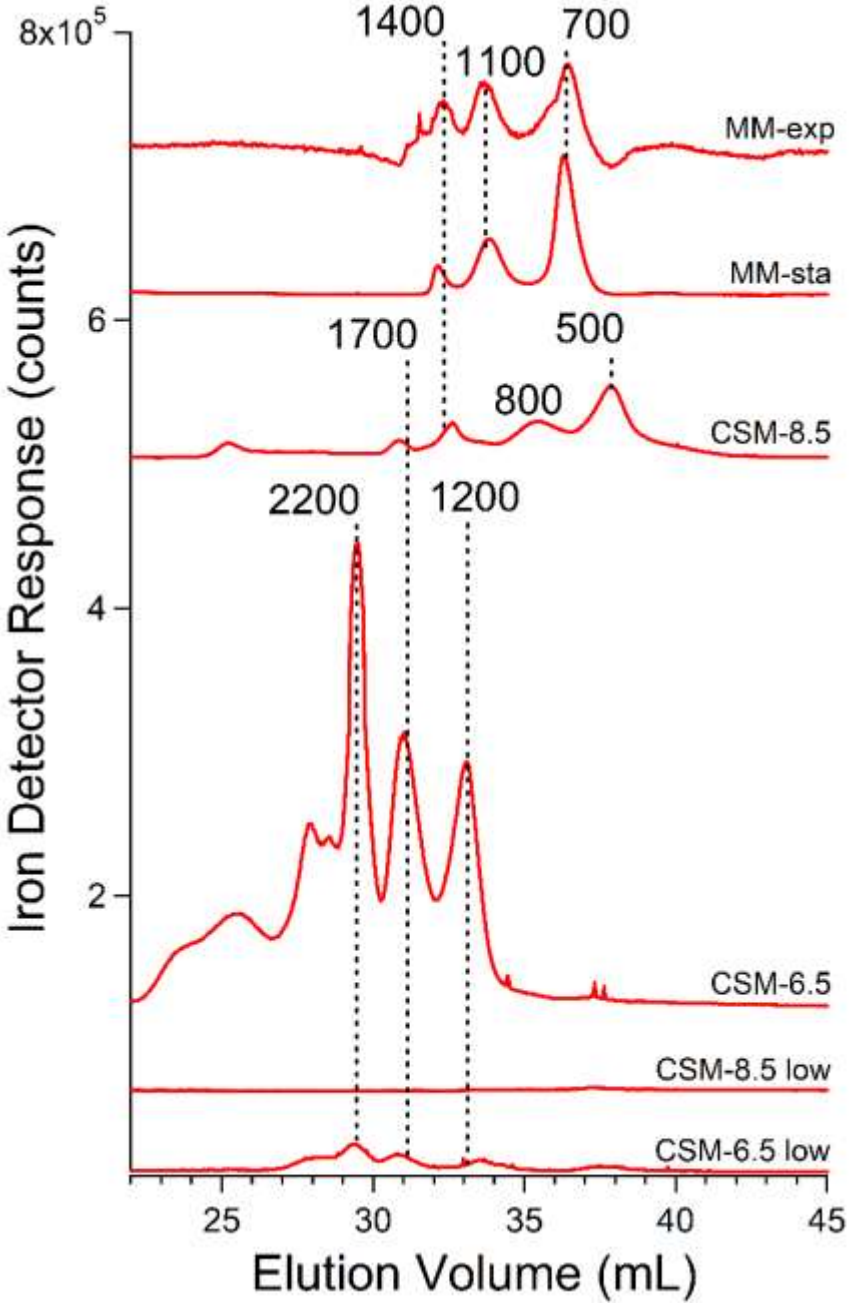

Figure 2.3: Averaged iron-detected chromatograms of FTS from isolated vacuoles (reprinted from reference 41)**.** *MM-exp*, average of traces obtained from MM-grown cells harvested under exponential conditions; *MM-sta*, average of traces obtained from MM-grown cells harvested under stationary conditions; *CSM-8.5*, averages of traces from CSM-grown cells using pH 8.5 mobile phase. *CSM-8.5 low*, same but for cells grown on 1 (rather than 40) μM Fe^{III} citrate; *CSM-6.5* and *CSM-6.5 low*, same but using pH 6.5 mobile phase (41).

of the peaks were lower (Figure 2.3, bottom 2 traces). This was almost certainly due to the lack of iron in vacuoles under nutrient iron-limited conditions. The intensity and position of zinc, manganese, and copper peaks from the same batches were similar to the corresponding peaks in iron-replete batches (see below), and they served as internal standards.

Phosphorus-detected chromatograms of FTS include phosphate and polyphosphate species

Vacuolar FTSs obtained from cells grown on CSM and harvested during stationary phase exhibited numerous phosphorus-detected chromatography peaks (Figure 2.4). The dominant peak migrated in accordance with an apparent mass of 500 Da. This peak represented 90–95% of the overall phosphorus-based intensity in these chromatograms. Sodium phosphate eluted at the same elution volume (Figure 2.S3, Supplemental Information). This was initially disconcerting since the mass of the $H_2PO_4^-$ ion is 97 Da, substantially lower than 500 Da. However, small highly charged ions migrate through standard Sephadex-based gel columns at rates that deviate from those expected, due to interactions between the mobile ions and the fixed charges within the column medium and/or due to the effects of different hydrodynamic volumes (41). Based on these considerations, we tentatively assigned the 500 Da peak to a mixture of phosphate ions and short (n = 6–8) polyP chains.

Our primary interest was in the lower-intensity higher-mass phosphorus-based peaks. An expanded view of chromatograms of vacuolar FTS was obtained from cells grown on MM and using the LC column equilibrated at pH 8.5. This view revealed peaks at 1400, 1100, and 700 Da (Figure 2.4). For cells grown on CSM, the equivalent chromatograms were similar but the main peak was shifted to 500 Da. Minor peaks at 2200 and 1700 Da are also evident. Using a mobile phase of pH 6.5, the peak at 1100 Da dominated the polyP region (Figure 2.4, trace CSM-6.5).

We tentatively assigned all of these peaks to polyP chains. In many batches, unresolved low-intensity phosphorus-based absorption was also evident between 9000–1700 Da (Figure 2.S6, Supplemental Information). This absorption, which is only evident by magnifying the plots and excluding the $P_{500/700}$ peaks, suggests that there is a low intensity broad statistical distribution of polyP chain lengths underlying higher-intensity peaks corresponding to particular polyP lengths.

We considered that some polyP chains hydrolyzed during isolation; this would explain the dominance of the 500 Da peak (as P_i). However, two batches isolated in the presence of phosphatase inhibitors cocktail did not yield significant changes in the intensities or elution volumes of our phosphorus-based chromatograms (Figure 2.S7, Supplemental Information), suggesting that degradation during isolation was not a major problem.

Evidence for iron:polyP complexes in vacuoles

Iron and phosphorus peaks comigrated in most batches. For example, using pH 8.5 mobile phase, iron and phosphorus peaks at 1700, 1400, 1100, and 500 Da comigrated. At pH 6.5, these same elements approximately comigrated at ca. 1200 Da. There were also unresolved minor phosphorus peaks in the region between 2200–1200 Da that comigrated with iron peaks. Iron and phosphorus peaks did not always comigrate, probably because the concentration of phosphorus was so much higher than the metal; thus the majority of observed polyP chains lacked iron and these would not comigrate.

Based on these results, we hypothesized that the comigrating peaks arose from Fe^{III}-polyP coordination complexes with masses between 1700–500 Da. One caveat was that with a mobile phase at pH 6.5, iron did not comigrate with the P_i peak at 500 Da.

The possibility that we were observing Fe^{III}-polyP complexes prompted us to prepare

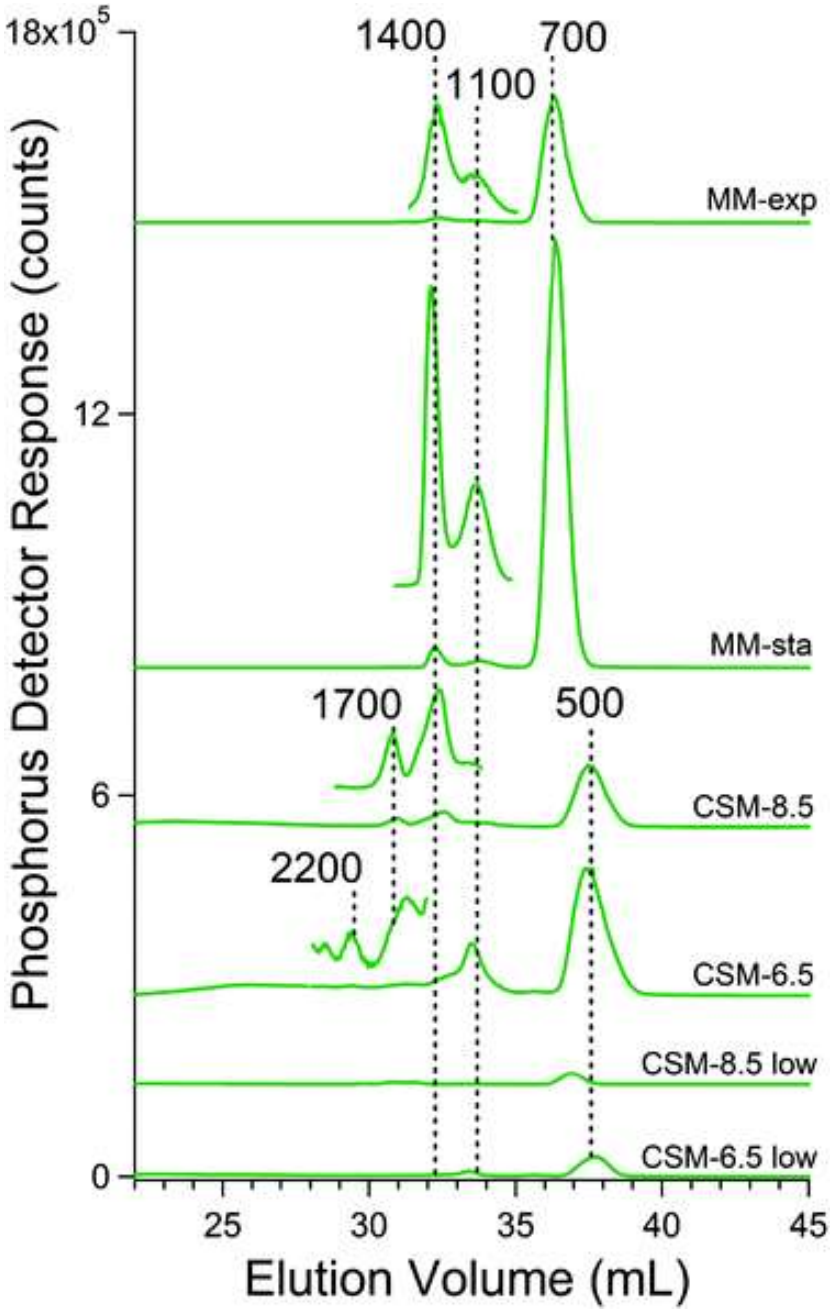

Figure 2.4: Averaged phosphorus-detected chromatograms of FTS from isolated vacuoles (reprinted from reference 41)**.** Trace labels are as in Figure 2.3 (41).

synthetic Fe^{III}-polyP complexes and examine their LC properties. Commercially purchased sodium polyP was incubated with $FeCl_3$ and passed through the 10 kDa cut-off membrane using the same procedure used to prepare vacuolar FTSs. Synthetic FTS was chromatographed as above, affording the traces shown in Figure 2.5 which included iron peaks with approximate masses of 1400, 1200, and 900 Da. Phosphorus-based traces also showed peaks in this region, albeit not always perfectly comigrating. The experiment was performed three times with similar results within the displayed region. When $FeCl_3$ was injected onto the column in the absence of polyP, only an iron-detected peak corresponding to a mass of 24 000 Da was observed (Figure 2.5 inset). This peak was probably due to nanoparticle aggregates. Some of the added iron probably adsorbed onto the column and was not detected. A control sample of polyP alone also did not exhibit any Fe-detected peaks in the LMM region (Figure 2.5). However, LC traces from polyP samples that had been incubated with $FeCl_3$ at increasing concentrations exhibited increasingly intense iron peaks between 1400–900 Da (Figure 2.5). No peaks at or near 24 000 Da were present. Two other experiments showed similar results (data not shown). We tentatively conclude that the iron and phosphorus peaks observed here arose from particularly stable Fe^{III}-polyP complexes with apparent masses of 1400, 1200, and 900 Da. This supports our hypothesis that the comigrating Fe and P peaks observed in the same region of the chromatograms of the FTSs of vacuolar extracts arose from Fe^{III}-polyP complexes of similar composition.

FTSs of vacuolar extracts arose from Fe^{III}-polyP complexes of similar composition. Complexes of particular masses were most evident in contrast to a broad binomial distribution of Fe^{III}-polyP complexes. The observed complexes must be either particularly stable or biosynthesized at higher levels.

If these peaks from vacuolar FTS arose from iron:polyP complexes, we reasoned that

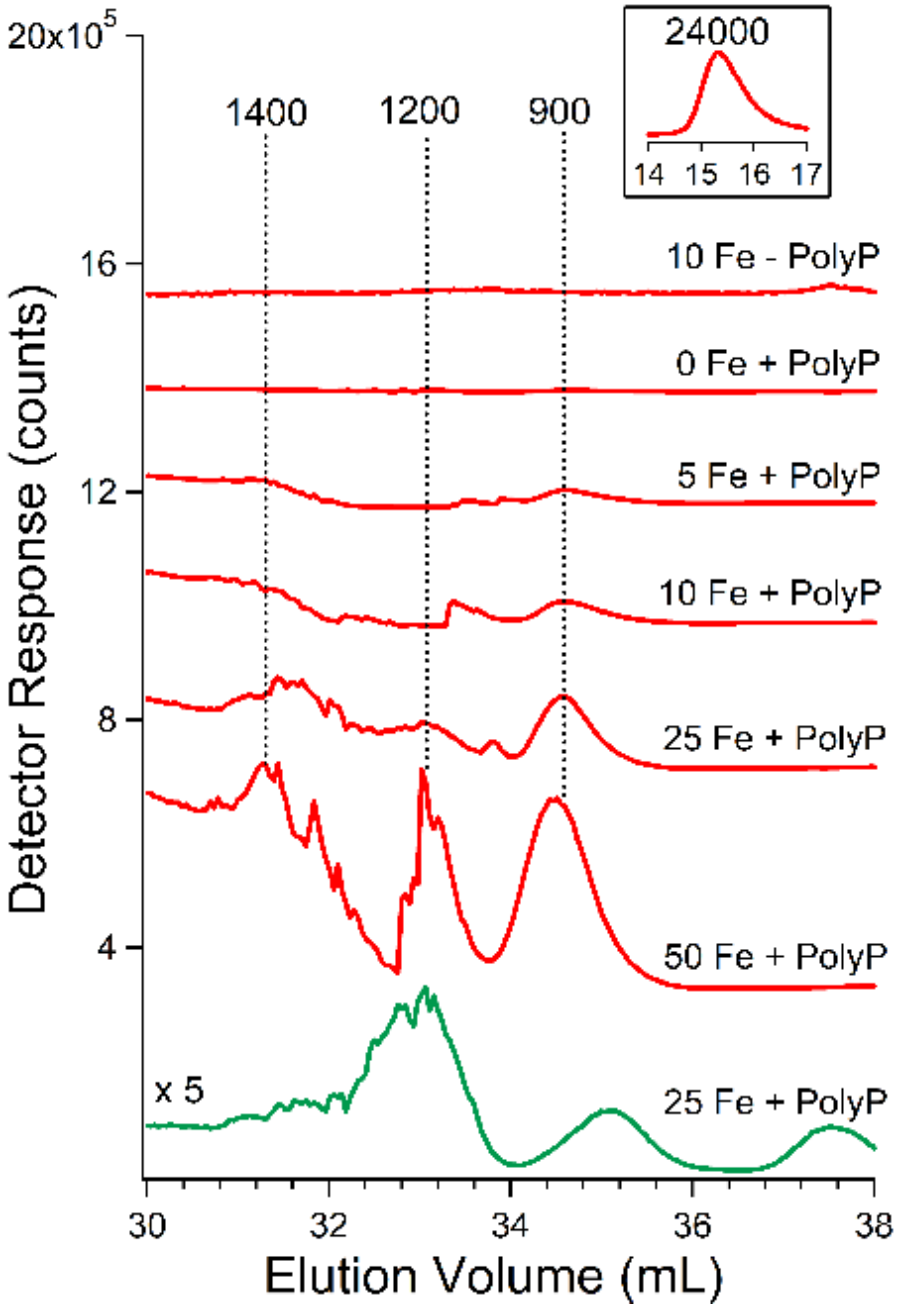

Figure 2.5: Chromatography traces of synthetic Fe^{III}-polyphosphate (reprinted from reference 41)**.** Red traces are Fe, green trace is P. The number before Fe indicates the concentration of $FeCl_3$ in μM used. The concentration of PolyP was 0.5 mg/mL in all runs. The inset above the top trace is of the same trace but at an earlier elution volume. The pH of the mobile phase was 8.5 (41).

treating vacuolar FTS with acid phosphatase ought to disrupt the complexes. The control trace for such an experiment (prior to treatment) exhibited iron peaks at 1400, 700, and 500 Da and phosphorus peaks at 1400 and 500 Da (Figure 2.6, *Fe-pre* and *P-pre*). Minor unresolved broad phosphorus-based peaks in the HMM region (ca. 5500 Da) were also observed. After treatment with acid phosphatase, the LMM iron peaks disappeared as iron peaks in the HMM void-volume region increased (Figure 2.6, *Fe-post*). After treatment, the resulting phosphorus-detected trace exhibited an intense peak at 500 Da, stronger than in the control, and the peaks at 5500 Da and 1400 Da were gone (Figure 2.6, *P-post*). We conclude that the FTS of vacuoles contain iron:polyP complexes with masses between 1400–500 Da, and that iron ions were released when the polyP chains were hydrolyzed by the phosphatase, generating P_i that contributed at 500 Da. The released iron aggregated to exhibit the void peak in the Fe-post trace.

Vacuoles also contains LMM zinc and manganese complexes

Zinc-detected chromatograms of vacuolar FTSs exhibited peaks at apparent masses between 1500–1200 Da (Figure 2.7). Zn_{1400} and Zn_{1500} dominated when the mobile phase was pH 8.5 whereas Zn_{1200} dominated at pH 6.5. Zinc peaks were generally more intense from batches that had been supplemented with zinc acetate in the growth medium (Figure 2.S4, Supplemental Information). These peaks were also affected by phosphatase treatment (Figure 2.6, *Zn-pre* vs. *Zn-post*) indicating that they also arose from zinc:polyP complexes. Most zinc ions eluted at the void volume after treatment, again suggesting aggregation. Curiously one peak (Zn_{1400}) remained after phosphatase treatment suggesting a different coordinating ligand. Zinc ions in vacuoles have been suggested to bind to glutamate and citrate (42).

The corresponding manganese-detected traces showed more variability than other metals

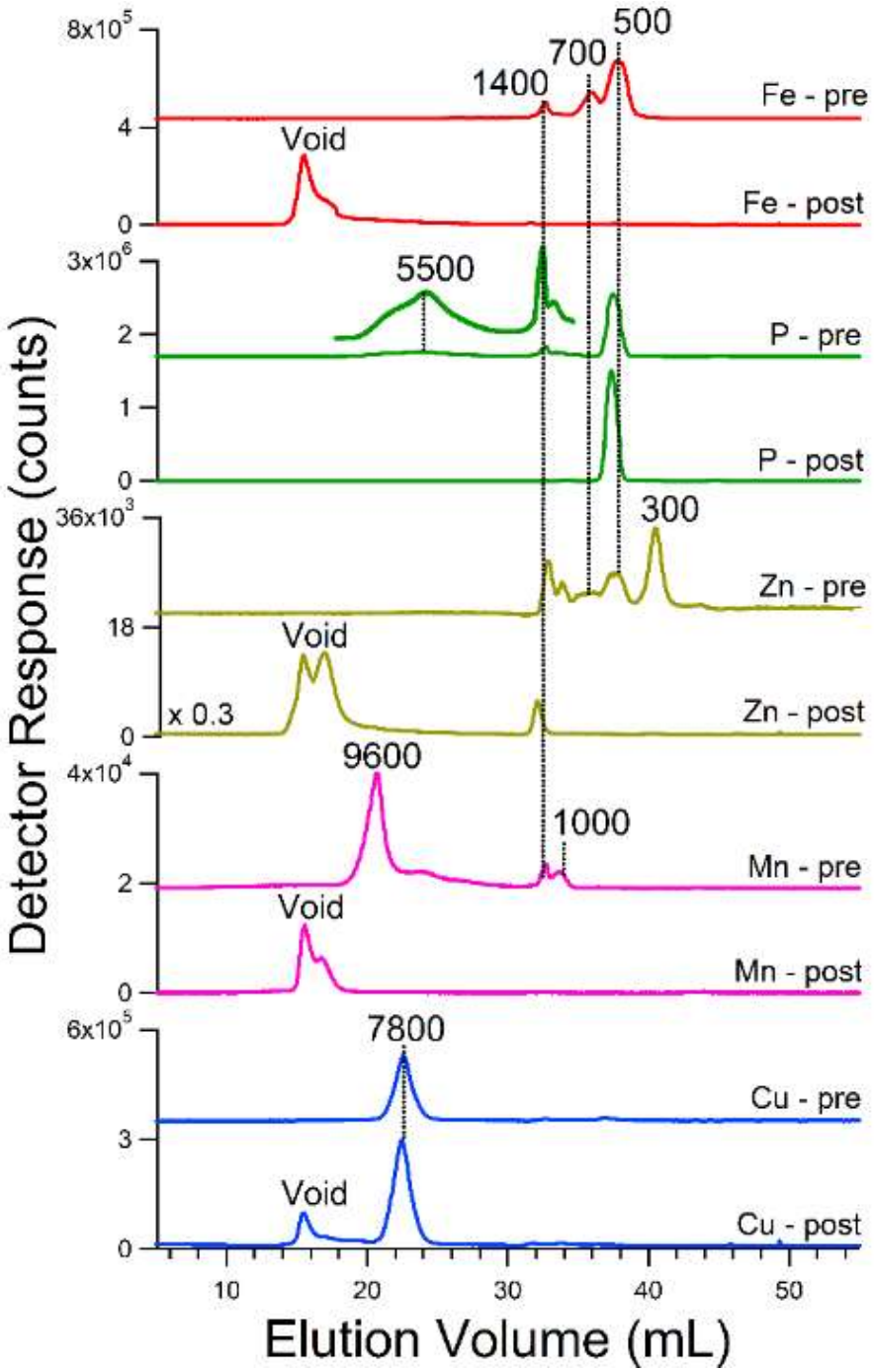

Figure 2.6: Effect of acid phosphatase on vacuolar FTS traces of batch 13 (reprinted from reference 41)**.** Element symbol: -*pre*, before treatment; element-symbol: -*post*, after treatment. See Experimental procedures for reaction details (41).

in terms of masses and intensities (Figure 2.8). Most traces exhibited peaks between 1700–1300 Da but some exhibited peaks with masses between 9600–4700 Da. Using a mobile phase pH of 8.5, LMM species dominated (especially Mn_{1400} for cells grown in MM, and Mn_{1300} and Mn_{1500} for cells grown on CSM). Using a mobile phase of pH 6.5, HMM species between 9600–4700 Da were evident. Broad low-intensity manganese and phosphorus absorption above 3000 Da were also evident (Figure 2.S6, Supplemental Information). Assuming that this absorption reflects polyP chains of all possible lengths, manganese appears to bind randomly to this distribution (more so than other elements). Supplementing the growth medium with $MnCl_2$ had no noticeable effect on the intensities of the LMM Mn species. Mn peaks were also sensitive to phosphatase treatment (Figure 2.6) suggesting that they (including the HMM species) arose from manganese:polyP complexes.

Vacuolar FTS contains both HMM and LMM copper species

Copper-detected traces of FTS exhibited both high- and low-molecular mass features, with relative intensities affected by the growth medium. Chromatograms of vacuolar FTS from cells grown on MM (Figure 2.9) contained a high-mass peak at ca. 7800 Da as well as a LMM peak at 1400 Da. Cu_{1400} was absent in the CSM-based traces. Traces from cells grown on CSM were dominated by peaks with masses between 7800–4800 Da. Low-mass peaks between 1400–600 Da were generally present but of minor intensity relative to the higher-mass peaks. Using a mobile phase pH of 6.5, copper-detected traces of vacuolar FTS were dominated by two HMM copper species at 6400 and 4800 Da (Figure 2.9), whereas at pH 8.5, the major species was at 7800 Da. Cu_{7800} remained in vacuolar FTSs treated with acid phosphatase (Figure 2.6, bottom panel), Cu_{7800} remained in vacuolar FTSs treated with acid phosphatase (Figure 2.6, bottom panel), suggesting

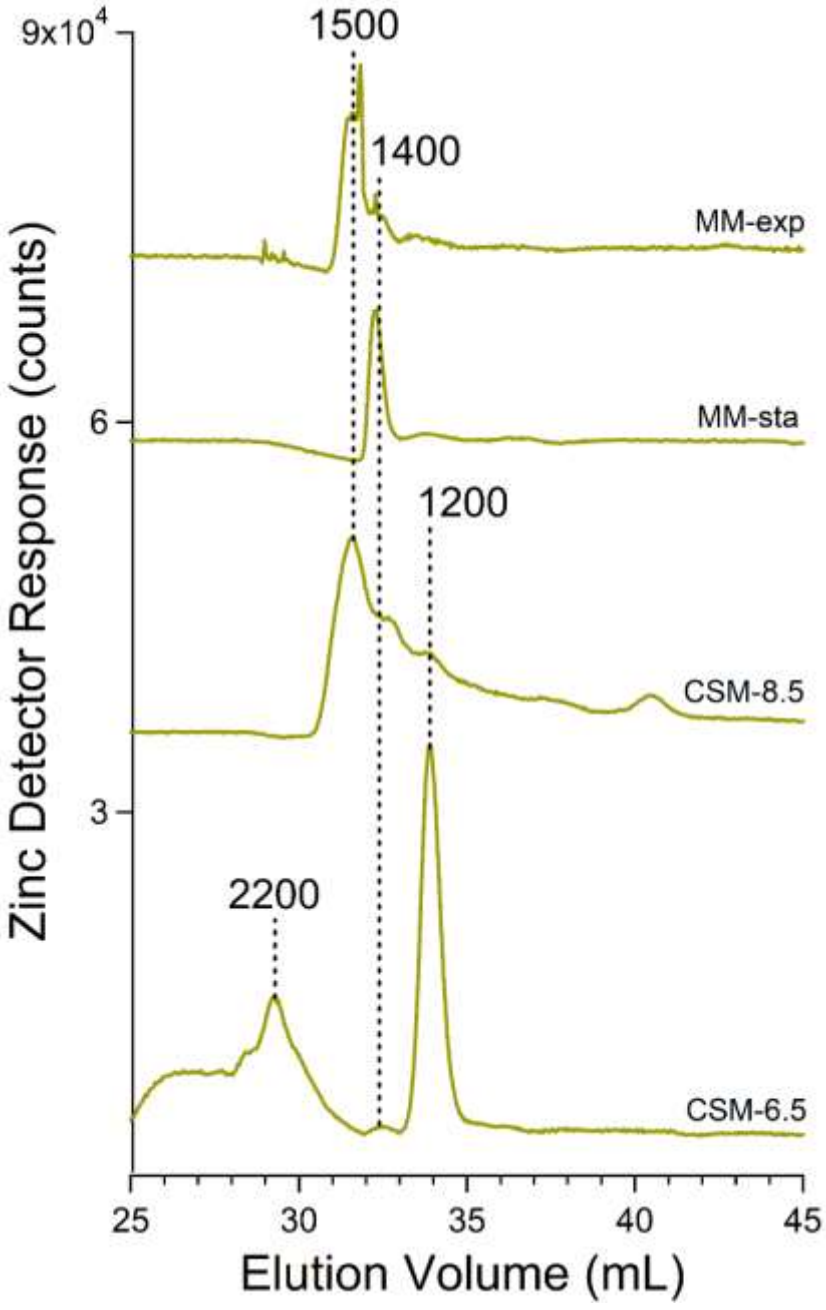

Figure 2.7: Averaged zinc-detected chromatograms of FTSs from isolated vacuoles (reprinted from reference 41)**.** Trace labels are as in Figure 2.3 (41).

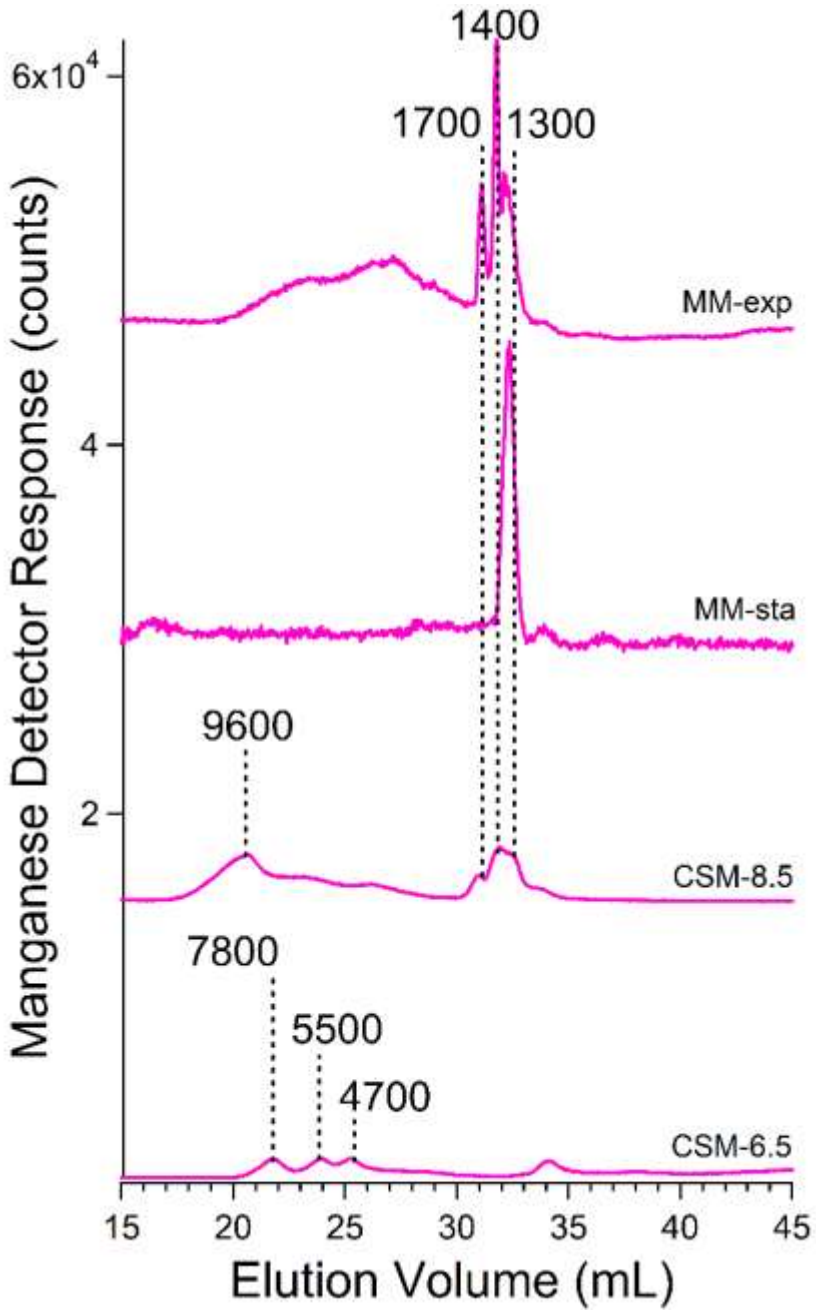

Figure 2.8: Averaged manganese-detected chromatograms of FTSs from isolated vacuoles (reprinted from reference 41)**.** Trace labels are as in Figure 2.3 (41).

that this species is not polyP-based.

We considered that one or both of the HMM copper species with masses of 7800–4800 Da was either Cup1 or Cox17. Cup1 is a ~6600 Da cytosolic copper-storage metallothionein protein (43). Cox17 is a ~7900 Da mitochondrial copper-binding protein that traffics copper to cytochrome c oxidase (44). To examine these possibilities, we isolated vacuoles from *cup1*Δ and *cox17*Δ cells that had been grown on CSM and harvested during stationary phase. *cup1*Δ cells grew slower than normal and reached an OD_{600} of only ~5 (WT cells typically reach an OD_{600} of 7–8). The resulting chromatogram of the FTS from cox17Δ cells in one batch was devoid of Cu7800 (Figure 2.10, panel A). The equivalent chromatogram from another batch contained a peak at ca. 7800 Da but the intensity was less relative to vacuoles from WT cells. The results using vacuolar FTS from *cup1*Δ cells were more definitive, in that the HMM copper species observed in WT batches was absent in each of the four batches examined (Figure 2.10, panel B). We conclude that the high- mass Cu peak is composed of Cup1. The deletion of Cox17 may exhibit pleiotropic effects that involve high-mass Cu peaks.

Relative to typical WT copper-based chromatograms, the FTS from *cup1*Δ and *cox17*Δ vacuoles contained more intense copper features in what we call the "true" LMM region (2000–500 Da) where proteins are unlikely to be coordinating ligands. The copper ions in this region appear to be coordinated to polyP chains as evidenced by comigrating phosphate-based species of similar masses (1700 and 1500 Da, see Figure 2.10 green lines).

Discussion

The vacuoles play major roles in the trafficking and homeostasis of metal ions in fungi and plants. This includes the dynamic storage and recycling of essential metal ions as well as the

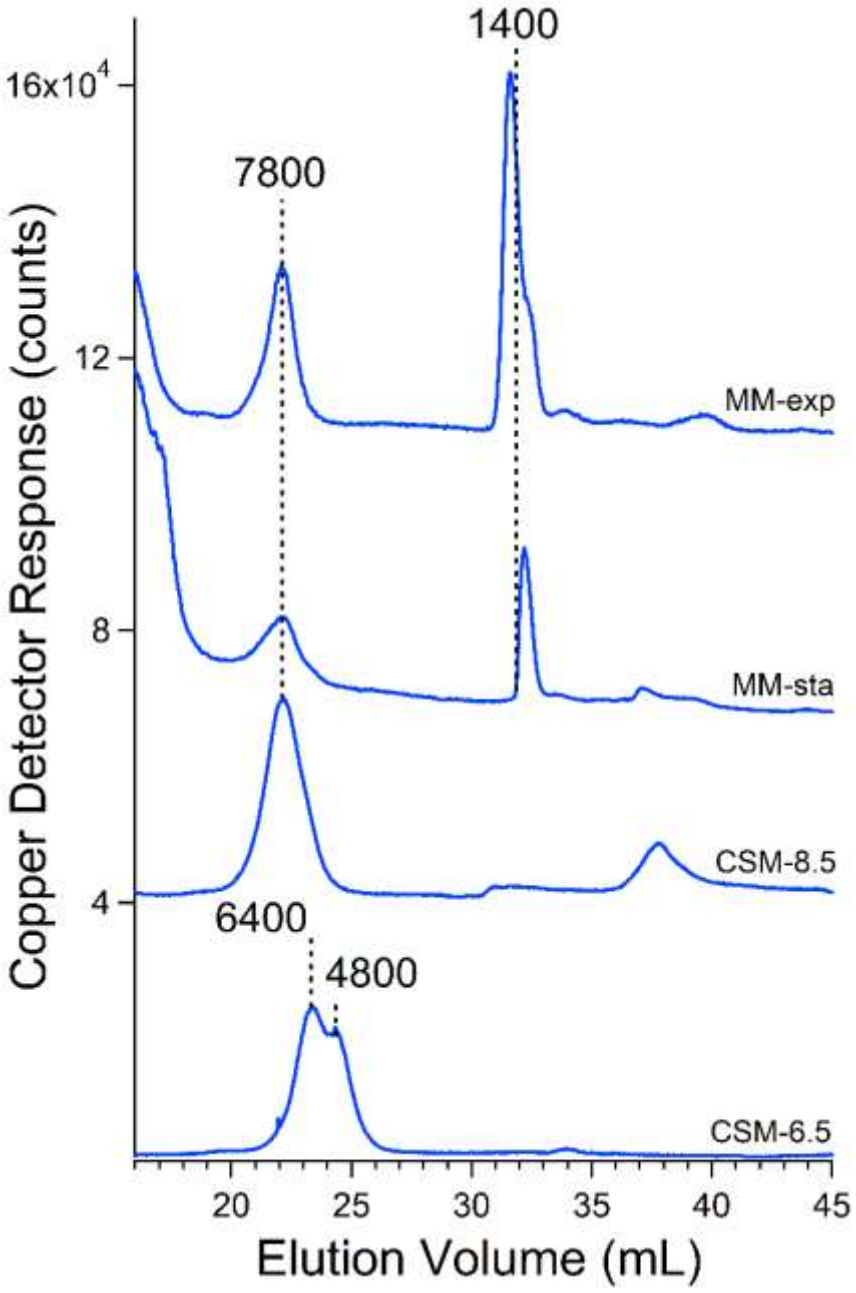

Figure 2.9: Averaged copper-detected chromatograms of FTSs from isolated vacuoles (reprinted from reference 41)**.** Trace labels are as in Figure 2.3 (41).

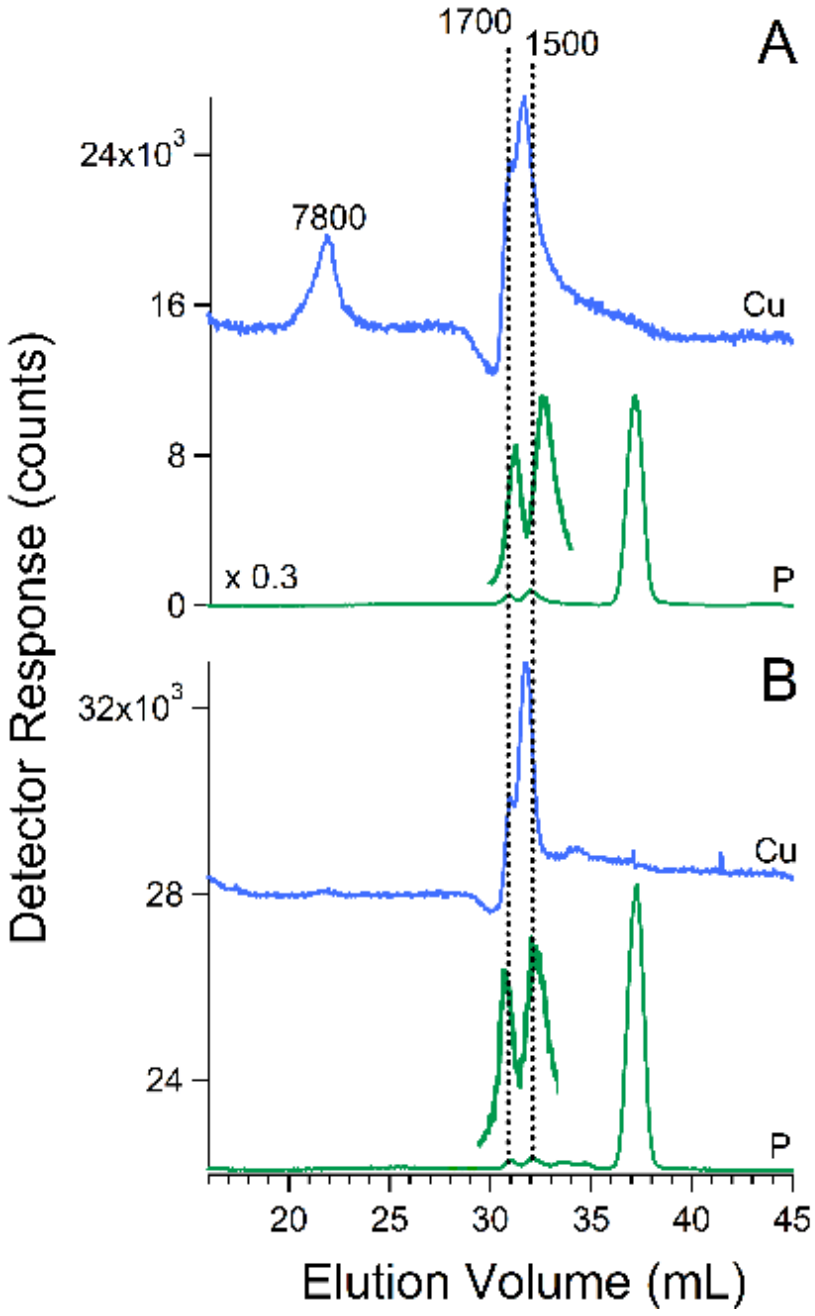

Figure 2.10: Copper and phosphorus-detected chromatograms of FTS from isolated vacuoles of *cox17*Δ and *cup1Δ* strains (reprinted from reference 41)**.** *cox17*Δ strain is panel A and *cup1Δ* strain is panel B. Blue trace is Cu, green trace is P. The pH of the mobile phase was 8.5 (41).

sequestration of what would otherwise be toxic metal ions. Despite these important roles, few mechanistic details are known regarding these processes. One reason is that vacuoles are difficult to purify, especially in the large quantities required for the biophysical, bioinorganic, and bioanalytical analyses that could tease-apart many of these details. In this study, we report a robust large-scale isolation method along with the first chromatographic characterization of the metal ions bound to polyphosphate in these organelles.

We first isolated vacuoles from cells grown exponentially on minimal media, but found that yields and reproducibility were better using cells grown on complete synthetic media and harvested in early stationary phase. Perhaps this is because vacuoles complete their biogenesis and morph into a single large structure during early stationary phase (45). Even under these optimized conditions, we were unable to purify vacuoles completely; Western blot and confocal microscopic analyses showed some contamination of ER and cytosol – but not mitochondria. Thus, our batches should be viewed as highly enriched in vacuoles but with minor cytosol and ER contamination. The contamination was not a severe problem for our iron-related studies because most cellular iron is either in vacuoles or mitochondria; the iron concentrations in ER and cytosol are lower. ER and vacuoles are involved in the receptor-mediated sorting pathway of soluble vacuolar hydrolases (46).As a result, it may not be possible to completely separate these two organelles. Due to these concerns and the lability of low-molecular-mass metal complexes, we decided to isolate a large number of batches and search for reproducible patterns. Rather than selecting one "representative" chromatogram for presentation, we present many traces and their averages to allow readers to assess for themselves the degree of reproducibility obtained. We regard this as laying the foundation for establishing the metal-related biochemistry associated with these delicate and intransigent organelles.

Our LC results provide the strongest evidence to date that most of the iron, zinc, and manganese ions (and some copper ions) in vacuoles are coordinated to polyP chains. Previous investigators used thermodynamic arguments based on the known strong coordination of these metal ions to polyP anionic chains in conjunction with the presence of high concentrations of iron and polyP in vacuoles to speculate that vacuoles contain such complexes. Previous studies from our lab focused on the spectroscopic properties of the iron in vacuoles which suggested the presence of Fe^{III}-polyP complexes. The behavior of vacuolar iron with variations of pH were also similar to those of authentic Fe^{III}-polyP complexes. The current study is the first to examine the metal and phosphorus content of isolated vacuoles using liquid chromatography.

Our results indicate that all of the four investigated metals in vacuoles are present in low-molecular-mass forms within vacuoles that migrate according to masses ranging from 10 000–500 Da (see following scheme 2.1).

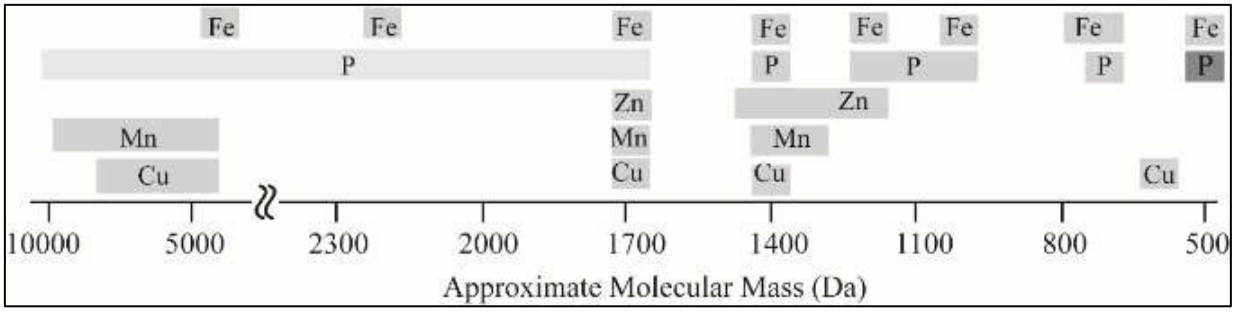

Scheme 2.1: Mass range of transition metals LMM complexes in vacuoles (reprinted from reference 41)**.**

Many (but not all) of the observed LC peaks comigrated with phosphorus, supporting the presence of metal:polyphosphate complexes in these organelles. Treatment with polyphosphatase disrupted these complexes, supporting this assignment. There were numerous instances in which the metals comigrated with each other, suggesting that multiple metals either bind to the same chain or to different chains of about the same length.

The length distribution of polyP chains in our samples was not primarily binomial. Rather, chains of 6–20 units long dominated, suggesting that these lengths were either especially stable or produced at especially high rates. We cannot explain these preferences but they must reflect the steady-state distribution resulting from opposing polyP synthesis and degradation processes. Metals may also preferentially bind to and/or stabilize chains of particular lengths e.g. due to chelation effects.

We calculated the molar ratio of phosphorus to iron, zinc, manganese and copper in the vacuolar FTS, and determined the percentage of each due to particular peaks in representative chromatograms. In most traces, the dominating $P_{500/700}$ peak represented 90–95% of the phosphorus in the sample. The LMM Fe species represented 80% of the iron in the sample. Thus, the P/Fe ratio for the LMM peaks should be roughly 10: 1. This implies that one iron ion is coordinated, on average, to an n = 10 polyP chain. For a given polyP chain, one or two metal ions should be bound on average. The drawing in Figure 2.11 represents a hypothetical metal-bound polyP chain.

Gerasimaite *et al.* reported that polyP was degraded during vacuolar isolation (31) and we considered that a similar phenomenon occurred here – i.e. a significant portion of the polyP may have hydrolyzed during our vacuolar isolation. However, our experiments in which phosphatase

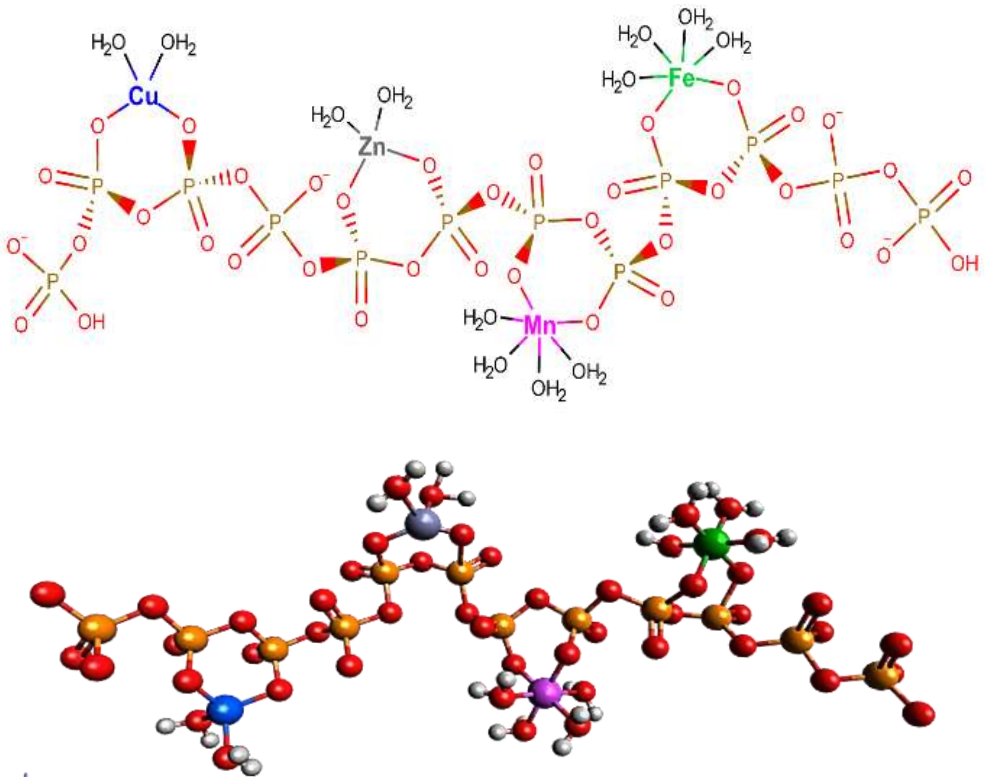

Figure 2.11: Hypothetical structure of a n = 12 metal:polyphosphate complex with a mass of ca. 1400 Da (reprinted from reference 41)**.** Metals are presumed to bind as chelates to a floppy chain. It is statistically unlikely that all four metal ions coordinate, as drawn, to a single chain of this length. No particular stereochemistry is implied. 2D and 3D structures were generated using MarvinSketch (https://chemaxon.com/products/marvin) and Avogadro (https://avogadro.cc/), respectively (41).

inhibitors were included during vacuolar isolation did not support this. Also, the masses of LMM metal:polyP species observed suggests polyP chain lengths in the same range as has been observed in previous studies. Trilisenko *et al.* reported an average polyP chain length (at pH 8.2) in isolated vacuoles of 5 ± 2 (47). They also found that 96% of phosphorus in isolated vacuoles was PolyP, with the remaining 4% present as P_i. The dominant phosphorus-detected peaks with approximate masses of 500–700 Da that we observe may arise from a mixture of short (n = 6–8) polyP chains and P_i.

Most copper ions in isolated vacuoles were present as 1–2 species with masses of 7800–4800 Da. These Cu peaks did not disappear after phosphatase treatment suggesting that they were not due to polyP complexes; we suspect that they are protein-bound and include Cup1. The situation may be different for the HMM manganese species, which migrated at the void volume after treatment with polyphosphatase. This suggests that high-mass manganese polyP complexes can form.

Whether the detected Cup1 copper protein was present within vacuoles or in the cytosol contaminants of our batches is unknown. We favor the former possibility because the HMM copper species in our chromatograms were intense and present in nearly all batches; this is not the typical behavior of contaminants in which wide variations in peak intensities would be expected.

Few copper ions in vacuolar FTSs from WT cells grown on CSM medium were present as nonproteinaceous LMM species. However, the proportion of LMM copper increased significantly in samples from *cup1*Δ and *cox17*Δ cells; this proportion also was higher in WT cells grown on minimal medium. We hypothesize that dysregulation of copper homeostasis caused by the absence of Cup1 and Cox17 (or by growth of WT cells on minimal media) resulted in higher concentrations of aqueous copper ions, which were ultimately trafficked into vacuoles and bound to polyP for

sequestration and detoxification. Gray and Jakob have suggested that the coordination of copper ions to polyP suppresses the tendency of copper to participate in Fenton-type reactions (48). We hypothesize that the proportion of copper present as LMM nonproteinaceous species is either related to the degree of copper dysregulation or to a lack of copper chaperones or storage proteins.

Our major foci for this study were iron and copper speciation in vacuoles, but we also probed zinc and manganese. Under most conditions of this study, isolated vacuoles contained 8 times more iron than zinc and 50 times more iron than manganese. Although some batch-to-batch variations were observed, it is clear that most of the zinc and manganese ions coordinate to polyP chains. The majority of vacuolar LMM complexes of zinc and manganese were found to bind to polyP between 1400–1300 Da. One or more of these LMM zinc species may be used to metallate Pho8 alkaline phosphatase. Qiao *et al*. showed that metallating alkaline phosphatase Pho8 depended on vacuolar zinc importers Zrc1 and Cot1 implying that vacuolar zinc is installed in apo-Pho8 (49).

With this foundation laid, further advances in understanding the important role of these organelles in the cellular biology of metals should be forthcoming. We are interested in probing the redox properties of iron in vacuoles and exploring the trafficking of vacuolar iron to and from other cellular compartments including cytosol and mitochondria. The effect of nutrient phosphorus levels and the vacuolar polyphosphatases on the metal and polyP content of vacuoles might also be revealing. We attempted to isolate vacuoles under low P_i medium to investigate the effect on the storage capabilities of transition metals. Unfortunately, our yields were insufficient for LC analysis. It may be useful to study vacuoles isolated from genetic strains in which vacuolar polyP levels are altered or in which another metallothionein (*CRS5*) is deleted.

References

1. Docampo, R., Ulrich, P., and Moreno, S. N. J. (2010) Evolution of acidocalcisomes and their role in polyphosphate storage and osmoregulation in eukaryotic microbes. *Philos. Trans. R. Soc. B Biol. Sci.* **365**, 775–784
2. Blaby-Haas, C. E., and Merchant, S. S. (2014) Lysosome-related organelles as mediators of metal homeostasis. *J. Biol. Chem.* **289**, 28129–28136
3. Gerasimaite, R., Sharma, S., Desfougeres, Y., Schmidt, A., and Mayer, A. (2014) Coupled synthesis and translocation restrains polyphosphate to acidocalcisome-like vacuoles and prevents its toxicity. *J. Cell Sci.* **127**, 5093–5104
4. Kane, P. M. (2016) Proton transport and pH control in fungi. in *Advances in Experimental Medicine and Biology*, **892**, 33–68.
5. Greenfield, N. J., Hussain, M., and Lenard, J. (1987) Effects of growth state and amines on cytoplasmic and vocuolar pH, phosphate and polyphosphate levels in *Saccharomyces cerevisiae*: a ^{31} P-nuclear magnetic resonance study. *BBA - Gen. Subj.* **926**, 205–214
6. McNaughton, R. L., Reddi, A. R., Clement, M. H. S., Sharma, A., Barnese, K., Rosenfeld, L., Gralla, E. B., Valentine, J. S., Culotta, V. C., and Hoffman, B. M. (2010) Probing in vivo Mn^{2+} speciation and oxidative stress resistance in yeast cells with electron-nuclear double resonance spectroscopy. *Proc. Natl. Acad. Sci. U. S. A.* **107**, 15335–15339
7. Bode, H. P., Dumschat, M., Garotti, S., and Fuhrmann, G. F. (1995) Iron sequestration by the yeast vacuole: a study with vacuolar mutants of *Saccharomyces cerevisiae*. *Eur. J. Biochem.* **228**, 337–342
8. Paidhungat, M., and Garrett, S. (1998) Cdc1 and the vacuole coordinately regulate Mn^{2+} homeostasis in the yeast *Saccharomyces cerevisiae*. *Genetics*. **148**, 1787–1798

9. Raguzzi, F., Lesuisse, E., and Crichton, R. R. (1988) Iron storage in *Saccharomyces cerevisiae*. *FEBS Lett.* **231**, 253–258

10. Okorokov, L. A., Lichko, L. P., and Andreeva, N. A. (1983) Changes of ATP, polyphosphate and K^+ contents in *Saccharomyces carlsbergensis* during uptake of Mn^{2+} and glucose. *Biochem. Int.* **6**, 481–488

11. White, C. M., and Gadd, G. M. (1987) The uptake and cellular distribution of zinc in *Saccharomyces cerevisiae*. *J. Gen. Microbiol.* **133**, 727–787

12. Ramsay, L. M., and Gadd, G. M. (1997) Mutants of *Saccharomyces cerevisiae* defective in vacuolar function confirm a role for the vacuole in toxic metal ion detoxification. *FEMS Microbiol. Lett.* **152**, 293–298

13. Nishimura, K., Igarashi, K., and Kakinuma, Y. (1998) Proton gradient-driven nickel uptake by vacuolar membrane vesicles of *Saccharomyces cerevisiae. J. Bacteriol.* **180**, 1962–1964

14. Bleackley, M. R., Young, B. P., Loewen, C. J. R., and MacGillivray, R. T. A. (2011) High density array screening to identify the genetic requirements for transition metal tolerance in *Saccharomyces cerevisiae*. *Metallomics*. **3**, 195–205

15. Li, L., Chen, O. S., Ward, D. M. V., and Kaplan, J. (2001) Ccc1 is a transporter that mediates vacuolar iron storage in yeast. *J. Biol. Chem.* **276**, 29515–29519

16. Pimentel, C., Vicente, C., Menezes, R. A., Caetano, S., Carreto, L., and Rodrigues-Pousada, C. (2012) The role of the Yap5 transcription factor in remodeling gene expression in response to fe bioavailability. *PLoS One*. **7**, e37434

17. Klompmaker, S. H., Kohl, K., Fasel, N., and Mayer, A. (2017) Magnesium uptake by connecting fluid-phase endocytosis to an intracellular inorganic cation filter. *Nat. Commun.* **8**, 1879

18. Urbanowski, J. L., and Piper, R. C. (1999) The iron transporter Fth1p forms a complex with the Fet5 iron oxidase and resides on the vacuolar membrane. *J. Biol. Chem.* **274**, 38061–38070

19. Portnoy, M. E., Liu, X. F., and Culotta, V. C. (2000) *Saccharomyces cerevisiae* expresses three functionally distinct homologues of the Nramp family of metal transporters. *Mol. Cell. Biol.* **20**, 7893–7902

20. Singh, A., Kaur, N., and Kosman, D. J. (2007) The metalloreductase Fre6p in Fe-efflux from the yeast vacuole. *J. Biol. Chem.* **282**, 28619–28626

21. Cockrell, A. L., Holmes-Hampton, G. P., McCormick, S. P., Chakrabarti, M., and Lindahl, P. A. (2011) Mössbauer and EPR study of iron in vacuoles from fermenting *Saccharomyces cerevisiae*. *Biochemistry*. **50**, 10275–10283

22. Cockrell, A., McCormick, S. P., Moore, M. J., Chakrabarti, M., and Lindahl, P. A. (2014) Mössbauer, EPR, and modeling study of iron trafficking and regulation in *Δccc1* and *CCC1*-up *Saccharomyces cerevisiae*. *Biochemistry*. **53**, 2926–2940

23. Park, J., McCormick, S. P., Cockrell, A. L., Chakrabarti, M., and Lindahl, P. A. (2014) High-spin ferric ions in *Saccharomyces cerevisiae* vacuoles are reduced to the ferrous state during adenine-precursor detoxification. *Biochemistry*. **53**, 3940–3951

24. Secco, D., Wang, C., Shou, H., and Whelan, J. (2012) Phosphate homeostasis in the yeast *Saccharomyces cerevisiae*, the key role of the SPX domain-containing proteins. *FEBS Lett.* **586**, 289–295

25. Auesukaree, C., Homma, T., Tochio, H., Shirakawa, M., Kaneko, Y., and Harashima, S. (2004) Intracellular phosphate serves as a signal for the regulation of the PHO pathway in *Saccharomyces cerevisiae*. *J. Biol. Chem.* **279**, 17289–17294

26. Gerasimaite, R., and Mayer, A. (2016) Enzymes of yeast polyphosphate metabolism: Structure, enzymology and biological roles. *Biochem. Soc. Trans.* **44**, 234–239

27. Hothorn, M., Neumann, H., Lenherr, E. D., Wehner, M., Rybin, V., Hassa, P. O., Uttenweiler, A., Reinhard, M., Schmidt, A., Seiler, J., Ladurner, A. G., Herrmann, C., Scheffzek, K., and Mayer, A. (2009) Catalytic core of amembrane-associated eukaryotic polyphosphate polymerase. *Science.* **324**, 513–516

28. Sethuraman, A., Rao, N. N., and Kornberg, A. (2001) The endopolyphosphatase gene: Essential in *Saccharomyces cerevisiae*. *Proc. Natl. Acad. Sci. U. S. A.* **98**, 8542–8547

29. Breitkreutz, A., Choi, H., Sharom, J. R., Boucher, L., Neduva, V., Larsen, B., Lin, Z. Y., Breitkreutz, B. J., Stark, C., Liu, G., Ahn, J., Dewar-Darch, D., Reguly, T., Tang, X., Almeida, R., Qin, Z. S., Pawson, T., Gingras, A. C., Nesvizhskii, A. I., and Tyers, M. (2010) A global protein kinase and phosphatase interaction network in yeast. *Science.* **328**, 1043–1046

30. Hurley, J. H., and Emr, S. D. (2006) The ESCRT complexes: Structure and mechanism of a membrane-trafficking network. *Annu. Rev. Biophys. Biomol. Struct.* **35**, 277–298

31. Gerasimaite, R., and Mayer, A. (2017) Ppn2, a novel Zn^{2+}-dependent polyphosphatase in the acidocalcisome-like yeast vacuole. *J. Cell Sci.* **130**, 1625–1636

32. Vagabov, V. M., Trilisenko, L. V., Kulakovskaya, T. V., and Kulaev, I. S. (2008) Effect of a carbon source on polyphosphate accumulation in *Saccharomyces cerevisiae*. *FEMS Yeast Res.* **8**, 877–882

33. Andreeva, N., Ryazanova, L., Dmitriev, V., Kulakovskaya, T., and Kulaev, I. (2013) Adaptation of *Saccharomyces cerevisiae* to toxic manganese concentration triggers changes in inorganic polyphosphates. *FEMS Yeast Res.* **13**, 463–470

34. Breus, N. A., Ryazanova, L. P., Dmitriev, V. V., Kulakovskaya, T. V., and Kulaev, I. S. (2012) Accumulation of phosphate and polyphosphate by *Cryptococcus humicola* and *Saccharomyces cerevisiae* in the absence of nitrogen. *FEMS Yeast Res.* **12**, 617–624

35. Van Wazer, J. R., and Callis, C. F. (1958) Metal complexing by phosphates. *Chem. Rev.* **58**, 1011–1046

36. Kulaev, I. S., Vagabov, V. M., and Kulakovskaya, T. V. (2004) *The Biochemistry of Inorganic Polyphosphates*, Wiley, Chichester.

37. Rees, E. M., Lee, J., and Thiele, D. J. (2004) Mobilization of intracellular copper stores by the Ctr2 vacuolar copper transporter. *J. Biol. Chem.* **279**, 54221–54229

38. Rees, E. M., and Thiele, D. J. (2007) Identification of a vacuole-associated metalloreductase and its role in Ctr2-mediated intracellular copper mobilization. *J. Biol. Chem.* **282**, 21629–21638

39. Kosman, D. J. (2003) Molecular mechanisms of iron uptake in fungi. *Mol. Microbiol.* **47**, 1185–1197

40. Dziuba, N., Hardy, J., and Lindahl, P. A. (2018) Low-molecular-mass iron in healthy blood plasma is not predominately ferric citrate. *Metallomics*. **10**, 802–817

41. Nguyen, T. Q., Dziuba, N., and Lindahl, P. A. (2019) Isolated *Saccharomyces cerevisiae* vacuoles contain low-molecular-mass transition-metal polyphosphate complexes. *Metallomics*. **11**, 1298–1309

42. Neddermeyer, P. A., and Rogers, L. B. (1968) Gel filtration behavior of inorganic salts. *Anal. Chem.* **40**, 755–762

43. Kitamoto, K., Yoshizawa, K., Ohsumi, Y., and Anraku, Y. (1988) Dynamic aspects of vacuolar and cytosolic amino acid pools of *Saccharomyces cerevisiae*. *J. Bacteriol.* **170**,

2683–2686

44. Winge, D. R., Nielson, K. B., Gray, W. R., and Hamer, D. H. (1985) Yeast metallothionein. Sequence and metal-binding properties. *J. Biol. Chem.* **260**, 14464–14470

45. Abajian, C., Yatsunyk, L. A., Ramirez, B. E., and Rosenzweig, A. C. (2004) Yeast Cox17 solution structure and copper(I) binding. *J. Biol. Chem.* **279**, 53584–53592

46. Conradt, B., Shaw, J., Vida, T., Emr, S., and Wickner, W. (1992) In vitro reactions of vacuole inheritance in *Saccharomyces cerevisiae*. *J. Cell Biol.* **119**, 1469–1480

47. Horazdovsky, B. F., DeWald, D. B., and Emr, S. D. (1995) Protein transport to the yeast vacuole. *Curr. Opin. Cell Biol.* **7**, 544–551

48. Trilisenko, L. V., Vagabov, V. M., and Kulaev, I. S. (2002) The content and chain length of polyphosphates from vacuoles of *Saccharomyces cerevisiae* VKM Y-1173. *Biochem.* **67**, 592–596

49. Gray, M. J., and Jakob, U. (2015) Oxidative stress protection by polyphosphate-new roles for an old player. *Curr. Opin. Microbiol.* **24**, 1–6

50. Kizawa, K., Aono, T., and Ohtomo, R. (2016) *PHO8* gene coding alkaline phosphatase of *Saccharomyces cerevisiae* is involved in polyphosphate metabolism. *J. Gen. Appl. Microbiol.* **62**, 297–302

Supplemental Information

Batch	Strain	Medium	Harvest	Non-default [M]
01	WT	MM	Stationary	
02	WT	MM	Stationary	
03	WT	MM	Stationary	
04	WT	MM	Stationary	
05	WT	MM	Exponential	
06	WT	MM	Exponential	
07	WT	MM	Exponential	
08	WT	MM	Exponential	
09	WT	MM	Exponential	
10	WT	CSM	Stationary	40 µM Cu; 200 µM Zn; 40 µM Mn
11	WT	CSM	Stationary	40 µM Cu; 200 µM Zn; 40 µM Mn
12	WT	CSM	Stationary	20 µM Cu; 100 µM Zn; 20 µM Mn
13	WT	CSM	Stationary	
14	WT	CSM	Stationary	
15	WT	CSM	Stationary	
16	WT	CSM	Stationary	
17	WT	CSM	Stationary	
18	WT	CSM	Stationary	
19	WT	CSM	Stationary	1 µM Fe
20	WT	CSM	Stationary	1 µM Fe
21	WT	CSM	Stationary	20 µM Cu; 100 µM Zn; 20 µM Mn
22	*cox17*Δ	CSM	Stationary	20 µM Cu; 100 µM Zn; 20 µM Mn
23	*cox17*Δ	CSM	Stationary	20 µM Cu; 100 µM Zn; 20 µM Mn
24	*cup1*Δ	CSM	Stationary	
25	*cup1*Δ	CSM	Stationary	
26	*cup1*Δ	CSM	Stationary	
27	*cup1*Δ	CSM	Stationary	
28	WT	CSM	Stationary	
29	WT	CSM	Stationary	

Table 2.S1: Batches of *Saccharomyces cerevisiae* vacuoles isolation used in this study (reprinted from reference 41). Final supplemented metal concentrations are given in µM. Default supplemented Fe, Cu, Zn, and Mn concentrations were 40, 10, 0, and 0 µM, respectively (41).

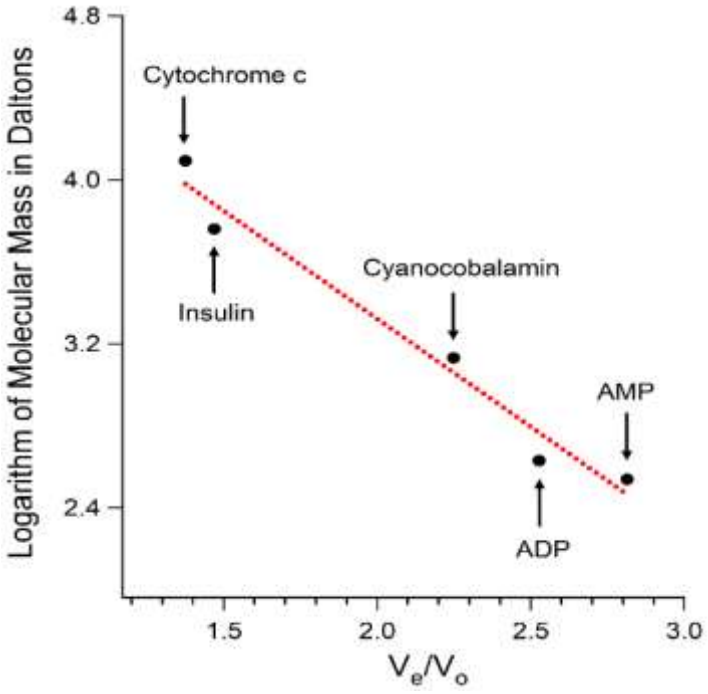

Figure 2.S1: Calibration curve of size exclusion column (reprinted from reference 41)**.** Best-fit line was *Log (Molecular Mass, Da)* = -1.0529×(V_e/V_o) + 5.4287 where V_e and V_o are elution volume and void volume, respectively. The void volume was determined to be 14.94 mL using Blue Dextran (Fisher Scientific). The correlation coefficient R^2 was 0.9607. The molecular masses of standards used for calibration curve were from a previous study (66): cytochrome c *Saccharomyces cerevisiae* (12,384 Da), insulin (5,777 Da), cyanocobalamin (1,355 Da), ADP (427 Da), and AMP (327 Da) (41).

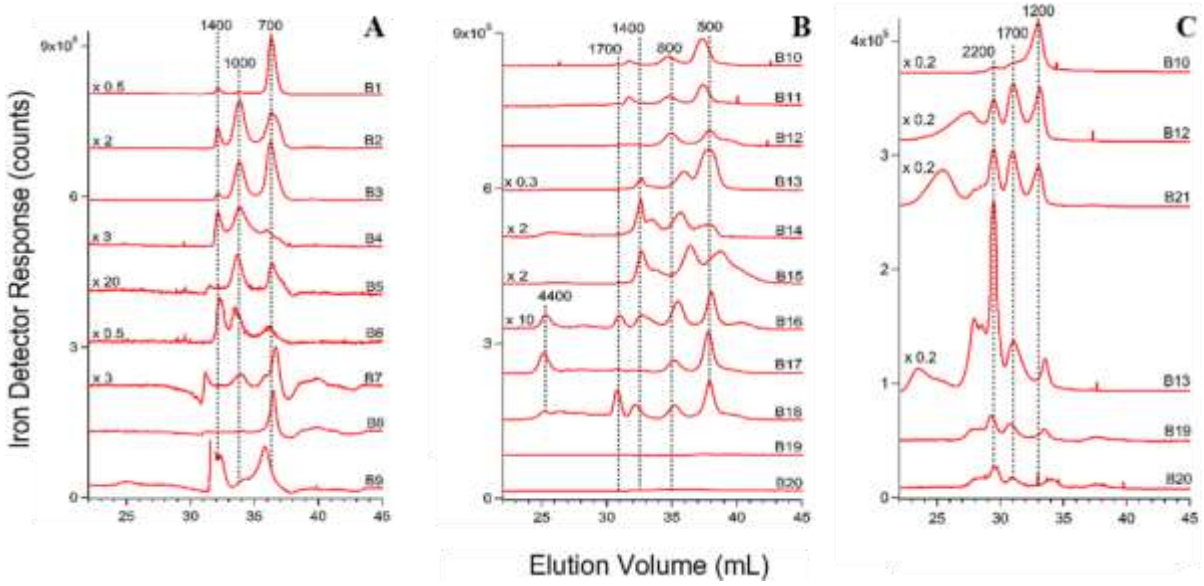

Figure 2.S2: Iron-detected chromatograms of vacuolar FTSs (reprinted from reference 41)**.**
A, Vacuolar FTSs from cells grown in minimal media containing 40 μM Fe^{III} citrate and harvested during stationary (B1 – B4) and exponential (B5 – B9) phases. The mobile phase pH was 8.5. Some trace intensities were multiplied by the indicated factor. Numbers above vertical dashed lines indicate approximate mass in Da for species at that elution volume (41).
B, Vacuole FTSs from cells grown in synthetic complete medium supplemented with 40 μM Fe^{III} citrate and harvested in stationary phase (B10 – B20). Vacuolar FTS of B19 and B20 were prepared in the same way but the media was supplemented with 1 μM Fe^{III} citrate. The mobile phase pH was 8.5 (41).
C, Vacuole FTSs prepared as in B with 40 (B10 – B18) or 1 (B19 – B20) μM Fe^{III} citrate. The mobile phase pH was 6.5 (41).

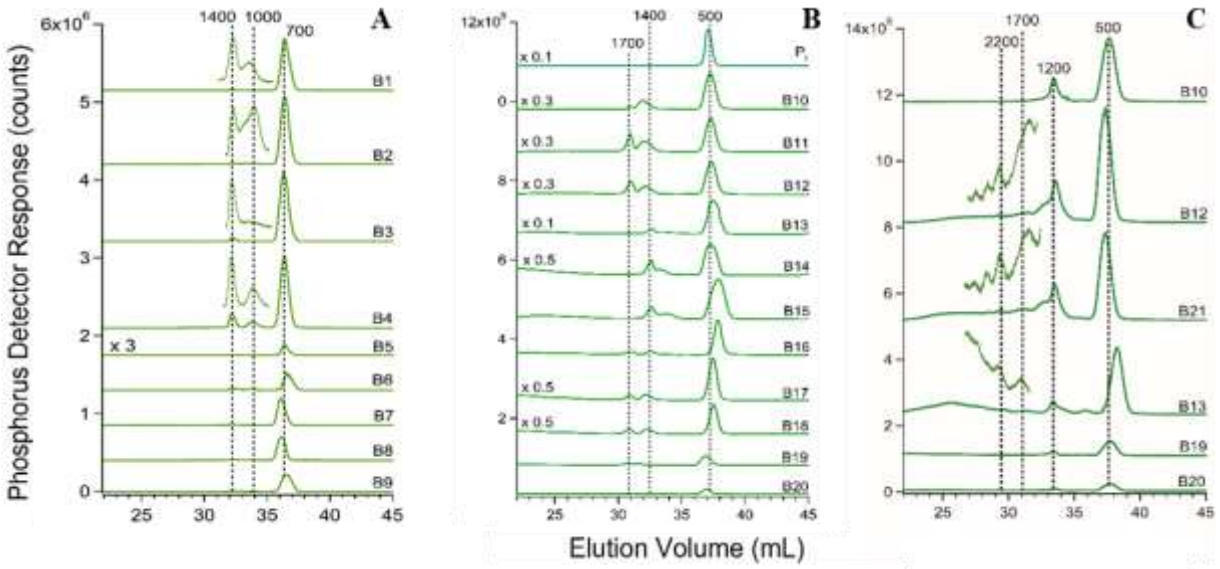

Figure 2.S3: Phosphorus-detected chromatograms of FTS from isolated vacuoles (reprinted from reference 41)**.**

A, Vacuolar FTSs from cells grown in minimal media containing 40 μM Fe^{III} citrate and harvested during stationary (B1 – B4) and exponential (B5 – B9) phases. The mobile phase pH was 8.5. Some trace intensities were multiplied by the indicated factor. Numbers above vertical dashed lines indicate approximate mass in Da for species at that elution volume (41).

B, Vacuole FTSs from cells grown in synthetic complete medium supplemented with 40 μM Fe^{III} citrate and harvested in stationary phase (B10 – B20). Vacuolar FTS of B19 and B20 were prepared in the same way but the media was supplemented with 1 μM Fe^{III} citrate. The mobile phase pH was 8.5 (41).

C, Vacuole FTSs prepared as in B with 40 (B10 – B18) or 1 (B19 – B20) μM Fe^{III} citrate. The mobile phase pH was 6.5 (41).

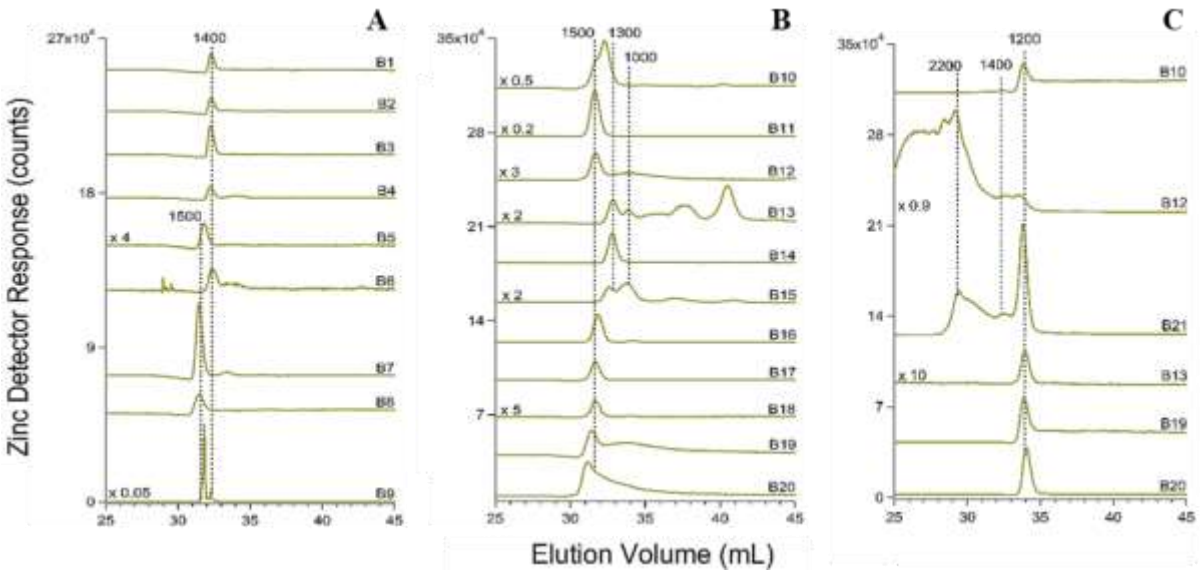

Figure 2.S4: Zinc-detected chromatograms of FTSs from isolated vacuoles (reprinted from reference 41)**.**

A, Vacuolar FTSs from cells grown in minimal media containing 40 μM Fe^{III} citrate and harvested during stationary (B1 – B4) and exponential (B5 – B9) phases. The mobile phase pH was 8.5. Some trace intensities were multiplied by the indicated factor. Numbers above vertical dashed lines indicate approximate mass in Da for species at that elution volume (41).

B, Vacuole FTSs from cells grown in synthetic complete medium supplemented with 40 μM Fe^{III} citrate and harvested in stationary phase (B10 – B20). Vacuolar FTS of B19 and B20 were prepared in the same way but the media was supplemented with 1 μM Fe^{III} citrate. The mobile phase pH was 8.5 (41).

C, Vacuole FTSs prepared as in B with 40 (B10 – B18) or 1 (B19 – B20) μM Fe^{III} citrate. The mobile phase pH was 6.5 (41).

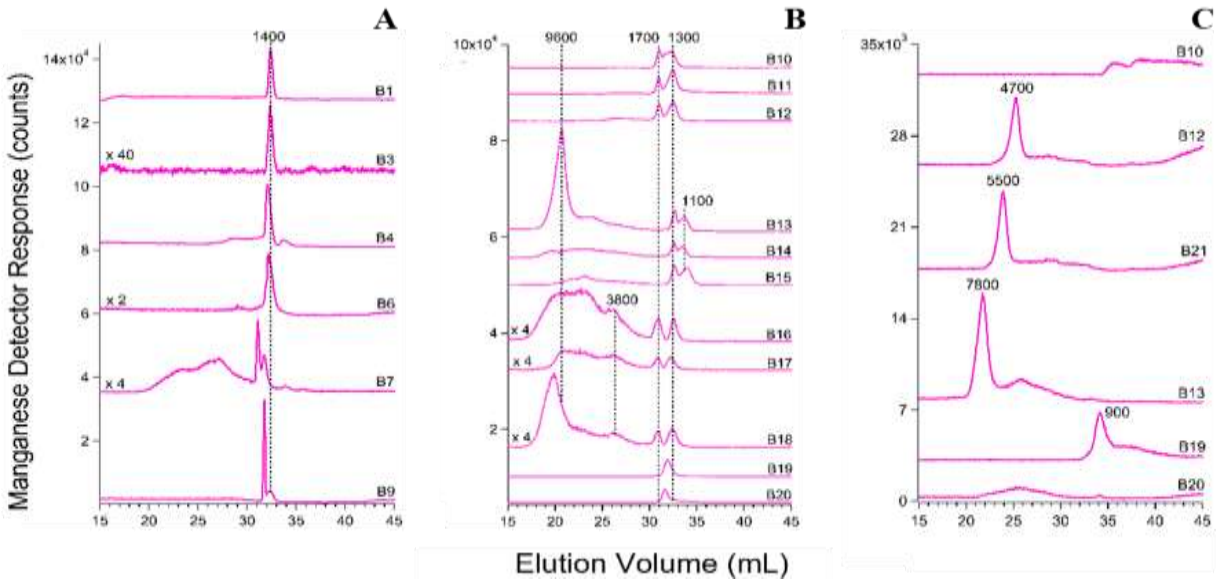

Figure 2.S5: Manganese-detected chromatograms of FTSs from isolated vacuoles (reprinted from reference 41)**.**

A, Vacuolar FTSs from cells grown in minimal media containing 40 μM Fe^{III} citrate and harvested during stationary (B1 – B4) and exponential (B5 – B9) phases. The mobile phase pH was 8.5. Some trace intensities were multiplied by the indicated factor. Numbers above vertical dashed lines indicate approximate mass in Da for species at that elution volume (41).

B, Vacuole FTSs from cells grown in synthetic complete medium supplemented with 40 μM Fe^{III} citrate and harvested in stationary phase (B10 – B20). Vacuolar FTS of B19 and B20 were prepared in the same way but the media was supplemented with 1 μM Fe^{III} citrate. The mobile phase pH was 8.5 (41).

C, Vacuole FTSs prepared as in B with 40 (B10 – B18) or 1 (B19 – B20) μM Fe^{III} citrate. The mobile phase pH was 6.5 (41).

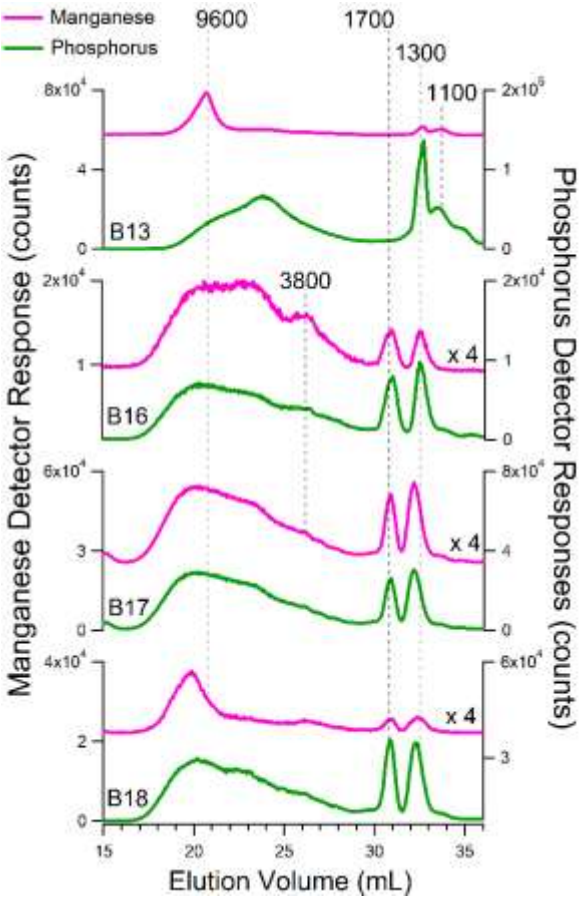

Figure 2.S6: Overlaying of Mn and P for batch 13, 16, 17, and 18 at pH 8.5 mobile phase (reprinted from reference 41)**.**

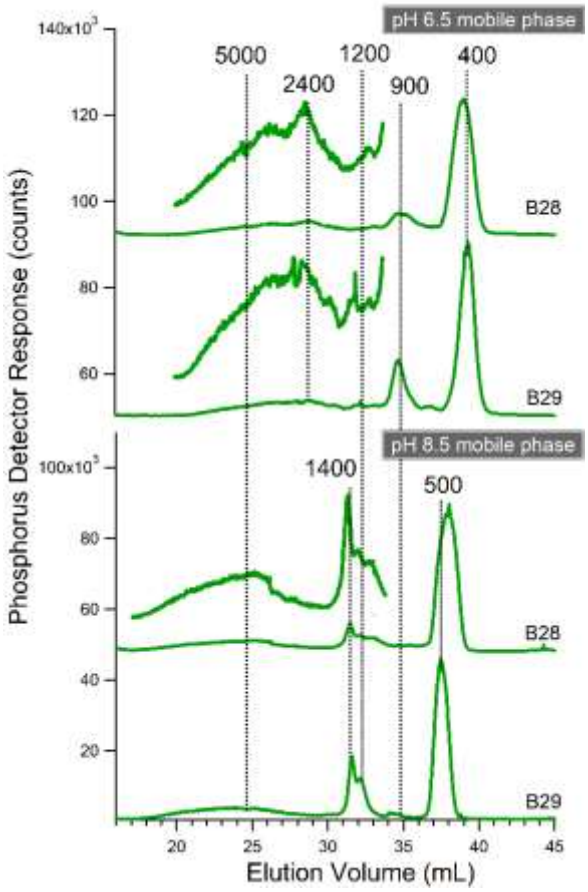

Figure 2.S7: Phosphorus-detected chromatograms of FTS from isolated vacuoles from WT strain in the presence of phosphatase inhibitors cocktail (reprinted from reference 41).

10 mM stock of phosphatase inhibitors cocktail (abcam, ab201113) containing imidazole, sodium fluoride, sodium molybdate, sodium orthovanadate, and sodium tartrate dihydrate was added to all buffers of vacuoles isolation procedure at a final concentration of 1 mM starting from the spheroplasting step and during the collection of vacuolar FTSs (n = 2) (41).

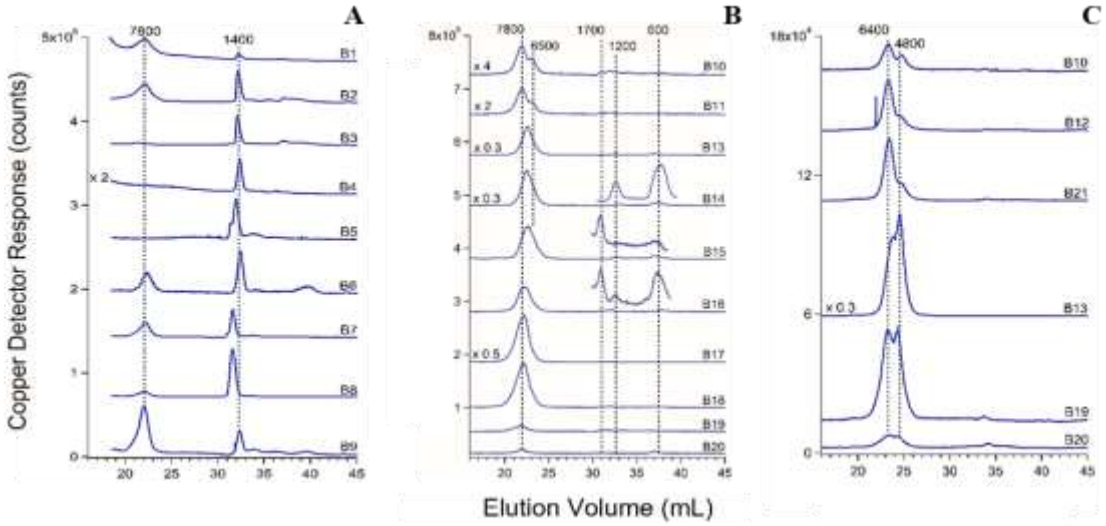

Figure 2.S8: Copper-detected chromatograms of FTS from isolated vacuoles of WT strain (reprinted from reference 41)**.**

A, Vacuolar FTSs from cells grown in minimal media containing 40 μM Fe^{III} citrate and harvested during stationary (B1 – B4) and exponential (B5 – B9) phases. The mobile phase pH was 8.5. Some trace intensities were multiplied by the indicated factor. Numbers above vertical dashed lines indicate approximate mass in Da for species at that elution volume (41).

B, Vacuole FTSs from cells grown in synthetic complete medium supplemented with 40 μM Fe^{III} citrate and harvested in stationary phase (B10 – B20). Vacuolar FTS of B19 and B20 were prepared in the same way but the media was supplemented with 1 μM Fe^{III} citrate. The mobile phase pH was 8.5 (41).

C, Vacuole FTSs prepared as in B with 40 (B10 – B18) or 1 (B19 – B20) μM Fe^{III} citrate. The mobile phase pH was 6.5 (41).

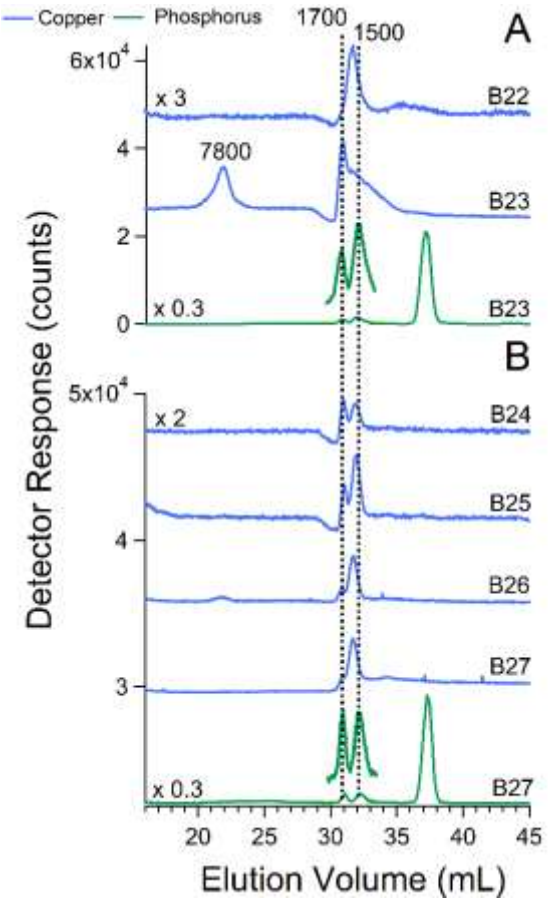

Figure 2.S9: Copper- and phosphorus detected chromatograms of FTS from isolated vacuoles from *cox17*Δ and *cup1*Δ cells (reprinted from reference 41)**.**

Panel A is *cox17*Δ and Panel B is *cup1*Δ. See Table S1 for other details. Vacuolar FTSs of B22 - B27 were analyzed with the mobile phase of pH 8.5

CHAPTER III

DETECTION OF LOW-MOLECULAR-MASS METAL COMPLEXES IN THE CYTOSOL OF SACCHAROMYCES CEREVISIAE

My contribution to this project was isolating cytosol from yeast cells of different genetic knockout strains. I prepared FTSs, obtained all LC-ICP-MS chromatograms and conducted elemental analysis of the isolated cytosolic fractions and their FTSs. I also designed the experiments, prepared figures and analyzed data.

Our lab was grateful to obtain the following yeast genetic strains: *vma2*Δ and *mrs3*Δ *mrs4*Δ strains from Dr. Andrew Dancis (University of Pennsylvania), *ccc1*Δ strain from Dr. Diane Ward (University of Utah), *cup1*Δ and *CUP1R* strains from Dr. Dennis Thiele (Duke University), *cox17*Δ strain from Dr. Vishal Gohil (Texas A&M University) and *fet3*Δ strain from Dr. Danish Khan (Stanford University).

Summary

Cytosol has been speculated to contain a pool of labile low-molecular-mass (LMM) metal complexes, which may involve in trafficking, signaling and other critical intracellular metabolic processes. Thirty eight batches of cytosol were isolated from *Saccharomyces cerevisiae*. Their Flow-through solutions (FTS) were collected by passage through a 10 kDa cut-off membrane and detection using an anaerobic liquid chromatography system coupled with an online ICP-MS. Iron chromatograms of cytosolic FTSs from wild type cells exhibits 4 major species with apparent masses between 700 – 1300 Da. Increasing the iron concentration in the growth media by 40 times only caused a 2-fold increase in the concentration of iron LMM complexes in the cytosol.

Interestingly, increased copper supplementation increased the concentration of LMM cytosolic copper complexes with masses between 300 – 1300 Da. A similar pool of copper complexes was also observed in cytosolic FTSs of genetic knockout strains which involved in copper dysregulation. Zinc and manganese LMM complexes were present in the cytosol at lower concentrations than iron. High zinc supplementation in the media upregulated the metallothionein Crs5, but not any LMM zinc complexes. Phosphorus-detected chromatograms were dominated by peaks at 700 – 800 Da, with minor peaks at 900 – 1500 Da. Sulfur chromatograms only contained one major species at 1000 Da. Phosphorus and sulfur peaks comigrated with iron, copper, zinc and manganese peaks at 700 – 1300 Da. Treatment with 2, 2'-bipyridine chelated perturbed the migration of all LMM cytosolic metal-containing species thus demonstrating the lability of these metal pools.

Introduction

The concept of a *labile iron pool* (LIP) in cells was introduced by Jacobs in 1977 and expanded by Williams a few years later (1) (2). They proposed, based on the available evidence, that cells contain nonproteinaceous, kinetically labile, low-molecular-mass (LMM) Fe^{II} complexes that are involved in iron trafficking, storage, and/or regulation. They predicted that these complexes, erroneously called "free" metals, are toxic and generate reactive oxygen species (ROS) such as hydroxyl radicals via Fenton chemistry. They and others argued that these labile LMM metal complexes should be present at low concentrations so as to minimize any potential damage to the cell (3).

These early researchers also emphasized the difficulty of distinguishing physiologically relevant complexes from artifacts generated during cell lysis and sample preparation. This

difficulty stems from the well-known lability (i.e. rapid ligand exchange rates) of the complexes. Isolating and characterizing dynamically changing species has been, and continues to be, a major unsolved challenge. Indeed, the LIP has been compared to the Loch Ness monster, “only to disappear from view before its presence or indeed its nature can be confirmed” (4). Thirty-five years later, a recent review concludes that “the molecular nature of the labile iron pool…(remains)…one of the least well understood aspects of iron cell biology" (5).

Cabantchik and coworkers developed a powerful strategy to investigate the beast; they loaded intact cells with the membrane-permeable fluorescent chelator probe calcein, a derivative of fluorescein whose fluorescence quenched upon iron binding (6). Cells were subsequently incubated with a stronger chelator (e.g. 2,2’-bipyridine, phenanthroline, or salicylaldehyde-isonicotinoyl-hydrazone SIH) which caused dequenching of the probe as iron dissociated and bound to the stronger chelator. The extent of fluorescence-recovery allowed the concentration of the LIP to be calculated. This strategy has become a popular and powerful method to quantify the LIP (3). Cabantchik reported an LIP concentration in the cytosol of K562 human cells (called cLIP) between 0.2 – 0.5 μM (7). Petrat and coworkers first reported a cytosolic LIP concentration of 10 ± 3 μM in isolated rat hepatocytes – values reflecting ca. 1.6% of total cellular iron (8) . Using Phen Green SK as a probe, they later reported 1 - 3 μM for the cytosolic LIP in cultured rat hepatocytes (9). Epsztejn *et al.* reported ca. 1 - 2 μM in a similar study (10).

Hider and coworkers developed another approach to studying the LIP, namely using thermodynamic binding strengths along with solubility properties and known concentrations of various potential ligands to predict the types of complexes that constitute the LIP. $Fe^{II}(glutathionate)_1(H_2O)_5$ currently leads the list (11). Since the oxidation state of iron in the cytosol is almost certainly Fe^{II} (12), Lewis bases in the cytosol that coordinate Fe^{III} but not Fe^{II} at

physiological pH are not good candidates; this excludes amino acids, ATP/ATP, inositol phosphates, and 2,5-dihydroxybenzoic acid. Citrate binds Fe^{II} but not strong enough to prevent autoxidation to Fe^{III}. In contrast, glutathione (GSH) is present in millimolar concentrations in the cytosol, it binds Fe^{II} strongly, and its antioxidant properties serve to maintain the Fe^{II} state (13).

Copper is also essential for cellular function, and like iron, is also potentially damaging to the cell. However, the mechanism of copper trafficking is thought to be different from that of iron in exclusively involving proteinaceous copper chaperones. O'Halloran and Culotta argued that cells do not contain "free" copper ("free" is an ambiguous term that could mean aqueous, chelatable, mobile, nonproteinaceous, or LMM) (14). Over the next 2 decades, this conclusion – that copper is exclusively passed from one protein chaperone to the next without involving a labile LMM copper pool - has become consensus (15).

Copper is imported via Ctr1 (among others) on the plasma membrane, affording the Cu^{I} state in the cytosol (16). Some cytosolic Cu^{I} binds Atx1, a chaperone which delivers copper to Ccc2, a P-type ATPase transporter on the trans-Golgi membrane. Some cytosolic Cu^{I} binds Ccs1, a cytosolic chaperone that installs copper into superoxide dismutase, and some bind the two metallothioneins Cup1 and Crs5. These proteins sequester and store cytosolic copper, and serve as a copper buffer.

How cytosolic Cu^{I} is delivered to mitochondria for import into the copper-containing respiratory complex cytochrome c oxidase during its assemble is a decades-old puzzle, as no chaperone for this process has been identified. Cox17 localizes to both the cytosol and mitochondria, prompting Glerum *et al.* to suggest that it was the sought-after chaperone (17). However, Winge and coworkers showed that this was unlikely, because anchoring Cox17 to the mitochondrial IMS did not prevent cytochrome c oxidase from being metallated. Cox17 is a copper

chaperone that functions in the mitochondrial IMS to deliver copper to two other chaparones (Sco1 and Cox11) that ultimately metallate Cu_A and Cu_B sites (18). The form(s) of copper that enters the cell and metallates Atx1, Ccs1, Cup1/Crs5, and Cox17 has (have) not been identified.

There actually is some evidence for a "labile copper pool" (LCP). Fahrni and coworkers obtained evidence for such a pool using copper-specific fluorescence-based chelator sensors (19). They found that copper is bound exceedingly tightly to the LCP ($K_D \sim 8$ aM) and that the ligands of this pool are probably thiols (but not GSH). The concentration of the LCP appears to increase transiently after cells are exposed to copper salts (e.g. 150 μM $CuCl_2$) in the growth medium. In these situations, copper rapidly enter cells, generating LCPs located mainly in mitochondria and Golgi (20). Also relevant is that the phenotypes of cells lacking copper-chaperones (e.g. Cox17, Sco2 and Coa6) can be rescued by exposing them to high concentrations of copper salts (17) (21) (22). Although the molecular basis for this has not been established, the implication is that the expanded LCP can substitute for unknown copper protein chaperones.

Zinc is found in nearly 600 eukaryotic proteins (23) and thus plays a major role in cellular metabolism. No zinc chaperones have been identified and it seems unlikely that each Zn-containing protein employs a specific chaperone for metallation (24). The concentration of nonproteinaceous labile LMM Zn in the cytosol of mammalian cells (called the labile zinc pool or LZP) is exceedingly low (25); estimates are in the *hundreds of pM* (26). Given the volume of a cell, this translates into less than 1 "free" Zn atom per cell averaged over time and space. Such low concentrations are apparently required to avoid mis-metallation in cells (Zn generally binds to protein sites tighter than do other metals). Somehow LZPs have been detected using either synthetic fluorescence-based probes or genetically-encoded FRET based sensors (26).

Yeast cells contain two major Zn importers on the plasma membrane, Zrt1 and Zrt2, and their expression is controlled by the transcriptional regulator Zap1 which is sensitive to the LZP. Some cytosolic Zn from the LZP is transported to the ER (Zhf1) and Golgi (Cis4 and Zrg17) for use in the secretory pathway. Other cytosolic Zn is bound to a buffer, proposed to be metallothioneins (27). In this case, aqueous Zn can be present at pM concentrations but be in equilibrium with a buffer at much higher concentration (μM). In *Bacillus subtilis* (and perhaps other gram-positive bacteria), the buffer is bacillithiol which is present at ~ 1 mM concentration (28). In Zn-shock experiments (adding 1-10 μM Zn salts to Zn-starved cells), chelator-sensitive Zn within the cell increases quickly and significantly, and then declines (29). This behavior suggests an expandable pool of mobile Zn ions in the cell, similar to the situation with copper.

Manganese ions constitute the active sites of numerous enzymes. Mn enters cells via various transporters, including DMT1, ZIP, SLC39A14, and Calcium channels (30). Cytosolic Mn^{II} ions are imported into the Golgi via SPCA1 and into lysosomes via ATP13A2. A significant proportion of Mn ions in cells exist as LMM complexes (30). The total Mn concentration in the cell, including both protein-bound and the labile manganese pool (LMP), is in the tens of μM. Mn^{II} ions have inherently low binding affinities toward most ligands and so it has been difficult to develop fluorescence-based probes that are Mn-selective (29). EPR, ENDOR, and ESEEM spectroscopies of intact cells have been more productive in investigating the LMP (31). Complexes of the LMP are coordinated by waters, phosphate and polyphosphate groups, carbonates, citrates, and histidines. Cells use compartmentalization to control which metal is metallated. In this way, Mn can metallate proteins that would otherwise be metallated by metals that bind more tightly (13). In mammalian cells, the low level of cytosolic Mn (10^{-7} M) is achieved by the action of membrane-bound ATPases which direct Mn^{II} to the Golgi apparatus and mitochondria. Under

these conditions Mn^{II} does not bind glutathione (11). Whether Mn chaperones deliver Mn to the active site of enzymes in the cytosol are unknown. When cells are exposed to high concentrations of Mn, excess Mn is found in the Golgi (29).

Metal-sensitive fluorescence-based chelators are the most popular means of detecting and characterizing labile metal pools in cells. Their main advantage is the ability to penetrate the membranes of intact cells without disrupting them. This avoids the concern, voiced by Jacobs and Williams 40 years ago and echoed ever since, that disrupting the cell and preparing extracts might alter the LMPs and create artifacts (31). Unfortunately, the chemical identity of these complexes remains unknown - *due* to the chelator-based approach. The fluorescence properties of these probes change in the presence of LMPs exactly because the chelators rip the metal from the complex(es) of interest. In essence, artifactual metal complexes are intentionally generated as the endogenous ligands, whose identities are sought, become permanently lost in the cellular milieu.

Another related problem with the chelator-based approach is that the detected concentration of the LMPs depends on the specific chelator used, the concentration of the chelator, the exposure time, the temperature of the reaction etc.; in contrast, the inherent concentration of LMPs should be independent of experimental conditions. Also, chelators are not perfectly specific for a particular metal or complex, and there is no guarantee that a chelator will exclusively detect metals that are part of the LMP – e.g. they might remove metals from protein sites (33).

Here we employ a chromatography-based method to characterize these labile metal complexes, in which such complexes are not destroyed but can be isolated and ultimately characterized by powerful downstream analytical methods. Towards this end we have installed a bioinert LC in an anaerobic glove box allowing the separation of LMM metal complexes within extracts of cells or cell compartments. The eluent from the column is split, with a portion flowing

to a fraction collector for downstream analytical characterization and the remainder flowing to an in-line ICP-MS for metal ion detection. Our objective was to detect, catalog, and characterize LMM metal complexes in the cytosol of budding yeast *S. cerevisiae*. We report the detection of numerous LMM metal complexes but have only begun to chemically identify such species. This study lays the foundation for their eventual chemical characterization.

Materials and Methods

Cell growth

The yeast strains used in this study are listed in Table 3.1. All strains were grown in 2 L of minimal medium (MM) except for *cup1*Δ cells which were grown in 1 L of complete synthetic media (CSM). The composition for MM and CSM has been described (34). Cells were harvested at early-exponential phase OD_{600} = 0.6 ± 0.2 for MM and OD_{600} = 3.0 ± 0.1for CSM. Additional conditions for individual cytosolic batches are listed in Table 3.2.

Isolation of cytosol

Harvested cells (typically 4 – 5 grams of wet pellet) were washed 2 times with 1 mM EDTA, pH ~ 8 and followed by 2 additional washes with DI water. Five mL of liquid was used per gram of wet pellet. Cells suspension was centrifuged at 4,000 × *g* for 5 min. All buffers and solutions were chilled in an ice bath. Washed cells were suspended in 5 mL of Buffer A (10 mM of dithiothreitol in 100 mM Tris, pH = 9.4) per g wet cell mass. After 10 min incubation at 30°C, cells were centrifuged and brought to a refrigerated nitrogen-atmosphere glovebox (Mbraun Labmaster, 4°C, ~ 2 ppm of O_2) where cytosol was isolated following the protocol of Herrera *et al.* with some modifications (35). Starting from this point, all buffers (B and C) were degassed on

Strain	Genotype	Source
W303 wild type	*MAT α ade2-1 his3-1,15 leu2-3,112 trp1-1 ura3-1*	Dancis Lab
*fet3*Δ	*MAT α ade2-1 his3-1,15 leu2-3,112 trp1-1 ura3-1 Δfet3::kanMX4*	Danish Khan
*ccc1*Δ	*MAT α ade2 can1 his3 leu2 trp1 ura3 Δccc1::HIS3*	Ward Lab
*mrs3*Δ *mrs4*Δ	*MAT α ade2-1 his3-1,15 leu2-3,112 trp1-1 ura3-1 Δmrs3::HIS3 Δmrs4::LEU2*	Dancis Lab
*vma2*Δ	*MAT α ade2-1 his3-1,14 leu2-3,112 trp 1-1 ura3-1 Δvma2:: HIS3*	Dancis Lab
*cox17*Δ	*MAT a his3Δ1 leu2Δ0 met15Δ0 ura3Δ0 cox17::HphMX4*	Gohil Lab
*cup1*Δ	*MAT α trp1-1 gall met13 can1 cup1S ura3-50 Ade$^-$ His$^-$ Δcup1::URA3*	Thiele Lab
CUP1R	*MAT α trp1 gal1Δ his3-532 ade1-100 leu2-3 leu2-112 CUP1R*	Thiele Lab

Table 3.1: Yeast strains used in this study.

Strain	Supplemented Metal Concentrations (μM)			Media	Number of Replicates
	Fe	Cu	Zn		
W303	1	10	0	MM	8
W303	40	10	0	MM	4
W303	100	10	0	MM	4
W303	40	0	0	MM	2
W303	40	50	0	MM	2
W303	40	10	100	MM	2
*fet3*Δ	100	10	0	MM	4
*ccc1*Δ	40	10	0	MM	2
*mrs3*Δ *mrs4*Δ	40	10	0	MM	2
*vma2*Δ	40	10	0	MM	2
*cox17*Δ	40	10	0	MM	2
*cup1*Δ	40	10	0	CSM	2
CUP1R	40	10	0	MM	2

Table 3.2: Growth conditions of 38 isolated cytosol batches.

a Schlenk line to make them anaerobic before contact with cells. Cells were resuspended in 5 mL of Buffer B (0.6 M sorbitol, 10 mM KP_i, pH = 7.4) per g of wet cells in the presence of 10 mM PMSF. In addition, 0.5 mg of 100 KU/g - Zymolyase (Amsbio, 120493-1) per g wet cells were freshly dissolved in 1 mL of Buffer B, and mixed well with the cell suspension. A 1-mL sample of the cell suspension was collected to monitor spheroplasts formation. The cells suspension and its 1 mL aliquot were removed from the glovebox in a sealed centrifuge bottle and incubated at 30°C for 15 min. The initial OD_{600} (immediately after adding Zymolyase) was measured by mixing 10 µL of cell suspension with 990 µL of water. Once the OD_{600} was decreased to 30% of the initial value (usually after 15 min), the suspension was centrifuged at 2,200 × *g* for 4 min and brought back to the glovebox where the supernatant was discarded. The spheroplast pellet was resuspended in a six-fold volume excess of Buffer C (10 mM Tris-MES, 0.1 mM $MgCl_2$, 12% Ficoll, pH ~ 6.8). The resulting suspension was divided in half. Each half (15-17 mL) was loaded one-at-a-time into a 40 mL Kimble® Dounce tissue grinder and fractionated with a glass pestle A (clearance 0.0030-0.0060 inches) for 10 strokes. The resulting homogenate was transferred to a centrifuge bottle, sealed, removed from the glovebox, and centrifuged at 1,000 × *g* for 15 min. The bottle was returned to the glovebox, the supernatant was transferred to a clean centrifuge bottle, which was sealed, removed from the box, and centrifuged at 15,000 × *g* for 30 min. The bottle was returned to the glove box and the process was repeated, except that the supernatant was transferred to 3 of 16 x 76mm polycarbonate bottles (Beckman Coulter, 355603) that fit a 70.1 Ti Fixed-Angle Titanium rotor (Beckman Coulter). After assembling the outer jackets, the sealed tubes were removed from the box to be centrifuged at 112,000 × *g* for 60 min. Bottles were brought back to the box. The supernatant was transferred to 2 clean sealed polycarbonate tubes, , removed from the box, and centrifuged at 185,000 × *g* for 150 min. At the end of this spin, the tubes were brought

back to the box where the supernatant was collected as the isolated cytosolic fraction. The top lipid layers and pellets were discarded. Scheme 3.1 summarizes all of the centrifugation steps to collect the isolated cytosolic fraction after the Dounce homogenization.

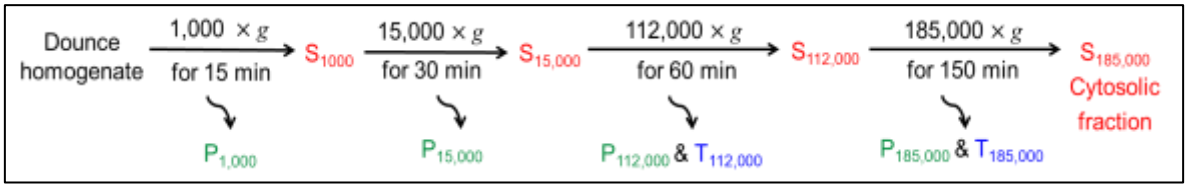

Scheme 3.1: Centrifugation steps for cytosol isolation after Dounce homogenization.
S: supernatant, P: pellet, T: top layer. The subscripts represent the centrifugation speed of each step.

Western blotting

Protein concentrations were quantified by 96-well plate Pierce™ BCA Protein Assay Kit (Thermo Scientific™). Whole cells protein extract and cytosolic fractions were run on a NuPAGE™ 10% Bis-Tris protein gel (Invitrogen™) at constant voltage of 40 V for 40 min then switched to 110 V for 110 min. A semidry Trans-Blot cell (Bio-Rad) was used to transfer separated proteins to activated PVDF membranes at constant voltage of 23V for 60 min. Membranes were blocked with a solution of 5% milk dissolved in Tris-buffered saline with 0.1% Tween (TBST-milk) for 1 hr at RT before being incubated with different primary antibodies overnight at 4 °C. All primary antibodies were diluted in TBST-milk solution as followed: 1:2000 dilution of anti-PGK antibody as cytosol marker (Life Technologies, H0460), 1:2000 dilution of anti-Kar2 antibody as endoplasmic reticulum marker (Santa Cruz Biotechnology, sc-33630), 1:2000 dilution

of anti-CPY antibody as vacuole marker (Life Technologies, A-6428), and 1:1000 dilution of anti-VDAC antibody as mitochondria marker (Thermo Fisher, 16G9E6BC4). Membranes were washed and incubated with 1:5000 dilution of either goat anti-rabbit IgG HRP-conjugated secondary antibody (Santa Cruz Biotechnology, clone sc-2004) or goat anti-mouse IgG HRP-conjugated secondary antibody (Invitrogen, clone G-21040) for 1 hr at RT. The blots were developed with Clarity™ Western ECL Substrate (Bio-Rad) for 2 min at RT and imaged using FujiFilm LAS-4000 mini with a 15 s exposure under chemiluminescence setting.

Preparation of cytosolic FTS and LC-ICP-MS chromatography

Four mL of isolated cytosolic fractions in Buffer C were passed through an Ultracel regenerated cellulose 10 kDa NMWL membrane (EMD Millipore) installed in an Amicon® EMD Millipore Stirred Cell (Model 8003, 3 mL) and pressurized with 70 psi Argon. Approximately 75% of the isolated cytosol fractions passed through the 10 kDa membrane in ca. 2.5 hr. The resulting flow-through solution (FTS) of 150 µL was loaded onto either a single or a dual size-exclusion (SEC) column SuperdexTM Peptide 10/300 GL (GE Life Sciences) connected to an Agilent 1260 Bioinert quaternary pump (G5611A). A mobile phase of 20 mM (NH_4) OAc, pH = 6.5 was used with a flow rate of 0.33- 0.35 mL/min for dual peptide columns and a flow rate of 0.6 mL/min for the single column. All LC-ICP-MS parameters, SEC calibration and molecular mass assignment have been described (36).

Elemental analysis

Elemental analysis was conducted using ICP-MS (Agilent 7700x) as described with some minor modifications (36). Cytosolic fractions and cytosolic FTSs of 4 independent batches were

separated into triplicates of 100 µL using 15 mL polypropylene screw-top vials. 300 µL of trace-metal-grade 70% w/v nitric acid (Fisher Scientific) was added to each vial. Vials were sealed with caps and electrical tape, then incubated at 70 °C for ca. 15 hr. Each replicate was thawed to room temperature, diluted with 5.60 mL high-purity trace-metal-free double distilled-deionized water and mixed well before analysis.

Results

Thirty eight batches of cytosol were isolated from yeast cells, as described in *Experimental Procedures* (See Table 3.2 for a compilation of all batches). Most batches were passed through a 10,000 Da cut-off membrane, and the resulting flow-through solutions (FTSs) were passed down a size-exclusion chromatography column (in a refrigerated glove box). The eluate from the column was then sent to an ICP-MS for metal-ion detection.

The purity of six of batches of cytosol was investigated by Western Blot; results are shown in Figure 3.2. The representative blot shown in Figure 3.1 was cytosol isolated from WT cells grown with 40 µM supplemented Fe-citrate and 10 µM $CuSO_4$. The blot exhibited an intense band for the cytosolic marker protein PGK1, indicating that the isolated fraction contained cytosol. There was minor contamination of vacuoles and endoplasmic reticulum, but no evidence of contamination due to mitochondria. A portion of the intensity of the band from Anti-CPY is likely due to pro-CPY, which is synthesized in the cytosol prior to the maturation in the vacuolar lumen and is detected by this antibody (37). Thus, our isolated cytosol preparations were less contaminated with vacuoles than is evidenced by the blot.

We determined concentrations of various elements in 16 batches of cytosol isolated from

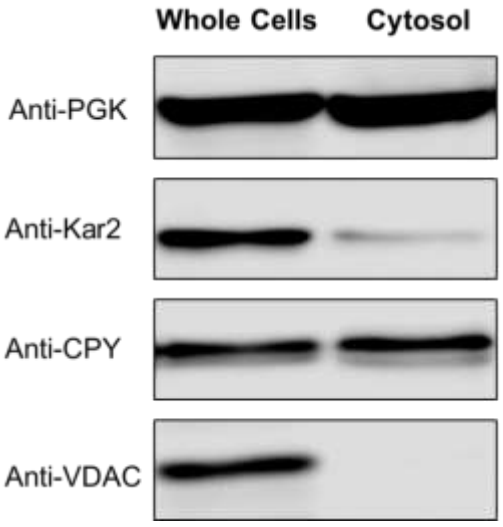

Figure 3.1: Purity of the isolated cytosolic fraction.

22 µg of proteins were loaded per lane. The dilutions of primary antibodies were used as followed: 2000X for anti-PGK (cytosolic marker), 2000X for anti-Kar2 (endoplasmic reticulum marker), 2000X for anti-CPY (vacuole/late endosome marker), and 1000X for anti-VDAC (mitochondria marker).

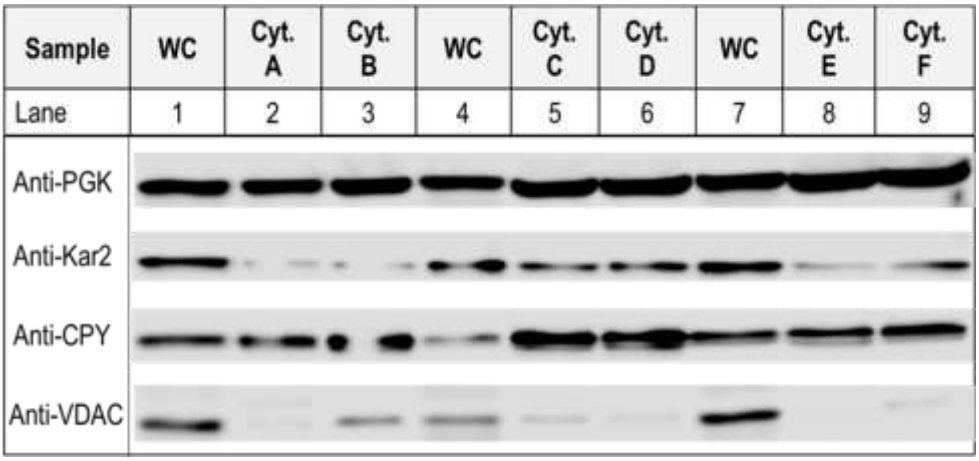

Figure 3.2: Purity of 6 isolated cytosol batches.

22 µg of proteins were loaded per lane. "WC": whole cells, "Cyt.": isolated cytosolic fraction. A, B, E, and F are 4 cytosol batches isolated from WT cells grown in MM with the supplementation of 40 µM Fe and 10 µM Cu. C and D are 2 cytosol batches from cells grown under the same condition but with 1 µM Fe. Primary antibodies were used as described in Figure 3.1.

WT cells grown under fermenting media of 3 different Fe conditions (Figure 3.2). Cytosol isolated from WT cells grown in MM supplemented with 1 μM Fe^{III} citrate contained 40 ± 10 μM Fe, 80 ± 40 μM Cu, 30 ± 10 μM Zn, 2 ± 1 μM Mn, and 50 ± 20 mM P. Under the same growth conditions but supplemented with 40 μM Fe^{III} citrate, the cytosol contained higher concentrations of Fe (110 ± 20 μM) and Cu (110 ± 60 μM), but unchanged concentrations of Zn and Mn. Thus, a 40-fold increase of iron in the growth media caused the concentration of iron in the cytosol to increase 2.7 fold. This is direct evidence that the cytosolic iron concentration is homeostatically regulated. Surprisingly, the concentration of Fe in cytosol from cells supplemented with 100 μM Fe^{III} citrate declined (to 70 ± 30 μM) as did Zn (to 14 ± 6 μM) whereas the Cu concentration increased to 200 ± 100 μM. The modest decline in cytosolic iron concentrations (110 → 70 μM) when the concentration of iron in the growth media increased from 40 → 100 μM Fe^{III} citrate may reflect a cellular response designed to prevent toxic levels of iron from entering the cell.

The iron concentrations of cytosolic FTSs were about half of those in cytosol: 20 ± 10 μM in FTS from WT cells grown on 1 μM Fe^{III} citrate, 80 ± 30 μM when grown on 40 μM Fe^{III} citrate, and 22 ± 2 μM when grown on 100 μM Fe^{III} citrate. These modest changes again probably reflect the homeostatic regulation of the LMM cytosolic iron pool. The labile copper pools constituted about 1/3 of the copper concentrations in the cytosol when cells were grown under 1 or 40 μM Fe^{III} citrate supplemented media. Other metal and P concentrations are given in Figure 3.2.

We subjected most batches of cytosolic FTS to LC-ICP-MS analysis. The FTS from fermenting WT cells grown in MM supplemented with 1 or 40 μM iron exhibited 3-4 partially resolved iron-containing peaks, with apparent masses of 1300, 1000, 900 and 800 Da (Figure 3.3, upper panel). The intensity of the peaks from the FTS from cells grown with 40 μM iron was approximately twice that of peaks from cells grown with 1 μM iron. The cytosol FTS from W303

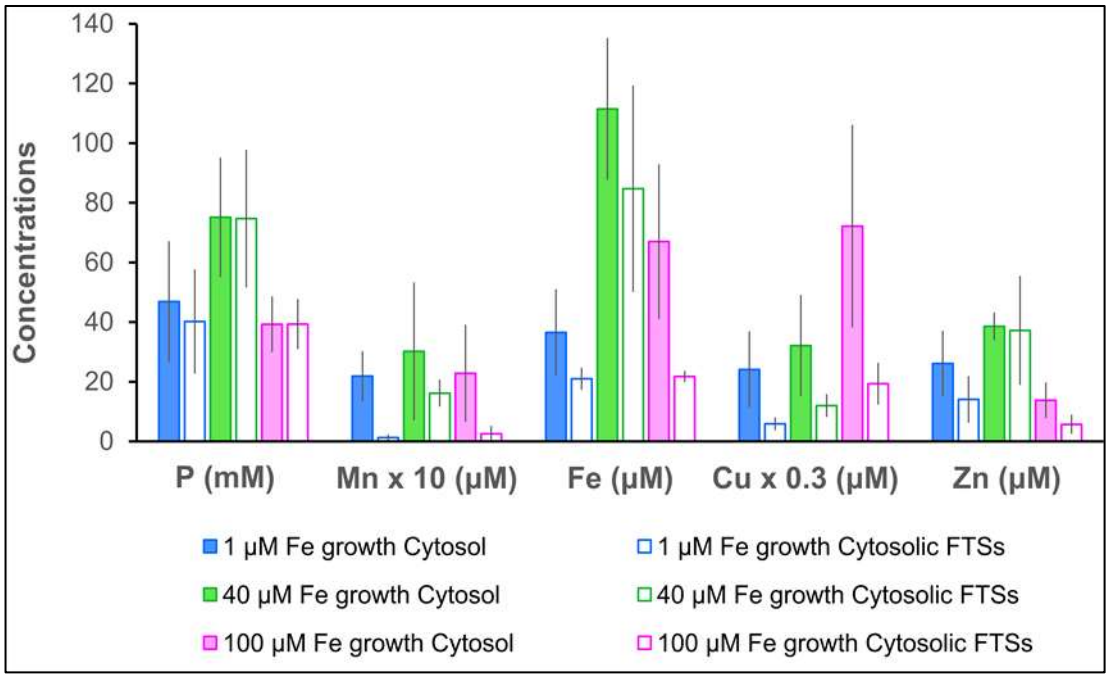

Figure 3.3: Elemental analysis of isolated cytosolic fractions and their FTSs under 1, 40 and 100 µM Fe growth conditions.

Solid bars represent the isolated cytosolic fractions. Empty bars represent the FTSs of the isolated cytosol. The concentrations of each element have been corrected with a dilution factor of 6 due to the isolation procedure (See Materials and Methods section). Replicates for each Fe growth condition have been described in Table 3.2.

cells grown in media supplemented with 100 μM iron exhibited an intense peak with an apparent mass of 700 Da (along with less-intense peaks with masses of 800 - 1300 Da).

Similar traces were obtained for cytosolic FTSs from various genetic strains of yeast, including *fet3*Δ , *mrs3*Δ*mrs4*Δ , and *ccc1*Δ (Figure 3.4, lower panel). These traces also exhibited iron peaks in the range between 600 – 1500 Da. We were able to interpret some of these traces better than others. The cytosolic iron contents of these iron-associated genetic strains appear perturbed, causing the formation of a somewhat different set of LMM iron complexes. FTS from strain *mrs3*Δ*mrs4*Δ exhibited an intense peak at 700 Da

Similar traces were obtained for cytosolic FTSs from various genetic strains of yeast, including *fet3*Δ , *mrs3*Δ*mrs4*Δ , and *ccc1*Δ (Figure 3.4, lower panel). These traces also exhibited iron peaks in the range between 600 – 1500 Da. We were able to interpret some of these traces better than others. Overall, we suspect that the cytosolic iron contents of these iron-associated genetic strains were perturbed, causing the formation of a somewhat different set of LMM iron complexes. *mrs3*Δ*mrs4*Δ exhibited an intense peak at 700 Da seems to have accumulated. On the other hand, this Fe-700 species was not dominant in chromatograms of *ccc1*Δ FTSs. Ccc1 is the major iron transporter into the vacuoles (38). Deletion of *CCC1* causes a decrease in total intracellular iron. We observe weak intensity peaks in the range of 900 – 1300 Da. The iron content of *fet3*Δ (deletion of high affinity transporter) exhibited numerous rather intense iron peaks. These iron species must have entered the cell via Fet4, the low affinity iron transporter (39). We added the phosphatase PPX to these solutions, and found that the iron peaks were altered. This implies that the original peaks might be associated with polyphosphate, as is found in vacuoles. However, polyphosphate chains are built as they are inserted into vacuoles and are generally not present in

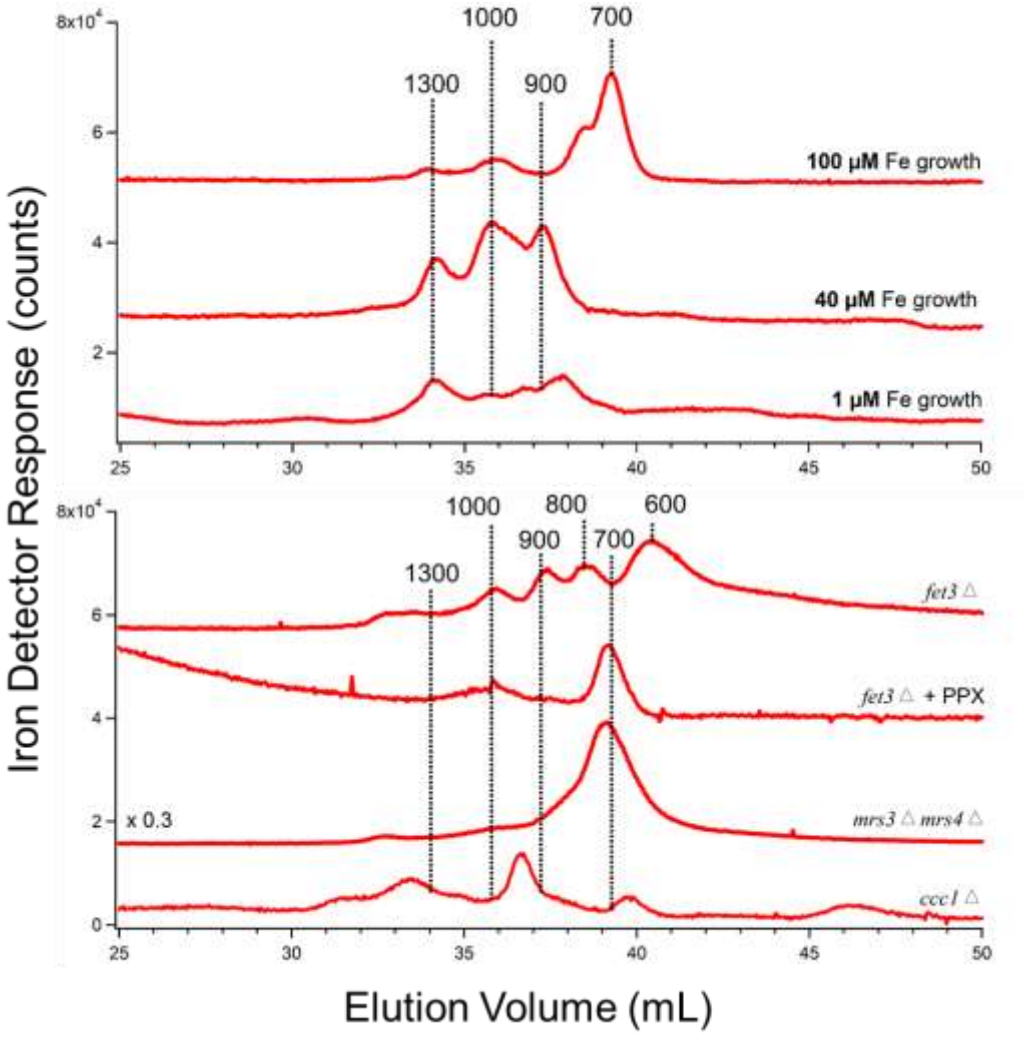

Figure 3.4: Averaged iron-detected chromatograms from FTS of isolated cytosol.
Cytosolic FTS of *fet3*Δ cells were incubated with acid phosphatase (PPX) for 2 hr and loaded to dual SEC columns. Growth conditions and replicates for cytosol isolation of different yeast strains have been described in Table 3.2. Each trace is the average of replicates of independent cytosol batches isolated from cells grown and harvested at the same condition (yeast strain, nutrient supplementation, and type of media).

cytosol, discounting this possibility.

The copper traces exhibited by cytosolic FTSs are shown in Figure 3.5. These traces were dominated by an intense peak at an apparent mass of ca. 5200 Da. This peak was absent in traces from *cup1*Δ cells, allowing us to assign it to Cup1 (Figure 3.5, bottom panel). Deletion of *CUP1* causes the upregulation of the other metallothionein Crs5 (40); thus, the Cu_{8500} signal of *cup1*Δ copper supplementation and observed some batch-to-batch variation in copper traces. Cup1 peak at 5200 Da and peaks due to LMM complexes of Cu were not present under extreme copper scarcity (Figure 3.5, top panel). We had not expected to observe any LMM copper peaks besides those due to the metallothioneins in FTS isolated from WT cells supplemented with 10 μM and 50 μM of $CuSO_4$. Surprisingly two minor copper peaks, with apparent masses of 1100 – 1300 Da were observed. The intensity of these peaks was small, and they were only evident by expanding the ordinate axis of the traces (See insets in Figure 3.5). However, the intensity of these LMM copper peaks increased dramatically in the cytosolic FTS from various genetic strains in which copper metabolism is perturbed, including *vma2*Δ, *cup1*Δ, *cox17*Δ, as well as in WT cells grown in high concentrations (50 μM) of copper. In each of these cases, copper peaks of significant intensities were observed between apparent masses of 300 – 1300 Da. *VMA2* encodes subunit B of the peripheral domain of vacuolar H^+/ATPase (41). Deletion of this gene results in V-ATPase dysfunction, which leads to alkalization of vacuoles and disruption of copper trafficking to post-Golgi compartments (42) (43). Cox17 is a copper chaperone which involves in copper metallation of cytochrome c oxidase (17). Deletion of *VMA2* and *COX17* both resulted in the accumulation of LMM copper peaks at 300 and 1300 Da, thus implying these species might play a critical role in copper trafficking to different organelles.

The cytosolic FTS exhibited at least two zinc peaks with apparent masses between 1300 – 1100 Da (Figure 3.6, top panel). This was the case for both WT cells and the various genetic strains mentioned above under no zinc supplementation. Cells grown with 100 μM of Zn supplementation resulted in no change in cytosolic zinc LMM species but increase in the signal intensity of the peak at 8500 Da. This signal is due to Crs5, which binds stronger to Zn than Cu (40). Crs5 is also overexpressed in *cup1*Δ cells, thus resulting in the increase of 8500 Da species signal in both Zn and Cu cytosolic FTSs chromatograms (Figures 3.5 and 3.6, lower panels).

Cytosolic FTSs exhibited multiple Mn peaks, with apparent masses ranging from 1200 – 100 Da (Figure 3.7, upper panel). Peak positions exhibited more batch-to-batch variability than was observed for the other metals, perhaps because the binding of Mn is generally not as strong. Interestingly, cytosol of *fet3*Δ , *mrs3*Δ*mrs4*Δ , and *cup1*Δ FTSs were dominated by a single Mn species at 1000 Da (Figure 3.8, lower panel). A Mn peak at 170 Da was also observed in *cup1*Δ manganese trace which is likely hexa-aqua manganese.

Cytosolic FTSs exhibited an intense sulfur peak at ca. 1000 – 1300 Da (Figure 3.9). We are uncertain whether the peak arises from glutathione or glutathione-related species. Phosphorus traces of FTS were dominated by a peak at 700 – 800 Da. There were other minor phosphorus peaks with masses between 900 - 1500 Da (Figure 3.8). Particular phosphorus and sulfur peaks comigrate with iron, copper, zinc and manganese in the 700 – 1300 Da region. Whether this indicates metal complexes with ligands that contain these elements is unknown.

Finally, we tested the lability of the LMM metal complexes in cytosol by treating FTSs with 100 μM of 2, 2'-bipyridine (Figure 3.10). After 2 hr incubation at pH 6.8, *all* of the LMM metal complexes disappeared, demonstrating the lability of these species.

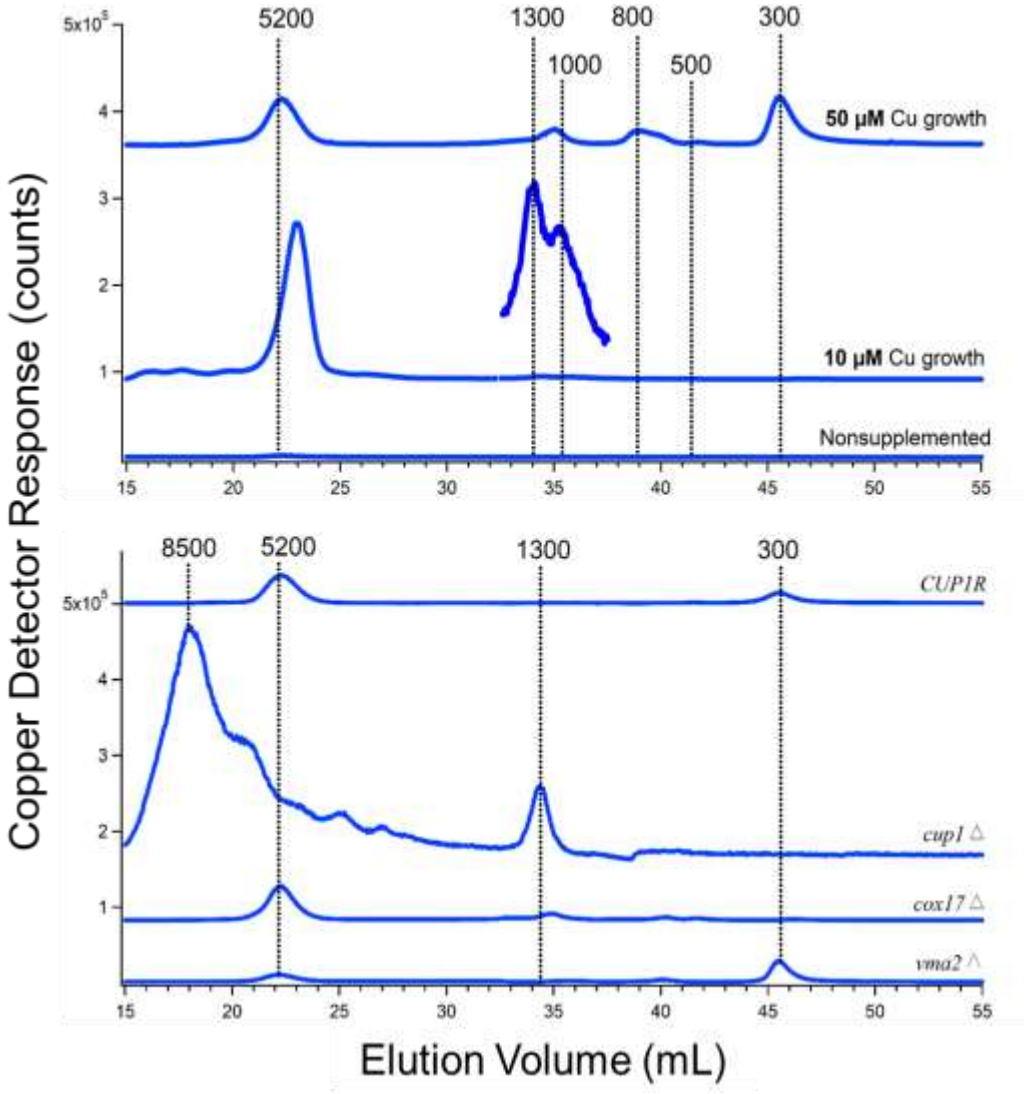

Figure 3.4: Averaged copper-detected chromatograms from FTS of isolated cytosol.
All traces except from the nonsupplemented Cu traces (upper panel) are the average of n=2. Growth conditions and replicates for cytosol isolation of different yeast strains have been described in Table 3.2.

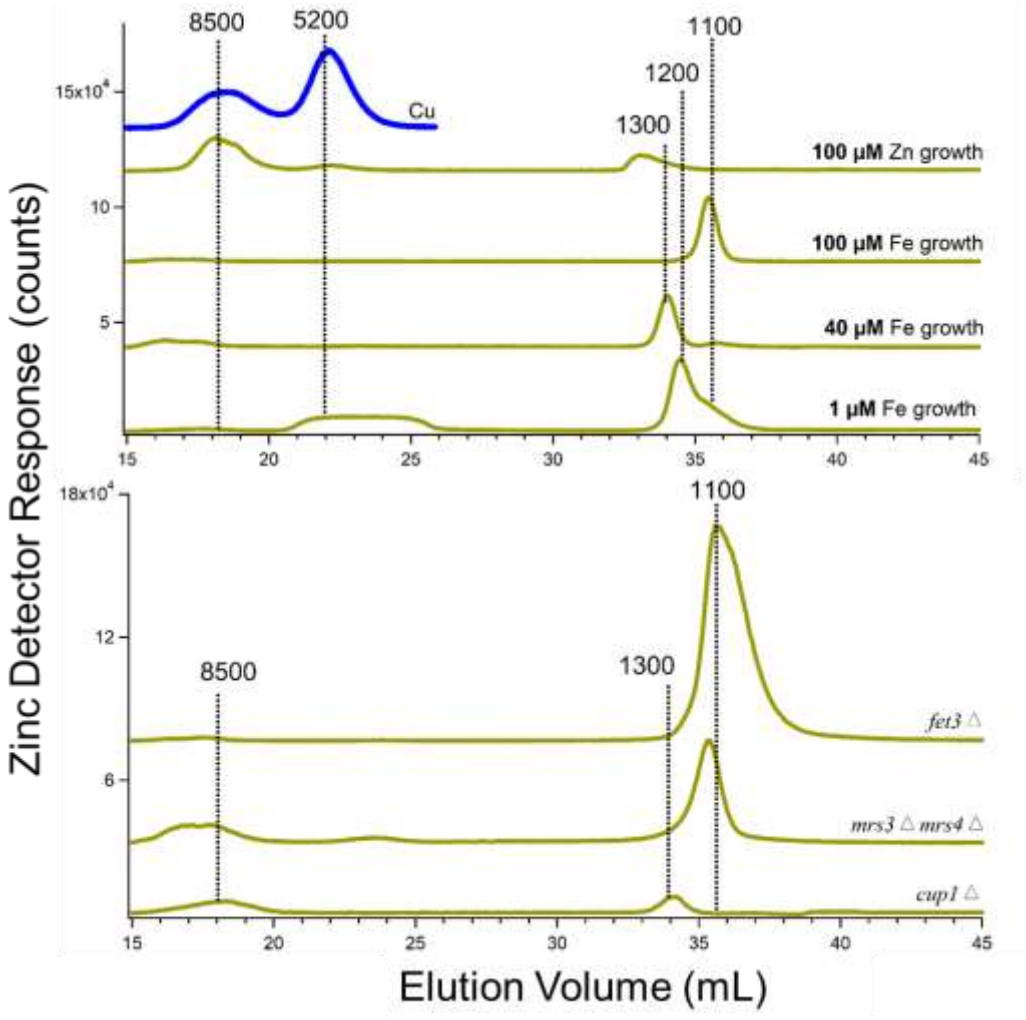

Figure 3.6: Averaged zinc-detected chromatograms from FTS of isolated cytosol.

Inset is the Cu chromatogram of cytosolic FTSs isolated from cells grown with 100 µM Zn. Growth conditions and replicates for cytosol isolation of different yeast strains have been described in Table 3.2.

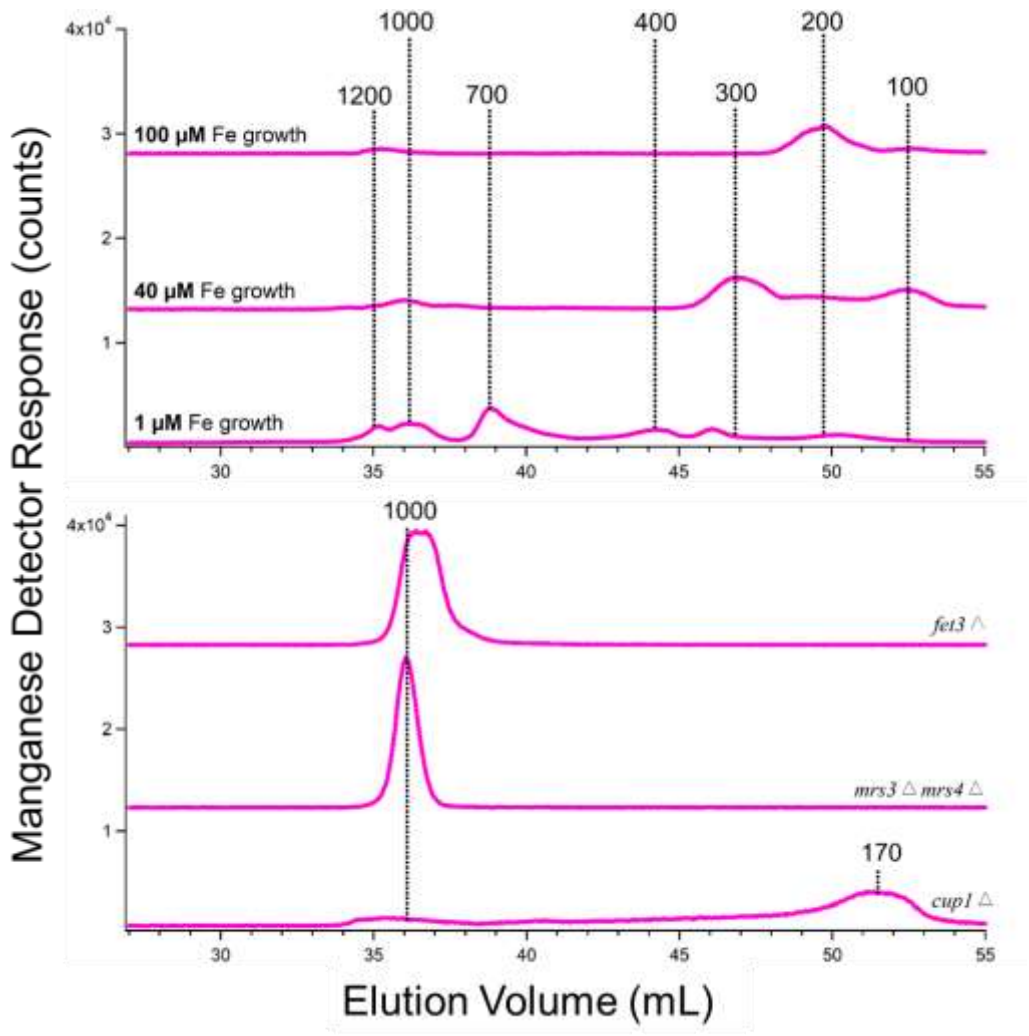

Figure 3.7: Averaged manganese-detected chromatograms from FTS of isolated cytosol.
Growth conditions and replicates for cytosol isolation of different yeast strains have been described in Table 3.2.

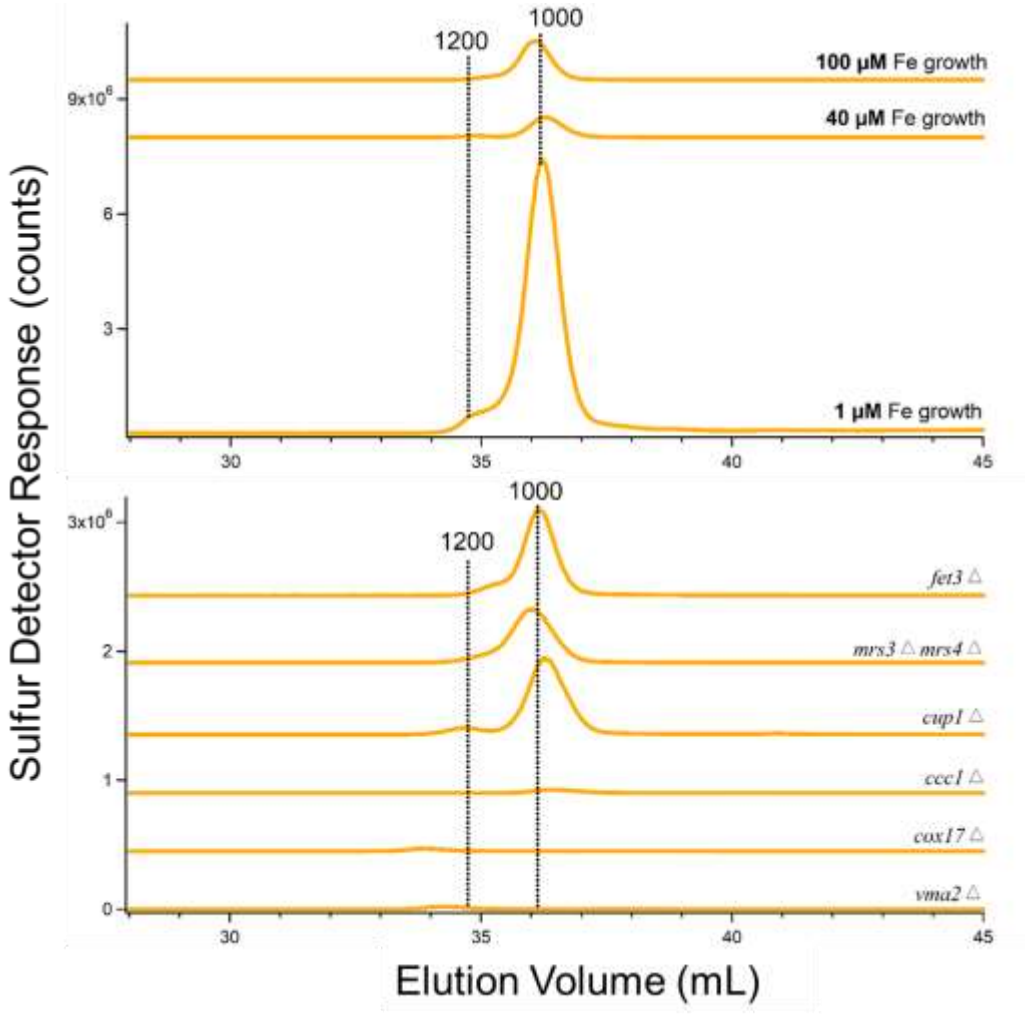

Figure 3.8: Averaged sulfur-detected chromatograms from FTS of isolated cytosol.
Growth conditions and replicates for cytosol isolation of different yeast strains have been described in Table 3.2.

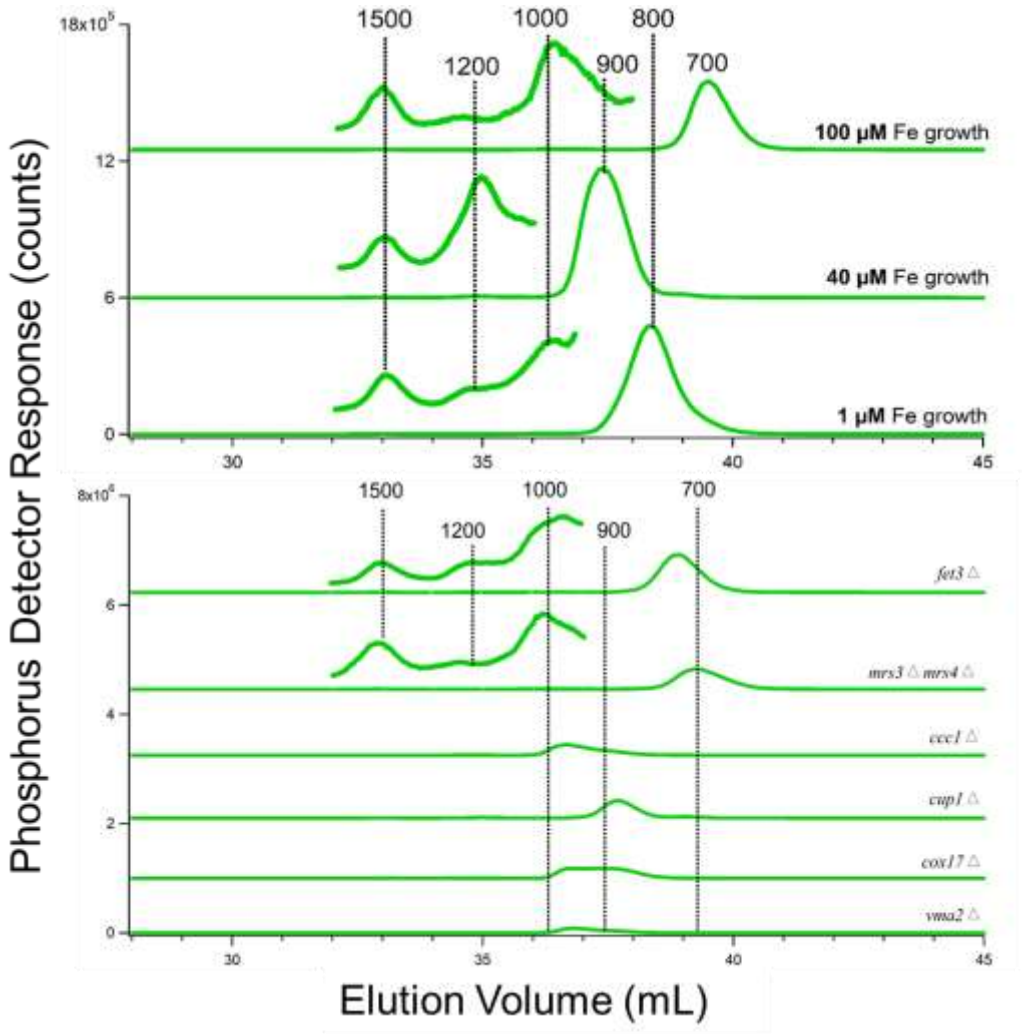

Figure 3.9: Averaged phosphorus-detected chromatograms from FTS of isolated cytosol. Growth conditions and replicates for cytosol isolation of different yeast strains have been described in Table 3.2.

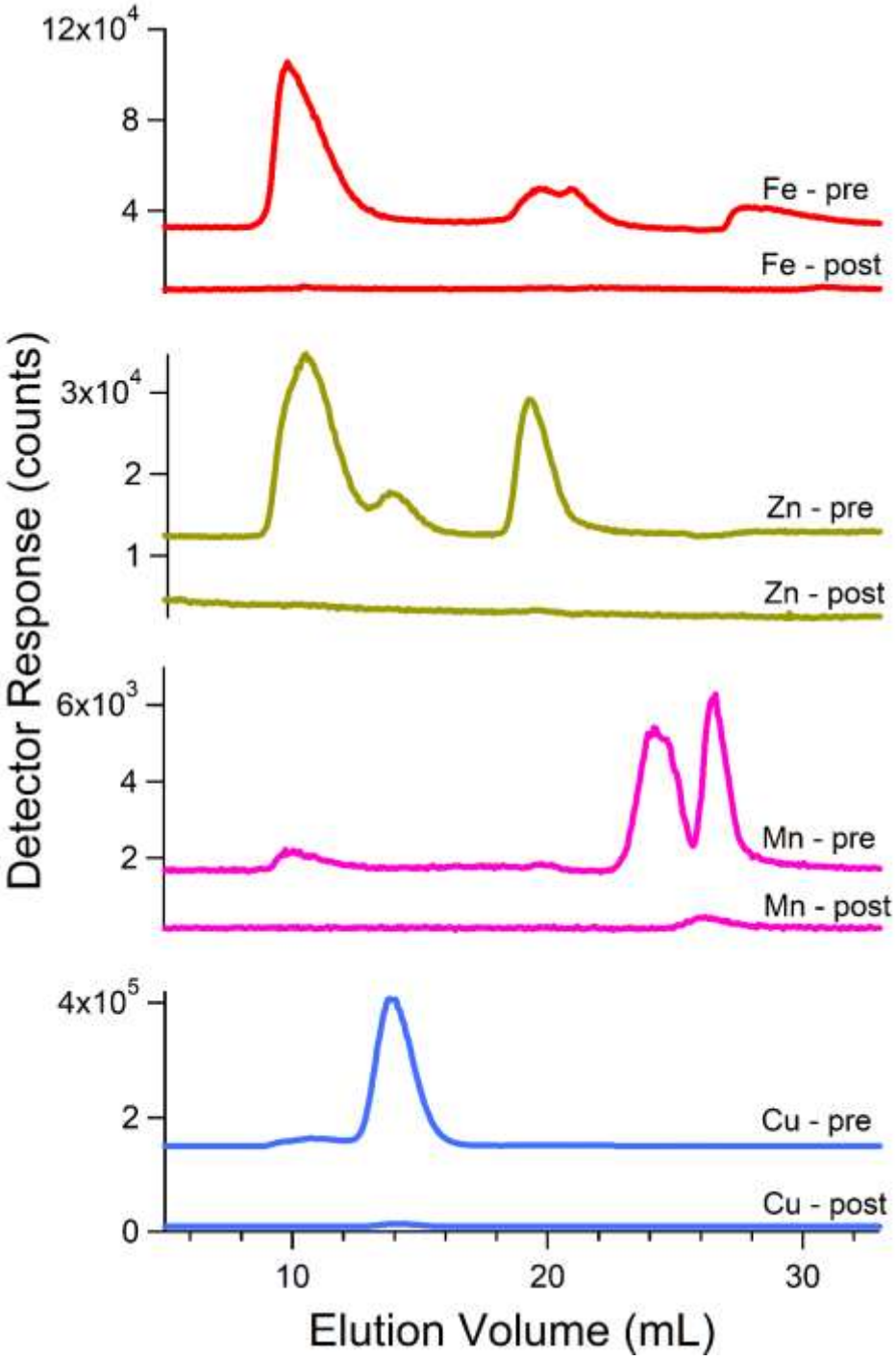

Figure 3.10: Lability of cytosolic LMM complexes as demonstrated with an Fe- chelator. Cytosolic FTSs were incubated with 100 μM of 2,2'-bipyridine for 2 hr at 37°C and injected to a single SEC column (n=2). *Pre-*: before treatment with 2,2'-bipyridine, *Post:* after treatment with 2,2'-bipyridine.

Discussion

This study reports the first chromatography-based determination of the iron content of cytosol from fermenting yeast cells. We focused on the LMM iron complexes in cytosol, by isolating the portion of the cytosol (the flow-through solution) that contained species with masses less than ca. 10 kDa. We discovered 3-4 LMM iron complexes with apparent masses between 800 – 1300 Da. We have not determined the chemical composition or cellular function of these LMM complexes but find that they are perturbed in mutant cells for which iron trafficking has been altered. Thus, we suggest that they are used in cellular iron trafficking.

We were (and are) concerned that some of the detected LMM iron complexes are artifacts or decomposition products of the endogenous labile iron complexes that serve cellular trafficking functions. We isolated many batches of cytosol in hopes that any artifacts or decomposition products would be generated sporadically and generate irreproducible LC traces. Given the difficulty of isolating cytosol from yeast cells, our LC traces were fairly reproducible, suggesting that most if not all of the peaks that we observed arise from endogenous complexes in the cell. We find it unlikely that artifacts would be generated so reproducibly (though this is certainly possible).

We are also more optimistic than Jacobs and others in the field that the LMM metal complexes detected here may not be as dynamically labile as is commonly assumed. The lability of Werner type coordination complexes with O, S, and N donors can be controlled by the denticity of the ligands and donor atoms. We suggest that the lability of LMPs in cells are fast enough for the metal ions to transfer efficiently to target proteins, but slow enough for the metal to effectively remain attached to these complexes while being trafficked to these targets. The shapes of the complexes likely dictate their binding properties to membrane-bound metal-ion transporters such

that if the complexes did not "hold together" long enough in the cell to allow for this recognition, metal ion traffic between various cellular compartments would be uncontrolled and chaotic.

This is the first report of the absolute concentration of iron (and other metals) in the cytosol of yeast (containing the iron-containing proteins of the cytosol) and in the flow-through solution (containing LMM iron species). We found that the iron concentration in the cytosol is sensitive to the iron concentration in the growth medium, as has been widely assumed in explaining numerous results – a 40-fold increase in media iron caused a 2.7-fold increase in cytosolic iron and slight increase for cytosolic copper. Cytosolic zinc and manganese increased slightly as increasing iron supplementation from μM to 40 μM. Interestingly, with 100 μM iron supplementation, cytosolic LMM complexes of iron, manganese, and zinc all decreased.

The overall concentration of iron in the cytosol (50 – 120 μM) was higher than we expected. About half of this was due to iron-containing proteins, and half to LMM iron complexes. We compared these values to the sum of concentrations of iron due to all iron-containing proteins that have been reported in yeast. Ho *et al*. have determined the concentration of each yeast protein (44). These authors integrated the concentrations reported in 21 quantitative proteomic studies (most were fermenting cells grown in rich media without iron supplementation). Using that information, we estimate that the cytosol should contain ca. 34 μM Fe bound to proteins (64% Fe_4S_4 clusters; 4% Fe_2S_2 clusters; 3% NHHS Fe^{II}; 23% Fe-O-Fe; 5% heme b). This collective concentration should be compared to the difference between the cytosolic Fe concentration (57 – 110 μM) and the Fe concentration in the FTSs (which should not contain these proteins) (25 – 65 μM) – namely 32 – 45 μM Fe. These calculated values are remarkably close to those that we measured here.

The LMM iron concentration in the cytosol (25 – 65 μM) is significantly higher than has been reported for the cytosol of human cells (1 – 5 μM). The difference may be due to the greater

use of LMM iron complexes in yeast than in human cells (which might rely more on iron trafficking chaperon proteins PCBP1/2).

Copper trafficking in the cytosol involves a variety of chaperones and cytosolic proteins. Here we provide the first direct evidence for a labile copper pool in the cytosol, with molecular mass less than 10 kDa and concentrations of 20 – 60 μM. Cup1 represents at least 80% of this pool suggesting that the concentration of labile LMM non-Cup1 Cu complexes in the cytosol is 4 – 12 μM. We are particularly intrigued by the copper species at 300 Da, 1100 Da and 1300 Da as the intensity of this species varied with the extent of copper supplementation in the media (in WT cells).

Similar LMM copper complexes also accumulated in cytosol isolated from several knockout strains, including *vma2*Δ, *cup1*Δ, and *cox17*Δ. All of these strains affect copper trafficking and regulation. The accumulation of these LMM copper species between masses of 300 – 1300 Da suggests that they might be involved in cellular copper trafficking. We have considered that the LMM cytosolic copper detected here might dynamically bind Cup1 and Crs5 metallothioneins. However, traces of *CUP1R* cytosolic FTSs exhibit peaks from both Cup1 and a peak at 300 Da. If the LMM Cu species binds metallothionins, we would expect that overexpressed Cup1 protein would bind LMM cytosolic copper (but this does not seem to have been the case).

The intensity of the single labile LMM Zn species that we observed (1100 – 1300 Da) in the cytosolic FTSs of WT cells and cells from genetic knockout strains varied with the extent of Zn supplementation in the growth medium as would be expected if this were an endogenous Zn species in the cell. Surprisingly, an increase in medium Zn resulted in an increased expression of Zn-bound Crs5, but not the accumulation of the LMM Zn complex. Zinc homeostasis might be

tightly regulated by Crs5 expression to prevent higher concentrations of the LMM Zn complex and thus the toxic effects of Zn mismetallation.

Manganese LMM complexes in the cytosol were more varied in molecular weights, ranging between 200 – 1300 Da, and overall were present at concentrations of only 0.3 – 1.6 μM. Culotta and coworkers demonstrated that nonproteinaceous manganese could replace Cu, Mn-superoxide dismutase to protect the cells against oxidative stress (45), and the species detected here may be involved in that.

Most cytosolic (poly)phosphates are LMM complexes with the chain lengths n = 10-15. Some cytosolic iron and phosphorus peaks comigrate in accordance with masses of 800, 900, 1000, and 1300 Da in FTSs traces of *fet3*Δ cells. The binding of iron and polyphosphate was disrupted after the treatment with acid phosphatase. This raises the possibility that polyphosphate is an endogenous ligands of some cytosolic iron LMM complexes. Ferrous ion has a dissociation constant around 10^{-14} with polyphosphate, while ferric ion has a K_D of 10^{-23} with polyphosphate (46). Another possible ligand is sulfur-relating species such as glutathione. There is a dominant peak of cytosolic S trace at 1000 Da and a small peak at 1200 Da, and these may be related to glutathione.

Treatment of the cytosolic FTSs with 2, 2'-bipyridine chelated all of the metal centers of cytosolic LMM complexes, thus further demonstrating the lability of the labile metal pools. Kosman and coworkers previously incubated growing yeast cells with 2,2'-bipyridine, and found that this caused cells to stop growing temporarily (47). They proposed that this chelator coordinated the LIP in the cytosol, and our results are consistent with this. Viewed collectively, the LMM metal complexes that we have detected here may be endogenous to the cell and critical

for cell growth and trafficking. Further studies are required to critically test these possibilities and bring out of the shadows these elusive little beasts.

References

1. Jacobs, A. (1977) Low molecular weight intracellular iron transport compounds. *Blood*. **50**, 433–439
2. Williams, R. J. P. (1982) Free manganese(II) and iron(II) cations can act as intracellular cell controls. *FEBS Lett.* **140**, 3–10
3. Petrat, F., de Groot, H., Sustmann, R., and Rauen, U. (2002) The chelatable iron pool in living cells: A methodically defined quantity. *Biol. Chem.* **383**, 489–502
4. Crichton, R. R. (1984) Iron uptake and utilization by mammalian cells II. Intracellular iron utilization. *Trends Biochem. Sci.* **9**, 283–286
5. Muckenthaler, M. U., Rivella, S., Hentze, M. W., and Galy, B. (2017) A red carpet for iron metabolism. *Cell*. **168**, 344–361
6. Breuer, W., Epsztejn, S., and Cabantchik, Z. I. (1995) Iron acquired from transferrin by K562 cells is delivered into a cytoplasmic pool of chelatable iron(II). *J. Biol. Chem.* **270**, 24209–24215
7. Shvartsman, M., and Ioav Cabantchik, Z. (2012) Intracellular iron trafficking: Role of cytosolic ligands. *BioMetals*. **25**, 711–723
8. Petrat, F., Rauen, U., and de Groot, H. (1999) Determination of the chelatable iron pool of isolated rat hepatocytes by digital fluorescence microscopy using the fluorescent probe, phen green SK. *Hepatology*. **29**, 1171–1179
9. Petrat, F., de Groot, H., and Rauen, U. (2000) Determination of the chelatable iron pool of

single intact cells by laser scanning microscopy. *Arch. Biochem. Biophys.* **376**, 74–81

10. Epsztejn, S., Kakhlon, O., Glickstein, H., Breuer, W., and Cabantchik, Z. I. (1997) Fluorescence analysis of the labile iron pool of mammalian cells. *Anal. Biochem.* **248**, 31–40
11. Hider, R. C., and Kong, X. L. (2011) Glutathione: A key component of the cytoplasmic labile iron pool. *BioMetals*. **24**, 1179–1187
12. Egyed', A., and Saltman, P. (1984) Iron is maintained as Fe(II) under aerobic conditions in erythroid cells. *Biol. Trace Elem. Res.* **6**, 357–364
13. Hider, R. C., and Kong, X. (2013) Iron speciation in the cytosol: An overview. *Dalt. Trans.* **42**, 3220–3229
14. Rae, T. D. (1999) Undetectable intracellular free copper: the requirement of a copper chaperone for superoxide dismutase. *Science.* **284**, 805–808
15. Keller, A. M., Benítez, J. J., Klarin, D., Zhong, L., Goldfogel, M., Yang, F., Chen, T.-Y., and Chen, P. (2012) Dynamic multibody protein interactions suggest versatile pathways for copper trafficking. *J. Am. Chem. Soc.* **134**, 8934–8943
16. Robinson, N. J., and Winge, D. R. (2010) Copper metallochaperones. *Annu. Rev. Biochem.* **79**, 537–562
17. Glerum, D. M., Shtanko, A., and Tzagoloff, A. (1996) Characterization of *COX17*, a yeast gene involved in copper metabolism and assembly of cytochrome oxidase. *J. Biol. Chem.* **271**, 14504–14509
18. Horn, D., and Barrientos, A. (2008) Mitochondrial copper metabolism and delivery to cytochromec oxidase. *IUBMB Life*. **60**, 421–429
19. Morgan, M. T., Bourassa, D., Harankhedkar, S., McCallum, A. M., Zlatic, S. A., Calvo, J.

S., Meloni, G., Faundez, V., and Fahrni, C. J. (2019) Ratiometric two-photon microscopy reveals attomolar copper buffering in normal and Menkes mutant cells. *Proc. Natl. Acad. Sci.* **116**, 12167–12172

20. Yang, L., McRae, R., Henary, M. M., Patel, R., Lai, B., Vogt, S., and Fahrni, C. J. (2005) Imaging of the intracellular topography of copper with a fluorescent sensor and by synchrotron X-ray fluorescence microscopy. *Proc. Natl. Acad. Sci.* **102**, 11179–11184
21. Glerum, D. M., Shtanko, A., and Tzagoloff, A. (1996) *SCO1* and *SCO2* act as high copy suppressors of a mitochondrial copper recruitment defect in *Saccharomyces cerevisiae*. *J. Biol. Chem.* **271**, 20531–20535
22. Ghosh, A., Trivedi, P. P., Timbalia, S. A., Griffin, A. T., Rahn, J. J., Chan, S. S. L., and Gohil, V. M. (2014) Copper supplementation restores cytochrome c oxidase assembly defect in a mitochondrial disease model of *COA6* deficiency. *Hum. Mol. Genet.* **23**, 3596–3606
23. Wang, Y., Weisenhorn, E., MacDiarmid, C. W., Andreini, C., Bucci, M., Taggart, J., Banci, L., Russell, J., Coon, J. J., and Eide, D. J. (2018) The cellular economy of the *Saccharomyces cerevisiae* zinc proteome. *Metallomics*. **10**, 1755–1776
24. Krężel, A., and Maret, W. (2016) The biological inorganic chemistry of zinc ions. *Arch. Biochem. Biophys.* **611**, 3–19
25. Qin, Y., Miranda, J. G., Stoddard, C. I., Dean, K. M., Galati, D. F., and Palmer, A. E. (2013) Direct comparison of a genetically encoded sensor and small molecule indicator: implications for quantification of cytosolic Zn^{2+}. *ACS Chem. Biol.* **8**, 2366–2371
26. Carpenter, M. C., Lo, M. N., and Palmer, A. E. (2016) Techniques for measuring cellular zinc. *Arch. Biochem. Biophys.* **611**, 20–29

27. Colvin, R. A., Holmes, W. R., Fontaine, C. P., and Maret, W. (2010) Cytosolic zinc buffering and muffling: Their role in intracellular zinc homeostasis. *Metallomics*. **2**, 306–317

28. Ma, Z., Chandrangsu, P., Helmann, T. C., Romsang, A., Gaballa, A., and Helmann, J. D. (2014) Bacillithiol is a major buffer of the labile zinc pool in *Bacillus subtilis*. *Mol. Microbiol.* **94**, 756–770

29. Choi, S., Hu, Y.-M., Corkins, M. E., Palmer, A. E., and Bird, A. J. (2018) Zinc transporters belonging to the Cation Diffusion Facilitator (CDF) family have complementary roles in transporting zinc out of the cytosol. *PLOS Genet.* **14**, 1–23

30. Das, S., Khatua, K., Rakshit, A., Carmona, A., Sarkar, A., Bakthavatsalam, S., Ortega, R., and Datta, A. (2019) Emerging chemical tools and techniques for tracking biological manganese. *Dalt. Trans.* **48**, 7047–7061

31. McNaughton, R. L., Reddi, A. R., Clement, M. H. S., Sharma, A., Barnese, K., Rosenfeld, L., Gralla, E. B., Valentine, J. S., Culotta, V. C., and Hoffman, B. M. (2010) Probing in vivo Mn^{2+} speciation and oxidative stress resistance in yeast cells with electron-nuclear double resonance spectroscopy. *Proc. Natl. Acad. Sci. U. S. A.* **107**, 15335–15339

32. Philpott, C. C., and Ryu, M.-S. (2014) Special delivery: Distributing iron in the cytosol of mammalian cells. *Front. Pharmacol.* **5**, 1–8

33. McCormick, S. P., Moore, M. J., and Lindahl, P. A. (2015) Detection of labile low-molecular-mass transition metal complexes in mitochondria. *Biochemistry*. **54**, 3442–3453

34. Nguyen, T. Q., Dziuba, N., and Lindahl, P. A. (2019) Isolated *Saccharomyces cerevisiae* vacuoles contain low-molecular-mass transition-metal polyphosphate complexes. *Metallomics*. **11**, 1298–1309

35. Herrera, R., Álvarez, M. C., Gelis, S., and Ramos, J. (2013) Subcellular potassium and sodium distribution in *Saccharomyces cerevisiae* wild-type and vacuolar mutants. *Biochem. J.* **454**, 525–532

36. Dziuba, N., Hardy, J., and Lindahl, P. A. (2018) Low-molecular-mass iron in healthy blood plasma is not predominately ferric citrate. *Metallomics*. **10**, 802–817

37. Bryant, N. J., and Stevens, T. H. (1998) Vacuole biogenesis in *Saccharomyces cerevisiae*: protein transport pathways to the yeast vacuole. *Microbiol. Mol. Biol. Rev.* **62**, 230–47

38. Li, L., Chen, O. S., Ward, D. M. V., and Kaplan, J. (2001) Ccc1 is a transporter that mediates vacuolar iron storage in yeast. *J. Biol. Chem.* **276**, 29515–29519

39. Li, L., and Kaplan, J. (1998) Defects in the yeast high affinity iron transport system result in increased metal sensitivity because of the increased expression of transporters with a broad transition metal specificity. *J. Biol. Chem.* **273**, 22181–22187

40. Pagani, A., Villarreal, L., Capdevila, M., and Atrian, S. (2007) The *Saccharomyces cerevisiae* Crs5 Metallothionein metal-binding abilities and its role in the response to zinc overload. *Mol. Microbiol.* **63**, 256–269

41. Forgac, M. (2007) Vacuolar ATPases: Rotary proton pumps in physiology and pathophysiology. *Nat. Rev. Mol. Cell Biol.* **8**, 917–929

42. Yuan, D. S., Dancis, A., and Klausner, R. D. (1997) Restriction of copper export in *Saccharomyces cerevisiae* to a late Golgi or post-Golgi compartment in the secretory pathway. *J. Biol. Chem.* **272**, 25787–25793

43. Marsh, T., and Debnath, J. (2015) Ironing out *VPS34* inhibition. *Nat. Cell Biol.* **17**, 1–3

44. Ho, B., Baryshnikova, A., and Brown, G. W. (2018) Unification of protein abundance datasets yields a quantitative *Saccharomyces cerevisiae* proteome. *Cell Syst.* **6**, 192–205

45. Reddi, A. R., Jensen, L. T., Naranuntarat, A., Rosenfeld, L., Leung, E., Shah, R., and Culotta, V. C. (2009) The overlapping roles of manganese and Cu/Zn SOD in oxidative stress protection. *Free Radic. Biol. Med.* **46**, 154–162

46. Chen, O. S., and Kaplan, J. (2000) Ccc1 suppresses mitochondrial damage in the yeast model of Friedreich's ataxia by limiting mitochondrial iron accumulation. *J. Biol. Chem.* **275**, 7626–7632

47. Romeo, A. M., Christen, L., Niles, E. G., and Kosman, D. J. (2001) Intracellular chelation of iron by bipyridyl inhibits DNA virus replication. *J. Biol. Chem.* **276**, 24301–24308

CHAPTER IV

CONCLUSION AND FUTURE WORK

Conclusion

The ultimate goal of this dissertation was to detect and characterize iron, copper, zinc, and manganese trafficking species in the vacuoles and cytosol of *Saccharomyces cerevisiae*. Such species were presumed to be nonproteinaceous, low-molecular mass, and labile (possessing rapidly exchanging ligands). Due to the lability of these complexes, the chemical composition and precise cellular functions of these species remain undetermined despite the abundant evidence that these species play essential roles in the cell biology of metal ions.

Previous studies in this field have universally employed the chelator-based approach of detecting such complexes, in which membrane-permeable fluorescence-based chelators are added to intact cells. Such chelators penetrate the cell and bind the labile trafficking metal. This alters the fluorescence properties of the chelators, thereby allowing detection of what are called *labile metal pools*. The approach has some important strengths but also some critical weaknesses. Most importantly, such an approach destroys the complexes of interest during their detection. Thus, it will not be possible to determine the chemical composition or cellular function of these complexes using this approach.

A chromatography-based approach was developed in this dissertation as an alternative in which it is possible, *at least in principle*, to isolate and characterize these labile metal complexes. The approach developed here was to first isolate a particular cellular compartment, in this case the vacuoles and cytosol, and then isolate a low-molecular-mass filtrate which was then analyzed using a liquid chromatography system present in a refrigerated anaerobic glove box and interfaced

to an on-line ICP-MS. The eluate from the column was split, allowing a portion to be collected in fractions and the remainder to be sent to the ICP-MS.

A major problem that was encountered initially was poor batch-to-batch reproducibility. Diagnosing and addressing this problem involved improving organelle isolation methods, altering column conditions, column cleaning methods, changing buffers, etc. Eventually an acceptable level of reproducibility was achieved. This is only the first step in establishing that the complexes detected are endogenous to the cell and physiologically relevant. In the future, this approach needs to be further developed so as to better distinguish endogenous species from artifacts. Going hand-in-hand with these improvements will be efforts to determine the chemical composition of these species, using powerful bioanalytical tools such as ESI and MALDI mass spectrometry, and NMR, EPR, Raman and Mössbauer spectroscopies.

Researchers in the 1980's predicted that iron was stored in vacuoles in the Fe^{III} oxidation state and bound to polyphosphate chains. This prediction was based on the high concentration of polyphosphate in this organelle, the binding strength of Fe^{III} ions to polyphosphate, the acidity of the organelle, and the assumption that the glutathione redox couple controlled the redox status of the organelle. There were no further investigations into this until Cockrell *et al.* isolated vacuoles from cells enriched in ^{57}Fe and performed EPR and Mössbauer spectroscopy on them. They found that the iron in vacuoles was high-spin $S = 5/2$ Fe^{III} and that the hyperfine coupling between the electron and nuclear spins was typical of Fe^{III} ions coordinated to "hard" oxygen-based ligands (as would be observed in an Fe^{III} polyphosphate complex) (1). This was the state of the field prior to my investigations.

Using liquid chromatography coupled with ICP-MS, my work in Chapter II supports this model of Fe^{III}-polyphosphate complexes and it further demonstrates that polyphosphate serves a

similar function to store vacuolar Cu, Zn and Mn ions in the vacuole. Based on the liquid chromatograms of vacuolar FTSs, phosphorus peaks coeluted with metal peaks at the masses of 500 – 1700 Da. We found the average chain length of vacuolar polyphosphate was 6 – 20 of phosphate units in which 1-3 metal centers were coordinated per chain. Hard oxygen ligands in polyphosphate are excellent Lewis bases for hard Lewis acids like ferric ions (2). Treatment with acid phosphatase disrupted the binding of polyphosphate with these LMM-metal bound species. This study was also the first to show that the majority of vacuolar Fe, Zn and Mn were stored as LMM complexes. This likely allows the cells to easily acquire and redistribute these metal ions under stress or deficiency of trace metals during cell growth conditions.

Among the metals in the vacuolar flow-through solution, only copper was primarily present in a form (with an apparent mass of 4800 – 7800 Da) that might be proteinaceous. Consistent with this, the species was resistant to phosphatase treatment, as would be expected for a protein-bound species. We conclude this species is likely due to Cup1 protein, since the copper trace of *cup1*Δ vacuolar FTSs lacked the 7800 Da species. Interestingly, copper:polyphosphate complexes also accumulated in *cup1*Δ and *cox17*Δ vacuolar FTSs. This suggests polyphosphate might play a role in copper detoxification when copper homeostasis is disrupted in these knockout strains.

As a single membrane-bound organelle, the vacuole is difficult to isolate in large scale for biophysical characterization. In addition, vacuoles actively interact with other subcellular compartments like endoplasmic reticulum and Golgi to participate in a wide variety of metabolic processes such as membrane trafficking, protein sorting and degradation (3). Vacuolar morphology is highly dynamic and “plastic” at different stages of cell division and different growth media (3) (4). Vacuoles at early stationary growth phase are fused into a single large lobe whereas cells at exponential growth phase contain multiple fragmented vacuoles, which are more fragile and

challenging to isolate in intact forms (5). This explains why iron traces of vacuolar FTSs from cells harvested during exponential phase were less reproducible than those harvested in stationary phase. Although the purity of the vacuolar extract was not perfect, vacuoles were highly enriched in the isolated fractions relative to other subcellular compartments (ER and cytosol). Ultimately, twenty-nine batches of vacuoles were isolated to obtain and ensure the reproducibility of metal chromatograms of vacuolar FTSs.

Using the same experimental approach, LMM complexes of iron and other transition metals in the cytosol were characterized for the first time (Chapter III). Studying cytosolic iron trafficking species has remained a challenge for the past 30 years due to the following: [1] cytosol is difficult to isolate in a pure form, [2] the iron in the cytosol is loosely bound and the ligand exchange rate is high, [3] multiple iron trafficking species could be present (6) (7). To solve these problems, I optimized the cytosol isolation procedure to obtain the cytosol that was largely free of ER, mitochondria and vacuoles. In this case, cells were harvested at early exponential phase, which minimizes the biogenesis of vacuoles and mitochondria allowing for better purity (8) (9) (10). These organelles are hardly ruptured during the cell lysing step, minimizing their contamination to the isolated cytosolic fraction. In addition, spheroplasts were fractionated using a gentle method by Dounce homogenization rather than other harsh lysing approaches with glass beads or sonication. A series of low-speed and high-speed centrifugations was developed to obtain clean cytosol fractions, free of lipid droplets and organelles with high lipid content such as the ER. Finally, the entire procedure was performed in a glove box (or under anaerobic conditions) such that cytosolic iron, which is generally presumed to be in the reduced Fe^{II} state, would not be oxidized.

With clean isolated cytosol from WT cells and cells of different genetic knockout strains, the FTSs were collected and characterized. Wild type cytosolic iron traces contained 3 major species at 900, 1000 and 1300 Da. These species increased 2-fold in concentration when iron supplementation in the media was increased from 1 μM to 40 μM. Surprisingly, under 100 μM Fe supplementation, iron species at 800 – 1300 Da decreased but a species with the mass of 700 Da dominated. Iron traces of cytosolic FTSs from cells lacking the high affinity mitochondrial transporters *mrs3*Δ *mrs4*Δ strain also showed an accumulation of the Fe_{700} species. This result implies that the Fe_{700} species is the cytosolic iron LMM complexes trafficking to the mitochondria, but further studies are required to investigate this. Interestingly, isolated mitochondria contain a single iron species called "Fe_{580}" (because it has an apparent mass of approximately 600 Da). It is intriguing to consider that the 700 Da species described here might be Fe_{580} or related to it.

Deletion of vacuolar Fe importer *ccc1*Δ strain did not result in an accumulation of any iron LMM species in the cytosolic FTSs. Future work is needed to test if vacuoles and mitochondria share the same Fe trafficking species as has been commonly assumed. Our approach of isolating cytosol from different genetic knockout strains involved in Fe homeostasis represents a foundation to understand the functions of these cytosolic Fe complexes. The fluctuation and redistribution of Fe species under high Fe growth conditions reflect the dynamicity of the labile iron pool as previously proposed in literature (6) (7). Treatment with 2,2'-bipyridine disrupted all cytosolic iron and other metals LMM complexes, thus providing more evidence for the labile property of these species. Previous experiments have shown that this same treatment causes whole intact growing yeast cells to stop growing abruptly. We suggest that the low-mass iron complexes that are chelated by 2,2'-bipyridine are essential for cell growth.

Copper traces of WT cytosolic FTSs exhibit strong signals at 5200 Da due to Cup1. Cu_{8500} is absent in *cup1*Δ cytosolic FTSs but a species of mass at 8500 Da dominates indeed. We propose the other metallothionein Crs5 gives rise to Cu_{8500} peak. Crs5 protein is overexpressed in order to buffer cytosolic Cu under conditions in which the cell lacks the *CUP1* gene. Unexpectedly, a pool of copper LMM complexes with masses of 300 –1300 Da was also present in the cytosolic FTSs of *cup1*Δ cells and in the FTS of other cell strains in which copper is dysregulated (*cox17*Δ, and *vma2*Δ). Increasing copper supplementation in the growth media also led to more intense copper peaks from 300 – 1300 Da. This is the first direct demonstration of LMM nonproteinaceous copper species in the cytosol. The presence of such species violates the well-accepted view that all copper trafficking in cells is performed by protein-based chaperones and that there is no "free" copper in the cell. Further studies are required to investigate this.

We also discovered a low-molecular-mass (1000 – 1300 Da) zinc complex in the cytosol of yeast. Curiously, increasing zinc salts in the growth media did not result in the increase of this Zn species which is routinely observed in cytosolic FTSs from cells without any Zn supplementation. We also provided evidence that a significant portion of cytosolic Zn is bound to Crs5 metallothionein (showing a peak at 8500 Da). Both cytosolic Cu and Zn traces of from cells grown with 100 μM Zn comigrate at 8500 Da because Crs5 can bind both Zn and Cu. This implies cytosolic zinc LMM complexes are tightly controlled at high Zn growth condition. Since Zn is at the top of the Irving William order series, it is reasonable that cytosolic zinc is mostly buffered by proteins and chaperones with more layers of regulation rather than LMM forms.

Finally, we detected a very small pool of cytosolic Mn LMM complexes in the range of 1 – 3 μM. This was from cytosol isolated from cells that were not supplemented with a Mn salt. Mn traces of cytosolic FTSs from WT cells have a broad distribution of low-intensity peaks with

masses ranging from 100 Da to 1200 Da. This is likely because manganese binds weaker than the other metals investigated here. Cytosolic manganese trafficking species are probably more loosely bound and easily disrupted during the isolation. Curiously, more intense Mn peaks were observed in cytosol isolated from various genetic strains in which metal ion homeostasis was disrupted. We don't understand this fully, but it may involve the cell's response to metal ion dysregulation.

Future Work

This dissertation has established a new foundation to further understand the mechanisms of cellular metal ion trafficking and regulatory homeostasis on the molecular level, especially the role of non-proteinaceous low-molecular-mass labile metal complexes. Further studies will be required to identify the cellular function of each species, and to identify any such species that are artifacts of isolation. The approach will be to examine systematically how the intensities of various chromatographic peaks vary as the metal content of the growth media varies. Such studies should be performed on WT cells and on various genetic strains in which some aspect of metal ion trafficking or homeostasis has been compromised. If the chromatographic intensities of particular labile metal species cells vary in ways that are expected based on the specific nutritional or genetic perturbation employed, such results can help identify the cellular function of a particular labile species.

Once important endogenous labile metal species have been identified from such studies, their chemical composition needs to be determined. This will involve various forms of mass spectrometry (ESI, MALDI, etc) and a wide range of powerful analytical and biophysical methods including NMR, EPR, XAS, and Mössbauer spectroscopies. At this point, it might become clear

how nature uses coordination chemistry to facilitate metal ion trafficking in cells (without toxic effects of Fenton chemistry and/or mismetallation).

Further developments in isolating large quantities of various cellular compartments may also be required. For example, methods for cell-synchronization may be required to completely "lock" the cells at certain metabolic modes before an organelle or cytosol is isolated. Organelle isolation procedures are usually lengthy and time-consuming. Cell synchronization might be ideal to further characterize metal LMM complexes in the cytosol and vacuoles at different growth stages and conditions, especially if the labile metal complexes change during cell cycle processes. Other technical aspects may also be improved. For example, use of different chromatography columns may afford significantly different results. Different mobile phases, and isolation conditions, buffers, pH etc may generate different results.

Polyphosphate has been demonstrated to play a significant role in storing metals in the vacuoles as LMM complexes. It will be revealing to investigate the relationship between polyphosphate synthesis and metal ion uptake. Culotta and coworkers demonstrated that phosphate accumulation increased the expression of the Aft1-dependent iron regulon (11). We also observed lower intensity of phosphorus peaks comigrating with iron in vacuolar FTSs from cells grown under low Fe supplementation. Does decreased metal uptake downregulate polyphosphate synthesis? Do low intracellular polyphosphate concentrations affect iron uptake and iron storage in the vacuoles? I attempted to isolate vacuoles from cells grown with low phosphorus media. Unfortunately, the yield of vacuolar extract was too low for biophysical characterization. This was likely due to the morphology of vacuoles which depend on intracellular polyphosphate concentration. Gopaldass *et al.* showed that yeast vacuole fused into a single large organelle to store polyP when phosphate was abundant whereas consumption of polyP caused the yeast

vacuoles to fragment into numerous smaller organelles (12). The latter problem was encountered trying to obtain high vacuolar yield from cells grown in phosphate deficient media. Mössbauer and EPR spectroscopies might be useful for studying the whole cells iron-ome at low and high phosphate.

Phosphate and pH homeostasis are directly linked, especially in the vacuoles (13). Cockrell *et al.* demonstrated that cells treatment with Concanamycin A, an inhibitor of the V-ATPase/H^+ pump resulted in the majority of NHHS Fe^{II} and nanoparticles in whole cells. They concluded that low vacuolar pH is essential to maintain intracellular NHHS Fe^{III} levels (14). That study motivated our lab to continue studying iron speciation in *vma2*Δ cells which the subunit B of V-ATPase/H^+ pump is deleted. We are currently characterizing the iron pools localized to different subcellular compartments of *vma2*Δ cells by Mössbauer and LC-ICP-MS. It will be exciting to understand the effect of disrupted pH homeostasis on the redox status of cellular iron.

Glutathione (GSH) has been speculated to be the primary ligand for cytosolic iron (15) due to its abundance in the cytosol and high affinity to ferrous ions. In 1989, Freedman *et al.* showed that GSH was coordinated to cytosolic copper before the metal was bound by metallothioneins (16). It would be interesting to isolate the cytosol at low S or blocking the biosynthesis pathway of GSH. If GSH is the endogenous ligand of labile metal pools, we hypothesize that lower levels of S species and lower intensity peaks of cytosolic Fe and Cu LMM complexes would be observed.

References

1. Cockrell, A. L., Holmes-Hampton, G. P., McCormick, S. P., Chakrabarti, M., and Lindahl, P. A. (2011) Mössbauer and EPR study of iron in vacuoles from fermenting *Saccharomyces cerevisiae*. *Biochemistry*. **50**, 10275–10283

2. Maret, W. (2016) The metals in the biological periodic system of the elements: Concepts and conjectures. *Int. J. Mol. Sci.* **17**, 1–8

3. Li, S. C., and Kane, P. M. (2009) The yeast lysosome-like vacuole: Endpoint and crossroads. *Biochim. Biophys. Acta - Mol. Cell Res.* **1793**, 650–663

4. Conradt, B., Shaw, J., Vida, T., Emr, S., and Wickner, W. (1992) In vitro reactions of vacuole inheritance in *Saccharomyces cerevisiae*. *J. Cell Biol.* **119**, 1469–1480

5. Zhang, C., Hicks, G. R., and Raikhel, N. V (2014) Plant vacuole morphology and vacuolar trafficking. *Front. Plant Sci.* **5**, 1–9

6. Crichton, R. R. (1984) Iron uptake and utilization by mammalian cells II. Intracellular iron utilization. *Trends Biochem. Sci.* **9**, 283–286

7. Muckenthaler, M. U., Rivella, S., Hentze, M. W., and Galy, B. (2017) A red carpet for iron metabolism. *Cell*. **168**, 344–361

8. Martínez-Diez, M., Santamaría, G., Ortega, Á. D., and Cuezva, J. M. (2006) Biogenesis and dynamic of mitochondria during the cell cycle: Significance of 3'UTRs. *PLoS One*. **1**, 1–12

9. Latterich, M., Hartley, C. A., and Watson, M. D. (1993) Plasticity of vacuole biogenesis in the yeast *Saccharomyces cerevisiae*. *J. Exp. Bot.* **44**, 307–313

10. Chan, Y. H. M., and Marshall, W. F. (2014) Organelle size scaling of the budding yeast vacuole is tuned by membrane trafficking rates. *Biophys. J.* **106**, 1986–1996

11. Rosenfeld, L., Reddi, A. R., Leung, E., Aranda, K., Jensen, L. T., and Culotta, V. C. (2010) The effect of phosphate accumulation on metal ion homeostasis in *Saccharomyces cerevisiae*. *J. Biol. Inorg. Chem.* **15**, 1051–1062

12. Gopaldass, N., Fauvet, B., Lashuel, H., Roux, A., and Mayer, A. (2017) Membrane scission driven by the Proppin Atg18. *EMBO J.* **36**, 3274–3291

13. Eskes, E., Deprez, M.-A., Wilms, T., and Winderickx, J. (2018) pH homeostasis in yeast; the phosphate perspective. *Curr. Genet.* **64**, 155–161

14. Cockrell, A., McCormick, S. P., Moore, M. J., Chakrabarti, M., and Lindahl, P. A. (2014) Mössbauer, EPR, and modeling study of iron trafficking and regulation in *Δccc1* and *CCC1*-up *Saccharomyces cerevisiae*. *Biochemistry*. **53**, 2926–2940

15. Hider, R. C., and Kong, X. L. (2011) Glutathione: a key component of the cytoplasmic labile iron pool. *BioMetals*. **24**, 1179–1187

16. Freedman, J. H., Ciriolo, M. R., and Peisach, J. (1989) The role of glutathione in copper metabolism and toxicity. *J. Biol. Chem.* **264**, 5598–5605